DAA/LANGLEY

FINAL REPORT

NASA Grant No. NAG-1-177-02

N85-28785

Investigation of Semiconductor Clad
Optical Waveguides

Submitted to:

National Aeronautics and Space Administration
Langley Research Center
Hampton, Virginia 23665

Submitted by:

T. E. Batchman
Associate Professor

Richard F. Carson
Graduate Student Participant

Report No. UVA/528207/EE85/103
Report Date: March 1985

SEMICONDUCTOR DEVICE LABORATORY
DEPARTMENT OF ELECTRICAL ENGINEERING
SCHOOL OF ENGINEERING AND APPLIED SCIENCES
UNIVERSITY OF VIRGINIA

UNIVERSITY OF VIRGINIA

SDL

FINAL REPORT

NASA Grant No. NAG-1-177-02

Investigation of Semiconductor Clad
Optical Waveguides

Submitted to:

National Aeronautics and Space Administration
Langley Research Center
Hampton, Virginia 23665

Submitted by:

T. E. Batchman
Associate Professor

Richard F. Carson
Graduate Student Participant

Report No. UVA/528207/EE85/103
Report Date: March 1985

TABLE OF CONTENTS

i

I. INTRODUCTION

Integrated optical devices offer a variety of interesting and useful possibilities for use in high-speed and high-volume information processing systems. Though integrated optical techniques have not been widely implemented, the needs of advanced information processing and transmission systems for direct fiber-optical switching, high-speed real-time processing, and high-volume on-chip or board-to-board interconnects warrant the continued development of the optical technologies.

A variety of techniques have been proposed for fabricating integrated optical devices using semiconductors, lithium niobate, and glasses as waveguides and substrates. This investigation has focused on the use of glass waveguides and their interaction with thin semiconductor cladding layers. Though the interactions of these multilayer waveguide structures have been analyzed here using glass, they may be applicable to other types of materials as well. The primary reason for using glass is that it provides a simple, inexpensive way to construct waveguides and devices.

Much of this study has been based on investigating the effects of a lossy cladding material on a lossless planar dielectric waveguide. The relative permittivity of a lossy material is given by a complex value where the imaginary portion represents the loss of the material at the frequency of interest (ω). The lossy material is a semiconductor since the properties of such materials can be changed by doping, electric fields and incident photons. Of particular interest is the absorption

coefficient, α , which may be related to the imaginary portion of the refractive index by the expression $\alpha = \frac{2\omega k}{c}$. The physical mechanisms of this absorption are discussed in detail in Section II. The discussion uses the particular case of absorption in GaAs, as it is the best candidate for use in constructing an optical modulator.

Guided-wave studies of the GaAs-clad waveguides for use as modulators are detailed in Section III, while Section IV introduces a semiconductor-clad guided-wave polarizer. Recent studies of spectral filtering are presented in Section V, while Section VI introduces a high-speed amorphous silicon guided-wave photodetector.

II. OPTICAL ABSORPTION IN GaAs

The optical parameters of absorption and dispersion in GaAs (and in other semiconductors), exhibit a number of interesting properties that may be exploited for use in various electro-optical and photo-conductive devices. In the following analysis, these properties are studied for possible use in light-controlled integrated-optical modulators and frequency filters.

For a material with finite conductivity, the parameter of interest is the permittivity, which influences electromagnetic wave propogation, as will be shown. For a plane wave of frequency ω , the electric and magnetic fields are given by vector representations as

$$\bar{E} = \bar{E}_0 e^{j(\underline{k} \cdot \underline{r} - \omega t)}$$
$$\bar{H} = \bar{H}_0 e^{j(\underline{k} \cdot \underline{r} - \omega t)} \tag{1}$$

2

where $\underline{r}$ is the unit direction vector and $\underline{\tilde{k}}$ is the complex propagation vector

$$\underline{\tilde{k}} + \underline{k}_1 + j\underline{k}_2 \tag{2}$$

The real part of $\underline{\tilde{k}}$ (k_1) controls dispersion, or phase-shift, while the imaginary part ($\underline{k}_2$) controls attentuation, or loss. For a material with unit relative magnetic permeability ($\mu_r = 1$)

$$\underline{\tilde{k}} \cdot \underline{\tilde{k}} = \mu_0 \varepsilon_0 \tilde{\varepsilon}_r \omega^2 = \frac{\tilde{\varepsilon}_r \omega^2}{c^2} \tag{3}$$

where ε_0 and μ_0 are the permittivity and permeability of free space and c is the speed of light. The only parameter that includes the effects of the medium is the complex relative dielectric constant

$$\tilde{\varepsilon}_r = \varepsilon_1 + j\varepsilon_2 = \varepsilon_1 + j\,\tilde{\sigma}/\omega\varepsilon_0 \tag{4}$$

where $\tilde{\sigma}$ is the "a.c. conductivity".

The complex index of refraction $\tilde{n}$, is then given by $\tilde{\varepsilon}_r = \tilde{n}^2$ such that

$$\varepsilon_1 = \tilde{n}^2 - \tilde{k}^2 \tag{5}$$
$$\varepsilon_2 = 2\tilde{n}\tilde{k}$$

where $\tilde{k}$ is the magnitude of propagation vector $\underline{\tilde{k}}$.[1]

The loss term associated with conductivity may be described by an attenuation constant, (also called an absorption coefficient), which is given by[2]

$$\alpha = \frac{2\pi\varepsilon_2}{\lambda_0} = \frac{4\pi nk}{\lambda_0} = \frac{2\pi\tilde{\sigma}}{\omega\varepsilon_0\lambda_0} = \frac{\tilde{\sigma}}{nc\varepsilon_0} \tag{6}$$

Given in nepers/meter, this constant defines the exponential rate

3

of decay of the amplitude of a given wave. Immediately, we see that if conductivity can be changed, then the absorption, and thus the attenuation of a light wave travelling through the lossy medium can be changed.

In a semiconductor, this a.c. conductivity (and the resulting attenuation coefficient) is a function of many different material mechanisms, which are, in turn dependent on the frequency of the propagating wave. These include classical free carrier absorption effects, and quantum effects such as photon-phonon interactions, intra-band and interband transitions, and band-gap shifts.

A. The Semiconductor-Clad Waveguide

The propagation effects to be discussed are of interest in several areas, including crystal-growth studies, self-focusing in solid-state lasers, and (for our work) modulation in an optical waveguide.[3,4,5] The waveguide structure of interest is shown in Fig. 1. Guided waves propagating in layer 3 couple into the high permittivity, lossy semiconductor cladding layer[5]. The resulting attenuations and phase shifts have been determined by a computer analysis for various thicknesses of several types of semiconductor cladding layers, as shown in Fig. 2 and Fig. 3 for GaAs. The results of the analysis for GaAs (with light propagating at $\lambda_0 = 0.827$ μm), show that when $\tilde{\sigma}$ (or subsequently ε_2) is varied by a given amount, then the attenuation and phase changes are shown in Fig. 4 and Fig. 5, respectively. These calculations, which assume the GaAs permittivity values and guiding-layer thickness shown in Fig. 2, will be discussed

further in Section III.

The changes shown in these figures are sufficient for modulation if $\tilde{\sigma}$ can be changed sufficiently from its initial value. The problem of modulating the guided light beam is then essentially that of finding a way to sufficiently vary the value of $\tilde{\sigma}$, and thus the value of loss term ε_2 and the absorption coefficient α. Thus, in the analysis that follows, various models for $\tilde{\sigma}$ and α will be studied. Particular attention is given to the possibility of varying $\tilde{\sigma}$ by injecting free carriers, using a second light source as a modulating beam. GaAs is of primary interest as it is a direct-gap semiconductor and thus should tend to be more photo-active than indirect semiconductors.

B. The Dispersion Relations

As a starting point for our understanding of the interactions between the real and imaginary portions of the complex permittivity, we use the relations that connect dispersive and absorptive processes. As derived by Kramers and Kronig, they are applicable to the real and imaginary parts of a complex quantity which describes a linear relation between two amplitudes. The frequency-dependent complex value $\tilde{\varepsilon}_r(\omega)$ is such a quantity, as it relates the amplitude of an electric field ($\underline{E}$) to its displacement ($\underline{D}$)

$$\underline{D}(\omega) = \varepsilon_0 \tilde{\varepsilon}_r(\omega) \underline{E}(\omega) = \varepsilon_0 (\varepsilon_1(\omega) + j\varepsilon_2(\omega))\underline{E}(\omega) \tag{7}$$

For a propagating wave, $\varepsilon(\omega)$ describes a phase shift between successive values of wave amplitude. For a metal or

5

semiconductor with a zero frequency value for conductivity of σ_0, this Kramers-Kronig relation takes on the following form

$$\varepsilon_1(\omega) = 1 + \frac{2}{\pi} p \int_0^\infty \frac{\omega^1 \varepsilon_2(\omega^1)}{\omega^{12} - \omega^2} d\omega^1 \tag{8a}$$

$$\varepsilon_2(\omega) = \frac{\sigma_0}{\varepsilon_0 \omega} - \frac{2\omega}{\pi} p \int_0^\infty \frac{\varepsilon_1(\omega^1)}{\omega^{12} - \omega^2} d\omega^1 \tag{8b}$$

Here, p is the Canchy principle value of the integral. These relations apply similarly to $\tilde{n}$ and $\tilde{k}$.

Absorption-reflection analysis, when applied to relation (8a), leads to the result that ε_1 will have maxima at frequencies where the derivative of ε_2 is large and positive, while minima at frequencies where $\frac{d\varepsilon_2}{d\omega}$ is large and negative. Relation (8b) leads to the same result for ε_2, as related to the derivative of ε_1.[1] It is interesting to note that a similar sort of relation holds between the attenuation and mode index of our waveguide structure, (as shown in Figs. 2 and 3) as they vary with GaAs thickness.

C. Free Carrier Absorption: The Classical Model

At longer wavelengths (far intrared) the incident photons associated with a wave propagating in a semiconductor do not have enough energy to excite many interband transitions, and the absorptive interaction of the material with the wave can be modeled by using classical means. This analysis has previously been applied to metals in the form of the Drude theory.

Here, the a.c. conductivity (from Eq. 4 and Eq. 6) is given by the classical relation between current density and electric

field

$$\tilde{J} = \tilde{\sigma}\tilde{E} \tag{9}$$

For the propagating wave case where electrons are the charge carriers, we use the equation of motion of an electron with effective mass m* in the electric field of the wave

$$m^*\dot{v}_x = -q\tilde{E}_x = -q\tilde{E}_0 e^{-j\omega t} \tag{10}$$

When the above equation is used to solve the Eq. (9), the following result is obtained

$$J_x = \frac{nq^2}{m^*}\left\{\left<\frac{\tau}{1+\omega^2\tau^2}\right> - jw\left<\frac{\tau^2}{1+\omega^2\tau^2}\right>\right\}E_x \tag{11}$$

where   is the mean carrier lifetime and n is the free carrier concentration. When the d.c. conductivity is expressed as

$$\sigma_0 = nq^2\tau/m^* \tag{12}$$

then Eq. (11) can be expressed in simplified form as[2,6]

$$\tilde{\sigma} = \sigma' + j\sigma'' = \frac{\sigma_0}{1+\omega^2\tau^2} + j.\frac{\sigma_0\omega\tau}{1+\omega^2\tau^2} \tag{13}$$

This classical treatment shows that (to first-order) the a.c. conductivity and thus the absorption is directly related to the d.c. conductivity and inversely related to frequency. For low frequency, $\omega\tau \ll 1$ so $\sigma' \gg \sigma''$, and $\tilde{\sigma} \approx \sigma'$(which corresponds directly to conductivity losses in a propagating wave). In the very low frequency range (radio frequency or microwaves) $\tilde{\sigma}=\sigma' \approx \sigma_0$. Thus $\tilde{\varepsilon}_r \approx i\varepsilon_2$ and, by Eq. (5)

$$|n| = |k| = \sqrt{\frac{\sigma_0}{2\varepsilon_0\omega}} \tag{14}$$

In such a case, the skin depth approximation, often used to describe propagation in good conductors, holds

7

$$\delta = \frac{1}{2} = \left(\frac{\varepsilon_0 c^2}{2\sigma_0 \omega}\right)^{1/2} \tag{15}$$

Of specific importance from this classical model is the fact that the absorption, which is proportional to the d.c. conductivity, is thus proportional to the free carrier concentration (n). We note this effect for semiconductors in the longer wavelength region (beyond the fundamental absorption edge) of Fig. 6, where curve A has the lowest doping level, and thus the lowest value for n, while curve C has the highest doping level.[2]

For the high frequency region of this classical model, $\omega\tau \gg 1$ and $\sigma'' \gg \sigma'$, which yields

$$\tilde{\sigma} \approx \sigma'' \approx j \frac{\sigma_0 \omega\tau}{\omega^2\tau^2} = j \frac{\sigma_0}{\omega\tau} \tag{16}$$

When combined with Eq. (4)

$$\tilde{\varepsilon}_r \approx \varepsilon_1 + j \left(\frac{j\sigma_0}{\varepsilon_0\omega^2\tau}\right) = \varepsilon_1 - \frac{nq^2}{m^*\varepsilon_0\omega^2} \tag{17}$$

Eq. (17), then, predicts that there is no loss or absorption associated with the material at high frequency (which is also the case of total reflection, as for metal-coated mirrors). The frequency where $\varepsilon = 0$ is known as the "plasma frequency" (where ω_p is in the short wavelength visible to ultraviolet).

$$\omega_p = q(n/m^*\varepsilon_0\varepsilon_1)^{1/2} \tag{18}$$

Physically, it corresponds to the case where an undamped plasma of electrons and positive ions can oscillate (in resonance) as a whole.[2] Ideally, this resonance produces a discontinuous change

8

in absorption, yielding a "plasma edge" as shown in Fig. 7. In reality, this change is not a perfect discontinuity, and the absorption is not zero, as will be predicted by taking quantum effects into account for semiconductors.

By using this classical development, Lee, et. al. has been able to construct an optically-controlled millimeter-wave modulator in silicon.[7] In this device, the millimeter waves propagate through the silicon with an absorption defined by the a.c. conductivity of Eq. (13). A thin plasma layer is then induced and conrolled in the surface of the silicon by a laser light source that propagates at a wavelength such that the frequency well above ω_p, as in Fig. 8. The amplitude and phase of the millimeter-wave is changed according to the properties of the plasma layer, as it is conrolled by the laser light.

D. Quantum Effects: I.R. and The Fundamental Absorbtion

For our case of optical propagation with optical control, the classical model does not provide a complete picture of the behavior of the absorption coefficient. In this region of propagation, the primary phenomena of interest are the various types of photon absorptions that may occur.

As the frequency of the incident (guided) wave advances through the infra-red region (for GaAs), photon absorption is a function of phonon interaction (due to lattice effects) and intra-band absorption as may occur between overlapping valence bonds (as shown in Fig. 9). The governing factor is that all photon-absorption processes such as energy transitions or phonon excitation can only occur when the photon energy, (hf or $\hbar\omega$), is

great enough to cause the carrier to span the "quantum jump" associated with that transition of phonon. These effects tend to perturb the general shape of the long-wavelength portion of the absorption curve of Fig. 6 (especially out in the far infrared, for semiconductors).

At some frequency, the photon energy associated with the light wave finally becomes large enough that electrons in the valence band can rise into the conduction band when they absorb photons. This condition is described by the following relation

$$h\nu_f = \hbar\omega_f = E_g \tag{19}$$

where E_g is the band gap (or forbidden region) shown in Fig. 10.[2] The rapid rise in absorption that results from this transition is called the "fundamental absorption", and ω_f (with its associated free-space wavelength, λ_f) is known as the "absorption edge", as shown in Fig. 6.

In a direct band-gap semiconductor (such as GaAs), the photon-induced transition from the conduction band to the valence band can take place with no change in the momentum ($\underline{K}$) vector as in Fig. 10(a). In an indirect bandgap (sch as with Si or Ge), the momentum vector must change for the energy gap transition, resulting in a multi-step transition as in Fig. 10(b), which involves phonons. Because the multi-step (indirect) transition is less probable, indirect-gap materials tend to be less photoactive. This explains our choice to use GaAs as a cladding layer for the modulator.

For GaAs, $\Delta E_g = 1.424$ eV at 300°K, so $\omega_f = 2.16 \times 10^{15}$

rad/sec or $\lambda_f = 8711 \overset{\text{o}}{A} = .8711\mu m$, (in the near infra-red).[8]

E. GaAs Absorption Spectra

The effects of free carrier absorption, intra-band and phonon absorbtion, and the inter-band fundamental absorption provide a reasonably complete model for total absorption in GaAs, as shown in the experimental data of Fig. 11, for the various doping levels at room temperature.[9] As expected, the fundamental absorption occurs near $\lambda = 0.87\mu$, and the rise is extremely steep, up to about $\alpha = 10^4$, as seen in Fig. 12.[10]   (Shifts and other characteristics of the fundamental absorption will be discussed shortly.) Recall from the free carrier theory that the more highly doped (n-type) samples should have a higher absorption (at wavelengths greater than the fundamental edge). The data in Fig. 11 certainly bears this out, which shows that the absorption can be modeled by the free carrier theory of Eq. (6). When approximated by the low frequency version of Eq. (13) this yields

$$\alpha \approx 7.5 \times 10^{-20} n_0 \lambda^3 (cm^{-1})$$

(20)

Of particular interest in Fig. 11 is the fact that, for $\lambda < 4\mu$, the absorption ceases to fall, (as would be predicted by the free carrier model) and may even start to climb slowly. This characteristic, a result of an "optically assisted" inter-conduction band transition, can be approximated (at $\lambda = 2\mu$) as[11]

$$\alpha_i = 6 \times 10^{-18} n_0 (cm^{-1})$$

(21)

Note that the effect seems to be diminished for the degenerately

n-doped ($5.4 \times 10^{18} cm^{-3}$) sample of Fig. 11.

For p-type samples, an inter-valence band transition is seen in the absorption spectrum, as shown in Fig. 13.[12] This "hump" in the absorption spectrum corresponds to a transition at .43 eV.

F.   Shifts in the Fundamental Absorption

As shown in Fig. 11b and as predicted by all models, temperature shifts tend to change all parts of the absorption spectrum. This is particularly true for the case of the fundamental absorption, where the width of the energy gap changes with temperature. This can be seen in Fig. 13, where the gap shrinkage at lower temperatures causes the energy of the absorption edge to shift downward (or the wavelength to shift upward). For simplicity, we will continue to concentrate on effects at room temperature ($\approx 300^\circ K$). This high temperature constraint also implies that additional effects due to excitons will be almost negligible, except perhaps for the small "hump" at the top of the "high purity" curves of Fig. 14.[3,13]

The fundamental absorption also changes with conduction band carrier density, doping and compensation. This could be particularly valuable for our application; as we desire as large a change in absorption as possible, with respect to induced carrier densities. While the absorption coefficient obtained from the free carrier theory can easily be changed over an order of magnitude with doping (as seen at $\lambda \approx 3\mu$ in Fig. 11), the span of the fundamental absorption is three to four orders of magnitude, as shown in Fig. 12.

As seen in Fig. 14a, increasingly high dopings in n-type

GaAs tend to make the absorption edge less steep, and shifts it toward higher energies (lower wavelengths). This is an example of the Burnstien-Moss effect, combined with a band-tailing effect, as will be discussed momentarily. For p-type doping, as seen in Fig. 14b, the absorption edge moves downward in energy (as a result of band-tailing) with higher dopings up to $p_0 \approx 10^{19}$ cm_{-3}, at which point the Burnstien-Moss effect pushes the absorption edge back toward higher energies.[11]

The Burnstien-Moss effect occurs (for heavy doping) when the lowest energy states of the conduction band become filled by donor electrons. Once these states are filled, any additional electrons excited into the conduction band by photo-induced transitions, must traverse a larger energy "jump" in order to reach an available state. Thus, the absorption edge is shifted to higher energy (or shorter wavelength). This process occurs as outlined in Fig. 15.[2]

While the Burnstien-Moss effect acts to shift the fundamental absorption edge to shorter wavelengths, band tailing tends to shift the absorbtion edge to lower energies (longer wavelengths) by reducing the effective band-gap. Band tailing occurs when the impurity levels of induced dopants interact with the band edges of the intrinsic semiconductors, creating new states just inside those band edges. This condition is shown in Fig. 16 for the density of states in the non-doped crystal vs. those of the highly doped crystal (as predicted by several reseachers).[14, 15] Note that the valence band has a larger band tail than the conduction band. This is due to. the fact that

electrons are screened much more than holes, and thus do not interact as strongly. The facts that band tailing (and subsequent lowering of the absorption edge energy) is more pronounced in p-doped GaAs and that the Burnstien-Moss effect is not as significant for the lower effective mass holes, serve to account for the differences between Fig. 14a and Fig. 14b.

The results discussed thus far have shown a definite relation between doping and absorption. The modulation mechanism of interest, in which a second light beam is used to "inject" carriers, and thus change the absorption is, however, a minority carrier effect.[8] Thus, it would be instructive to find out how the absorption coefficient changes with injected minority carriers. Such a contribution has been studied for application in GaAs lasers as a model for gain and self-focusing.[4,16] The calculated results, which take band tailing into account, show a strong dependence of absorption on free-carrier injection, which is similar to that of Fig. 14.

The result shown in Fig. 17 is for highly compensated p-type material. As n-type carriers are injected, they first act to reduce the energy required for the absorption edge slightly (as for level 2 in Fig. 16) by increasing the length of the band-tail. As the injected carrier concentration rises, however, the states in the band-tail fill, and the absorption edge shifts back to higher energies (shorter wavelengths). As the states fill, the carrier density at the bottom of the conduction band again becomes high enough that the Bernstien-Moss effect again is seen, and the fundamental absorbtion shifts to energies higher than that of the intrinsic edge (at 1.424 eV).

G. The Injection of Free Carriers: Photo-Conductivity

As previously stated, the injected carriers which are to modulate the guided beam are to result from illumination of the GaAs waveguide cladding by a second "signal" light beam. From our previous analysis, it becomes obvious that injection may be most easily obtained when the second beam propagates at a wavelength such that the photon energy is well above that of the absorption edge, so that electron-hole pairs are "created" by the resulting band-gap transitions. This quantity is given simply in terms of excess minority carriers. For p-type material the _excess_ minority carriers are given by

$$\Delta n = a\alpha I'/\hbar\omega \tag{22}$$

where I' is the intensity of the beam _in_ the material, a is an adjustment factor called quantum efficiency. For our case, we will only consider band-to-band transitions where one electron is excited by each 100 photons, so a = 0.01) α is the absorption coefficient, and ω is the frequency of the light beam.[2]

For normal incidence on a thin layer of thickness d such that $\alpha d \ll 1$, I' is given by an interference, due to reflections from the back surface.[2] For normal illumination of visible light on our GaAs cladding layer of Fig. 1, $\alpha = 10_4(\frac{1}{cm})$ and $d < 2500$ $\overset{o}{A}$ = 5 x 10_{-5} cm, so this is indeed the case. Thus, the wavelength of the incoming light must be matched to a given thickness such that a maximum amount of light can be absorbed. The conditions for this criterion will be discussed in Appendix A.

Assuming that absorbed intensity is maximized and is uniform

throughout the layer for a given GaAs thickness, and solving for Eq. (22) at a visible light wavelength of $\lambda = 6328 \overset{O}{A}$ or $\omega = 2.977 \times 10_{15}$, then $\alpha = 10_4$

$$\frac{\Delta n}{I} = 3.1855 \times 10^{20} \frac{electrons}{w - cm^3} \qquad (23)$$

Thus, the maximum value from Fig. 17 of $\Delta n = 4 \times 10_{18}$ could be achieved with

$$I = 12.56 \frac{mW}{cm^2} \text{ (absorbed power density)} \qquad (24)$$

(at ideal quantum efficiency) which is a very realistic value for modulation with small amounts of power in the modulating signal beam.

H. The Dispersion Relation-Revisited

The Kramers-Kronig relations of Eq. 8 have been used in their corresponding index of refraction form to calculate the changes in the real part of the index of refraction with injected carrier concentrations. When a numerical solution of these equations was applied to the data corresponding to Fig. 17, the results shown in Fig. 18 were obtained.[16] Thus, as might be expected, both the real and imaginary parts of the index of refraction change with injected carrier concentrations.

This fact holds a strong implication concerning our ability to obtain modulation in a 4-layer GaAs-clad waveguide structure. Recall, for the curves of Fig. 4 and Fig. 5, that maximum modulation of amplitude and phase will occur at certain very sharply defind thickness values for the cladding layer. These values for GaAs thickness at which the modulation is maximized,

16

tend to change, however, with the real part of the refractive index. The changes caused by carrier injection could cause a shift away from this "sweet spot" as the modulating signal is applied. Thus, the GaAs thickness must be chosen and controlled very carefully so as to insure that such an effect does no limit modulation too severely. Such changes in the real part of the refractive index must eventually be incorporated into our computer analysis to determine their total effect on modulation.

I. Summary

The models discussed herein for absorption in GaAs, have been studied in order to provide a more complete understanding of the mechanisms by which an optical modulator might work. From these models we may conclude that the propagating beam should be at a wavelength near that of the fundamental absorption edge in order to take advantage of shifts in that edge and thus to obtain the greatest possible depth of modulation. We may also conclude that modulation can be achieved by shifting the absorption edge through the "injection" of hole-electron pairs by a second light beam (which propagates at a reasonable power level) at a photon energy above that of the absorption edge. We also note that we will need to be careful with interference patterns in the GaAs layer and that the effects of changes in the real part of the index of refraction with injected carriers must be studied further. In the final analysis, the results look encouraging, with respect to the feasibility of using light--light interactions in GaAs to build

an optical modulator.

III. PROGRESS ON THE OPTICAL MODULATOR

    A. Material choice: GaAs at $\lambda = 0.827$ Microns

       As discussed in Section III, a direct band-gap semiconductor such as GaAs is much more likely to absorb free carriers and thus to show a change in its absorption or ac conductivity than is an indirect band-gap material such as Si. In addition, for any given value of percent conductivity change, the percent values of change of attenuation and phase (shown in Fig. 4 and 5, respectively) are relatively high for the GaAs clad waveguide with $\lambda = 0.827$ μm. Note in Fig. 4 that the modulation of attenuation ranges from + 40% to -140% (depending on thickness).

    The wavelength of propagation should be near the band-edge of the cladding material, as discussed in Section II, so that propagating light does not "self-modulate" by generating its own excess carriers. This also happens to increase the range of modulation due to the smaller value of the base absorption or conductivity, σ_o. Our calculations have shown that a longer absorption tends to cause the oscillations of Figs. 2 and 3 to damp out very quickly and to be much less in magnitude. This reduces the coupling and decoupling effects that lead to the large modulation depths (as will be discussed). Since the absorption drops radically near the band-edge, the oscillations and thus the modulation effects are increased. This is illustrated by a comparison of Figs. 4 and 5 with Figs. 13 and 14 of ref. 17 (also Fig. 4 in semi-annual status report

UVA/528207/EE81/101) where the attenuation modulation only ranges over 70% for a silicon-clad waveguides at a propagation wavelength of 0.6328 µm (n = 4.1 - j.21) as opposed to 180% for the GaAs cladding of Fig. 4 were n = 3.6 - j.066. A review of the oscillatory effect follows.

B.   Review of the Modulation Mechanism

The mechansim for this modulation is the same as that previously discussed for the oscillatory effect, and is described in detail in ref. 5 (Appendix B).   Briefly, the attenuation and phase characteristics of Figs. 2 and 3 are generated by varying the cladding thickness from 0.01 to 1.0 microns at the chosen propagation wavelength of .827 microns.   As the cladding thickness is increased, the GaAs layer supports successively higher orders of the guided cladding "submodes."   At cladding thickness values where each of the submodes are just barely supported, the effective index associated with that submode is at a value which matches that of the dielectric waveguide.   A maximum amount of energy is then transferred into the lossy cladding and is thus attenuated in the guide.   This results in a local maximum in the attenuation characteristic of Fig. 2.

This coupling effect is illustrated in Fig. 19, where the mode index of an equivalent three-layer GaAs waveguide is plotted.[5]   When each of the successive mode orders of the GaAs layer (cladding) are supported, the effective index values rise from the dielectric guide value of n = 1.588.   For example, at +GaAs = 0.02, 0.14, and 0.23 µm, the TE_0, TE_1 and TE_2 modes are just at their cutoff values and their effective indices are given

19

by $n = 1.588$. A look at Fig. 2 reveals that these are the exact points where attenuatin maxima occurs in the four-layer guide. The electric field plot of Fig. 20 shows that for $t_2 = 0.14\ \mu m$ this corresponds to a high value of field at the interface of the dielectric guide with the cladding. Conversely, when the field value crosses zero at the interface as in Fig. 21, very little energy is exchanged into the cladding and thus there is very little attenuation. Fig. 21 also shows that a second order submode is supported in the GaAs, corresponding to the third local minimum on the four-layer attenuation curve at a cladding thickness of $0.34\ \mu m$.

This coupling of the modes is the mechanism which leads to the large changes in attenuation and phase as the absorption in the cladding is changed. When the cladding thickness is such that the attenuation is near a peak (at the dark conductivity, σ_0) the submode in the cladding is near cutoff. Thus, when the conductivity is reduced by even a small amount, the cutoff of that submode is shifted such that that mode is extinqished, so the attenuation is greatly reduced. A similar effect occurs at the attenuation minima. When the conductivity changes, the electric field is shifted so as to no longer be zero at the guide-cladding interface. Energy is then coupled into the cladding, and the attenuation is raised. That effect is less pronounced however, due to the fact that the submodes are only shifted, rather than extinquished.

C. Constructing a Modulator

The semiconductor-on-glass structure that has been

examined is very useful for theoretical and conceptual studies, but there are several problems with fabrication. First, the semiconductor must be deposited on an amorphous substrate, so it too must be amorphous. This results in a lowered quantum efficiency due to traps and imperfections, and it makes the deposition of thin GaAs films particularly difficult. Our experiments have shown that the thermal migration of the silver ions (in the ion exchange waveguide that we presently use) precludes the use of the Molecular Beam Epitaxy and other GaAs deposition techniques which would require high substrate temperatures. We have sputtered amorphous silicon, but have not been able to obtain photo-active films due to the high density of dangling bonds on the surface. We are currently experimenting with hydrogen in our sputtering process, in order to alleviate this problem.

Another fabrication approach, which would allow more flexibility in the use of a GaAs semiconductor cladding, is shown in Fig. 22. Here, a GaAs substrate with a thin active layer (etched to a mesa) is used. A buffer layer of low refractive index boron-doped SiO_2 (n = 1.43)[18] is deposited on the surface of the GaAs, in order to optically isolate the waveguide from the lossy substrate. Our calculations have shown that this layer should be about 1.0 microns thick for effective isolation. The surface is then planarized to expose the active layer, and a high index guiding dielectric is deposited. Finally, the GaAs substrate is etched away with a selective etch, and the area is back-filled with low index SiO_2 in order to optically isolate the

21

active semiconductor cladding region. This structure will have similar properties to that already analyzed, and would have the advantages of a crystalline semiconductor cladding. In addition, the substrate could be used to build lasers and active electronic devices on the same chip with the modulator, while the advantages of the lossless dielectric guide are maintained. Isolated dielectric guiding layers have been used successfully on silicon substrates in order to take advantage of these features.[19]

One caution is in order concerning the values used in our calculations. The complex refractive index of a given semiconductor cladding is highly dependent on the deposition method and system used. Thus, in actual construction the optical parameters will have to be measured before exact computer predictions are generated.

IV. A SEMICONDUCTOR-CLAD WAVEGUIDE POLARIZER

The semiconductor-clad dielectric waveguide can be used as a TE-TM polarizer, due to the different coupling conditions of the TE or TM waves in the guide. The polarizer and our results are discussed here and in ref. (20) (in Appendix B).

Waveguide polarizers have been constructed by using selective attenuation in metal claddings,[21,22] cutoff effects in the waveguide due to cladding interaction,[23] or birefringent claddings such as calcite.[24] Unlike metal claddings on dielectric guides which mainly attenuate the TM mode,[21] a silicon cladding allow the selective attenuation of either the TE or TM polarization simply by choice of the thickness of the deposited cladding layer.

22

The planar waveguide structure analyzed is the four-layer cross section shown in the inset of Fig. 23. The air and the dielectric substrate layers are taken as semi-infinite, while the dielectric guiding layer is a constant (1 μm) thickness and the silicon layer thickness, t_2, is variable. The refractive indices used in the computer predictions are also shown in the inset, where the air and dielectric layers are considered to be lossless. The silicon layer, being absorptive at 633 nm, is characterized by a complex refractive index (for amorphous thin films)[25]

$$\eta = 4.1 - j\, 0.21 \tag{25}$$

or a relative permittivity of

$$\varepsilon_r = \varepsilon' - j\varepsilon'' = 16.76 - j\, 1.75. \tag{26}$$

As illustrated in Fig. 23 and discussed in previous references for the TE_0 case, the attenuation constant for the four-layer guide exhibits a damped oscillatory behavior as the silicon layer thickness is increased from 0.005 to 1.0 microns.[26] These oscillations are due to coupling between the zero-order mode propagating in the dielectric waveguide and the various orders of the modes which are supported by the silicon layer. As the silicon thickness is increased, each successive maximum on the attenuation curve represents a point were the silicon layer is supporting a successively higher order mode.

In order to study the modes of the silicon layer itself, the TE_0 and TM_0 mode indices are generated for an equivalent three-layer air-silicon-dielectric guide, where the dielectric substrate now has the $\eta = 1.588$ index value of the dielectric guide in the four-layer structure. The results, shown in Fig.

23

24, indicate that a given mode in the silicon can only exist at thickness values which allow the mode index to be greater than 1.588 for that mode. When the silicon is too thin, the mode index falls below 1.588 for a given mode, which is then said to be in "cut-off". When the mode index is just above 1.588, the mode still propagates, but it is "matched" with the substrate, and there is large exchange of energy across the silicon-dielectric boundary. In the four-layer guide, these "match" points correspond to large amounts of energy being coupled from the dielectric guide into the absorptive silicon. Thus, as shown by comparing the mode index curve of Fig. 24 to the attenuation curve of Fig. 1, the attenuation maxima for the four-layer air-silicon-dielectric case. Similar behavior has been seen by Sasaki, et.al. in II-VI compounds for the TE_0 case. [27]

Of special interest here is the fact that, for the TM case, the three-layer silicon waveguide is below the cut-off thickness and hence does not support any modes below 0.04 microns. It follows that the attenuation of the TM_0 mode in the four-layer guide has an attenuation peak in Fig. 23 at a silicon thickness were the TE_0 or TM_0 modes may be selectively absorbed into the silicon and thus are attenuated in the guide.

This extinction ratio between the TM_0 and TE_0 modes is plotted in Fig. 25 where the theoretical intensity relation between the two modes is plotted by the solid line using data from Fig. 23. The extinction is defined as

$$\text{TE-TM Extinction (dB)} = 10 \log (I_{TE}/I_{TM}) \tag{27}$$

and the ratio of output intensities is

24

$$\frac{I_{TE}}{I_{TM}} = e^{-(\alpha_{TE} - \alpha_{TM})z} \tag{28}$$

where z is the 100 micron width of silicon shown on the top view of the waveguide in the inset. The rectangles along the dotted curve show actual experimental measurements, taken by measuring the prism-coupled input and output of waveguides with a 100 micron wide strip of sputtered amorphous silicon cladding, having the thickness values shown. The predictions and results indicate that high extinctions can be obtained for either mode simply by changing the thickness of the silicon cladding layer.

The suppression in the negative peak of the experimental data is due to the large amount of scattered and stray light in the measurement system, which caused the noise level to be at about -40 dB. The slight shift in the negative peak may be due to the fact that the experimental waveguides are ion-exchange graded-index guides, rather than the slab guides analyzed by the computer program. The refractive index of the sputtered silicon may also be different from that used in the computer prdictions due to varying sputtering conditions.

Views of the scattered light in the guide are shown for both polarizations in Fig. 26. For the TE_0 mode, the beam passing under the 0.04 μm thick (100 μm wide) silicon strip is much less attenuated than the beam which encounters the 0.007 μm thick silicon. When the polarization is changed to the TM_0 mode the 0.04 μm thick silicon layer attenuates the beam much more than the 0.007 μm thick layer.

Our silicon-clad waveguides have yielded a high performance selective TE-TM polarizer, and the measurements of Fig. 25 have provided good experimental verification of the mode coupling

characteristics predicted by the computer runs. The observed results were made possible by the use of the very narrow (100 μm) strip of silicon as a cladding. This narrow width (one-tenth of that previously used) was achieved by the use of a photolithographic pattern defining technique in which the entire waveguide, except for the strip, is masked off so that the excess sputterd silicon is lifted off. This process is outlined in Fig. 27.

The use of the narrow strip has allowed the observation of the polarization effects, and has reduced the need for any dielectric buffer layer that would reduce the attenuation induced by the semiconductor cladding. Thus, the dielectric buffer layers discussed in ref. (28) have not been actively pursued, except as "tuners" for the spectral filters that will be discussed in Section V.

V. SEMICONDUCTOR-CLAD WAVEGUIDES AS SPECTRAL FILTERS (from reference 28)

The attenuation characteristics of semiconductor-clad waveguides are a function of the material permittivities for a particular wavelength. Based on observed changes in period and amplitude of the attenuation curve oscillations as the material parameters vary with wavelength, it is evident that selective frequency filtering, can be realized with a semiconductor-clad waveguide. Although the permittivities of all four materials (air, cladding, guide, and substrate) in the planar waveguide structure vary with wavelength, the semiconductors (due to the effects discussed in Section II), are particularly sensitive to

frequency variations. In particular, for a given semiconductor cladding thickness, the attenuation will vary drastically as the material permittivities and thus the coupling characteristics of the submodes vary with wavelength.

A. Silicon-Clad Waveguide Filters

Attenuation and mode index versus silicon cladding thickness curves similar to those of Figs. 2 and 3 (for GaAs) were generated as the wavelength was allowed to change from 0.35 to 1.55 μm and the permittivities of the four layers consequently varied.[25,29] All attenuation curves retained their characteristic oscillations; howver, the amplitude and period of the oscillations were significantly altered. Similarly, the mode index versus silicon thickness curves retained their characteristic oscillatory behavior although the frequency and amplitude of the oscillations changed.

Figures 28 to 30 were obtained by assuming a given silicon thickness in the four-layer planar structure and allowing the wavelength to vary (and consequently, the material permittivities). The resulting attenuation (dB) for a 1 mm wide silicon bar is plotted vertically in Figs. 28 to 30.

A high-pass frequency filter is realized in Figure 28. Insertion loss is less than 7 dB for a wavelength greater than 1.0 μm for the three silicon thicknesses considered ($t_{Si} = 0.09$, 0.10, 0.11 μm), and the extinction for wavelengths less than 0.7 μm is more than 50 dB. The particular filter characteristics in the wavelength region of 0.7-1.0 μm may be adjusted by changing the thickness of the silicon cladding.

Filters with passband wavelengths of 0.7-0.9 µm are shown in Figure 30. Note that the exact location of the passband may be varied for the three silicon thicknesses of interest (t_{Si} = 0.15, 0.17, 0.19 µm) and that high attenuation (>100 dB) occurs immediately outside of this passband region. Insertion loss, however, is approximately 20 dB for a 1 mm length of Si.

Even relatively short sections of silicon-clad waveguides are lossy, and for a practical device the insertion loss must be reduced significantly. Thin dielectric buffer layers have been used to lower the attenuation losses of metal-clad dielectric waveguide.[5,21] These layers are placed between the dielectric core and the metal and act as buffers to remove a large portion of the field from the metal cladding. The effect of a silicon dioxide (SiO_2) buffer layer on the filter response curve was investigated. The results are shown in Figure 30. A silicon thickness t_{Si} = 0.13 µm was assumed and the attenuation versus wavelength was calculated for a four-layer structure. Note that an insertion loss of approximately 40 dB is apparent in the passband region of 632.8 nm, although rapid extinction is evident (>400 dB) immediately outside of the passband region. A silicon dioxide buffer layer (t_{Si} = 0.2 µm) of refractive index n = 1.46 was then added, and the filter response curve for the five-layer structure was calculated. Insertion loss is now less than 9 dB at a wavelength of 632.8 nm while rapid extinction (>200 dB) is still evident immediately outside of this passband. Further reduction of the passband attenuation may result from optimization of the buffer layer and silicon thicknesses.

Although no attempt has been made to optimize the filter characteristics, Figures 28 and 29 indicate the low frequency cutoff and the attenuation peaks may be adjusted by proper choice of cladding thickness.

In addition to the suggested application as a frequency filter, the structure may also be used as a wavelength demultiplexer. The frequency response of silicon-clad guides with thicknesses t_{Si} = 0.03 μm and t_{Si} = 0.13 μm is shown in Figure 31. Note that the t_{Si} = 0.03 μm curve lies in a region of low attenuation with respect to the t_{Si} = 0.13 μm curve for a guide wavelength of 800 nm. The roles are reversed for a guide wavelength of 1150 nm: t_{Si} = 0.13 μm lies in a region of low attenuation while t_{Si} = 0.03 μm lies in a region of high attenuation. One structure utilizing this effect is a wavelength demultiplexer in which the semiconductor cladding thicknesses are chosen such that one wavelength is attenuated while the other wavelength is selectively passed (Figure 32).

Filter calculations and experimental results for a guide with a silicon cladding, t_{Si} = 0.03 μm, are presented in Figure 33. The computer calculations have been appropriately normalized for a 0.1 mm interaction width. Again, scattered light measurements were taken over the wavelength range 570 nm - 640 nm. Good correlation between the computer predictions and experimental results was obtained over the wavelength range. Two series of measurements were performed on the same guide. For the first series of measurements (RUN 1), the peak in attenuation at a wavelength of 580 nm and the subsequent decrease in attenuation at the higher wavelength region are apparent. In the second

29

series of measurements (RUN 2), the attenuation decreases steadily at the longer wavelengths.

B. Gallium Arsenide Clad Waveguide Filters

The frequency filtering characteristics of GaAs-clad waveguides were also examined. Attenuation vs gallium arsenide cladding thickness curves were generated as the wavelength was allowed to vary from .3 μm to 1.0 μm and the permittivities of the four layers consequently varied.[30] All attenuation curves retained their characteristic oscillations; again, the amplitude and period of the oscillations were significantly altered.

Figures 34 and 35 were obtained by assuming a given GaAs thickness in the four-layer planar structure and allowing the wavelength to vary (and consequently, the material permittivities). The resulting attenuation (dB) for a 1 mm wide GaAs bar is plotted vertically in Figures 34 and 35.

The clad guides, themselves, may be used as coarse frequency filters; a more probable application, however, is as a wavelength demultiplexer, as shown in Fig. 32 for a silicon-clad structure. The device utilizes the order of magnitude difference in attenuation for different semiconductor thicknesses in the region of 0.8 - 1.0 μm. In Figure 34, note that the $t_{GaAs} = 0.11$ μm curve lies in a region of high attenuation with respect to the $t_{GaAs} = 0.16$ μm curve for a guide wavelength of 800 nm. The roles are reversed for a guide wavelength of 1000 nm: $t_{GaAs} = 0.16$ μm lies in a region of high attenuation while $t_{GaAs} = 0.11$ μm lies in a region of low attenuation. Similar behavior is observed in Figure 35 for $t_{GaAs} = 0.13$ μm ad 0.17 μm. In this

case, however, demultiplexing could be effectively accomplished between the wavelengths 900 nm and 1000 nm, rather than 800 nm and 1000 nm. Also, the insertion loss of the structure may be decreased considerably by reducing the interaction width from 1 mm, and by using a low refractive index buffer layer.

C. Summary

In this section, we have shown how silicon and gallium arsenide waveguides can be used as spectral filters and demultiplexers. The changes in permittivity and coupling with wavelength result in high attenuations at various wavelengths for various cladding thicknesses. Some of these results were presented at the 1983 Conference on Lasers and Electro-Optics and the submitted paper summary appears in Appendix B.[31]

VI. PERIODIC COUPLING IN PLANAR WAVEGUIDE THIN-FILM PHOTODEC-TECTORS

As discussed in the previous sections of this report, semiconductor cladding layers on planar dielectric waveguides exhibit periodic coupling characteristics which have been studied for use in filters, modulators, and polarizers. This coupling occurs between the lossless modes of the dielectric waveguide, and the lossy modes supported by the absorptive semiconductor cladding. Large amounts of absorption have been observed both experimentally and theoretically for certain thickness values of amorphous silicon claddings, making them likely candidates for photodetector structures. Here, the coupling characteristics of an easily fabricated metal-silicon-metal cladding are analyzed in

31

order to determine its suitability for use as a waveguide photodetector.

Johnson, et.al. have developed an amorphous silicon thin-film photodetector that employs a microstripline structure as in Fig. 36.[32] Here, the semi-transparent top electrode made of gold-on-overlaps an aluminum bottom electrode, sandwiching a layer of hydrogenated amorphous silicon. The chromium forms a Schottky barrier with the silicon, and the light is absorbed by the silicon as it passes through the top electrode in the area of overlap. Due to the short carrier lifetimes and low capacitance in this thin-film geometry, the researchers have obtained 40 picosecond response times and internal quantum efficiencies of 36 percent.

For waveguide use this structure is inverted and modified as shown in Fig. 37 so that the light couples into the silicon through the gold-chromium electrode. Our computer program is used to analyze the propagation characteristics of this seven-layer waveguide-cladding structure. The metal electrodes are held constant at the thicknesses shown in Fig. 37 while the silicon layer thickness, t_3 is varied over an appropriate range of values. The changes in silicon layer thickness result in the attenuation characteristics of Fig. 36 for a wavelength of $\lambda = 632.8$ nm. As discussed in the previous sections, the damped oscillatory behavior of the attenuation is characteristic of thin absorbing layers on a dielectric guide, and indicates a periodic coupling effect between the lossless dielectric guide and the lossy metal-silicon-metal cladding. Thus, at silicon thickness

values where the most coupling occurs, there is a maximum amount of energy coupled into the cladding and absorbed, resulting in a maximum in attenuation.

These points of maximum coupling are more clearly illustrated by the mode index characteristics of a six-layer metal-silicon-metal waveguide on a dielectric substrate (with refractive index $\eta = 1.588$) as in Fig. 39. These TE´and TM´ modes correspond to sub-modes in the cladding of the seven-layer waveguide. Thus, at silicon thickness values where the index of a sub-mode is most nearly matched to the guide value (when that sub-mode is at cut-off), a maximum amount of energy is transferred from the TE_0 or TM_0 mode of the wave guide into the TE and TM sub-mode of the cladding. The absorption of this energy results in an attenuation maximum in Fig. 38 for the seven-layer guide.

This coupling and its effect on attenuation and absorption is illustrated in detail for the transverse magnetic polarization where the silicon layer is .13 µm thick. As shown in Fig. 3, the transverse magnetic field has a large value at the cladding-guide interface and is falling exponetially in the dielectric guide, indicating a large amount of energy being transferred from the guide into the silicon and metal layers. This thickness value also corresponds to a mode-match or cut-off condition for the TM sub-mode as shown in Fig. 39 at point A. Because of the absorption in the silicon, the attenuation characteristic of the seven-layer guide at this silicon thickness of 0.13 µm is a maximum, as shown by point A on Fig. 38. It follows that these silicon thickness values corresponding to maximum attenuation

33

points in Fig. 38 potentially provide the highest efficiency for a waveguide photodetector.

The field plot of Fig. 40 reveals several implications for photodetector response and efficiency. When the maximum field (and thus the maximum energy) is near the silicon-chromium Schottky barrier, a higher efficiency will tend to result due to the fact that the excited carriers have a small chance of recombining before reaching the junction. The TM polarization, however, induces a surface plasma layer in the thin aluminum top electrode as characterized by the sharp positive-to-negative transition in that region in Fig. 39. Because this plasma layer is outside the silicon region it will tend to excite few carriers and will reduce detector efficiency. These and other effects are described more completely by an analysis of the Poynting vectors in the structure.

In conclusion, this analysis has shown how periodic coupling between layers influences the response and efficiency of an easily fabricated fast-response photodectector adapted for waveguide use. Additional methods which might be used to increase the detector efficiency and reduce step scattering losses include grating and/or taper coupling. between layers influences the response and efficiency of an easily fabricated fast response photodetector adapted for waveguide use. Additional methods which might be used to increase the detector efficiency and reduce step scattering losses include grating and/or taper coupling.

VII. CONCLUSION

Over the period of this contract we have shown that
clad dielectric waveguide structures can be used for both passive
and active integrated optical devices. Passive devices studied
and fabricated included a guided wave polarization filter and a
spectral filter. Both of these devices need to be optimized to
achieve the performance needed for integrated circuit
applications. This will require additional theoretical studies
and fabrication of a number of devices for experimental
verification.

The active devices considered in this study were a modulator
and a waveguide clad photodetector. The theory for the modulator
has been developed but experimental devices await the development
of the capability to produce photosensitive amorphous silicon
films or superlattice GaAs structures in our laboratories. Work
was well under way to fabricate amorphous silicon films when this
contract was terminated. Future work should explore the
development of GaAs superlattice structure for use with
dielectric waveguides. Superlattice materials offer a number of
exciting structures on dielectric waveguides including bistable
elements for optical memory.

FIGURES

N_1 AIR $(\hat{\epsilon}_R = 1.0 + j0)$

N_2 SEMICONDUCTOR $(\hat{\epsilon}_R = \epsilon_R^{\mathfrak{l}} + j\epsilon_R^{\mathfrak{n}})$

N_3 DIELECTRIC $(\hat{\epsilon}_R = 2.522 + j0)$

N_4 SUBSTRATE $(\hat{\epsilon}_R = 2.2577 + j0)$

(For GaAs: $\epsilon^{\mathfrak{l}} = 14.3$, $\epsilon^{\mathfrak{n}} = 1.21$)
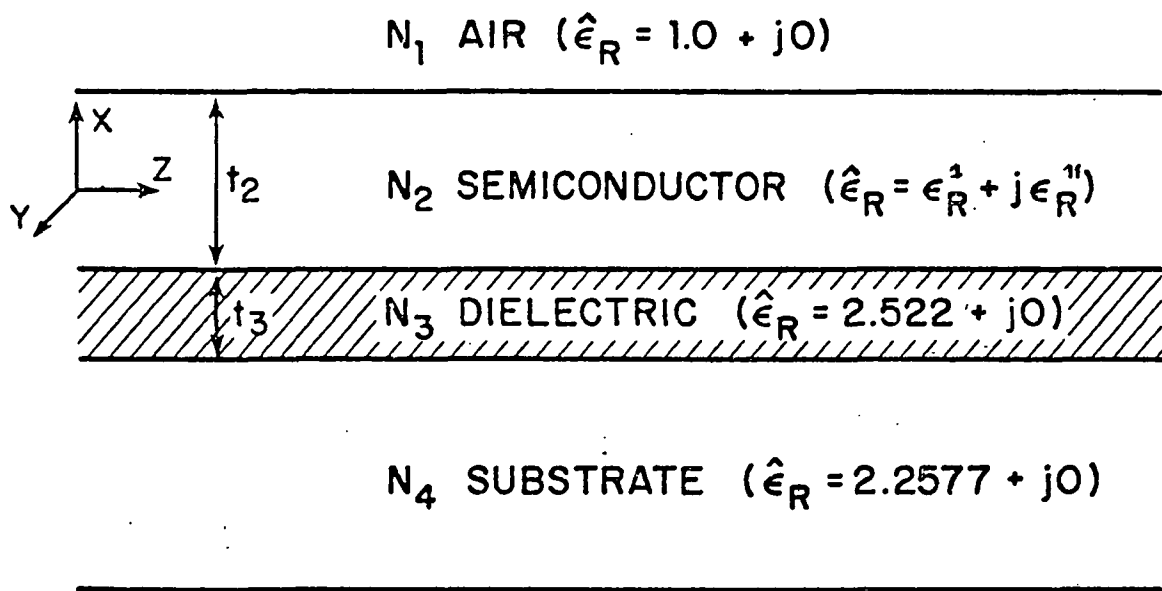
FIGURE #1. FOUR LAYER PLANER WAVEGUIDE STRUCTURE.
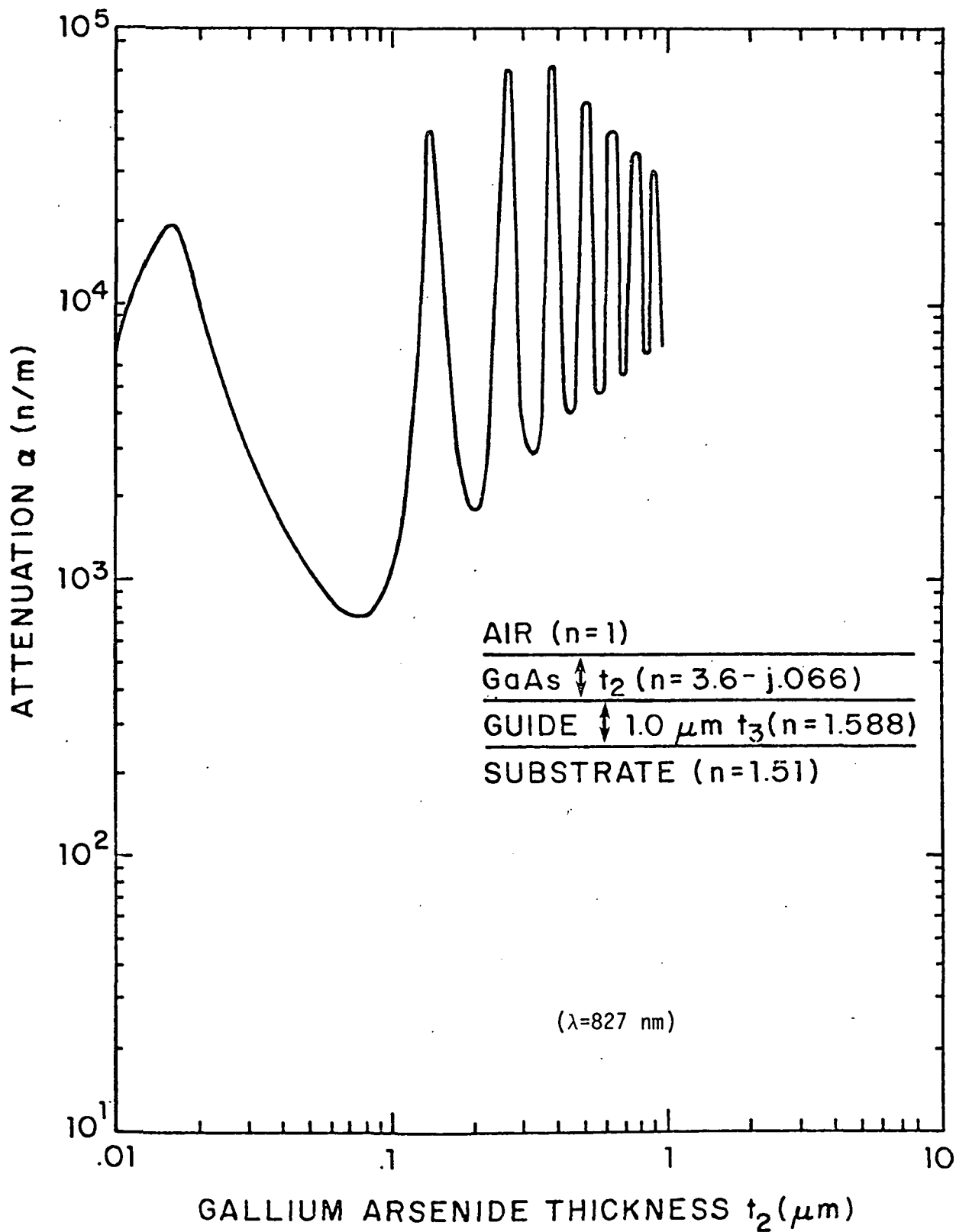
FIGURE #2. ATTENUATION CHARACTERISTIC OF FOUR LAYER STRUCTURE.
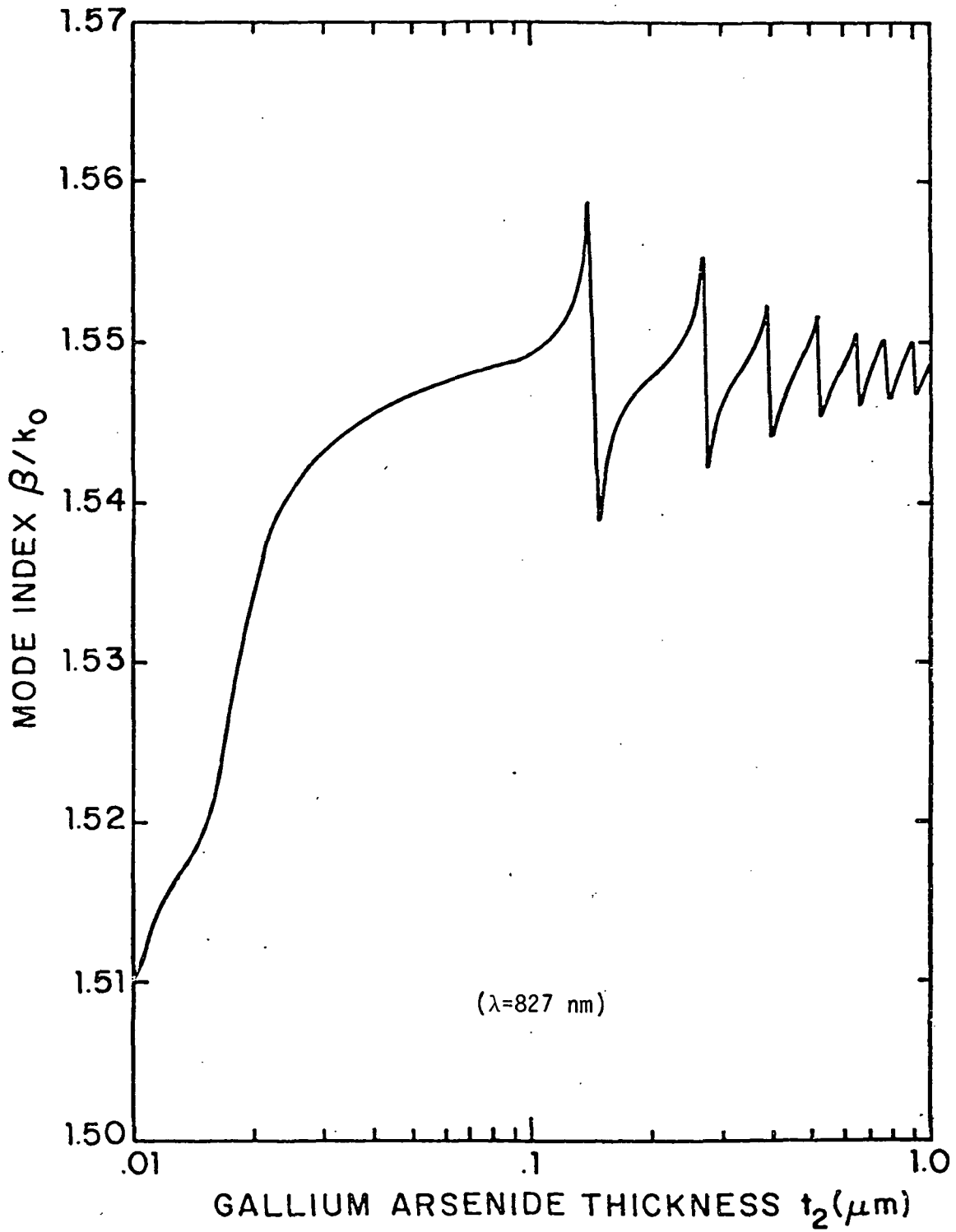
FIGURE #3. MODE INDEX CHARACTERISTIC OF FOUR LAYER STRUCTURE.
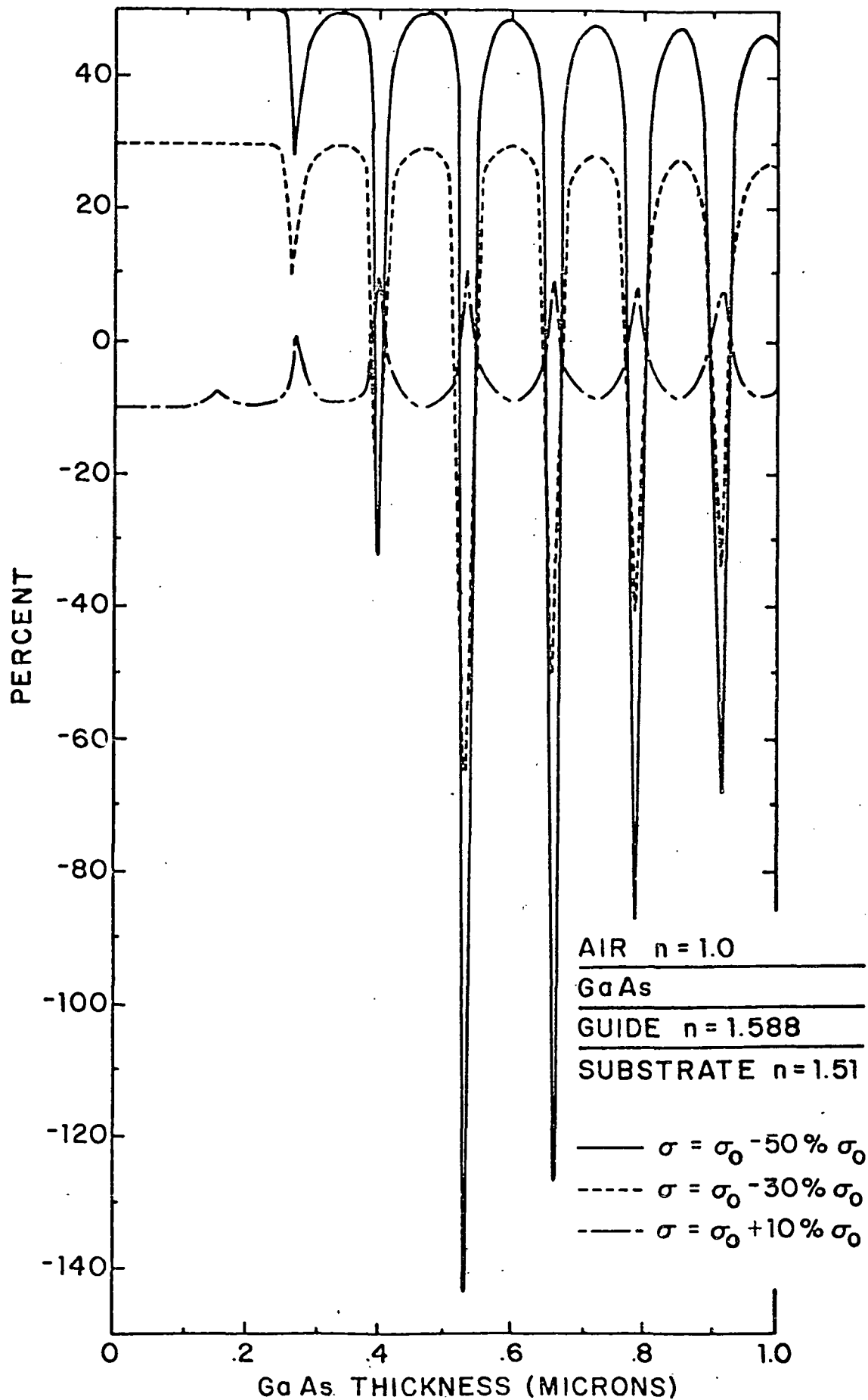
FIGURE #4. CHANGE IN ATTENUATION WITH RELATIVE CHANGE IN CONDUCTIVITY (σ_0).
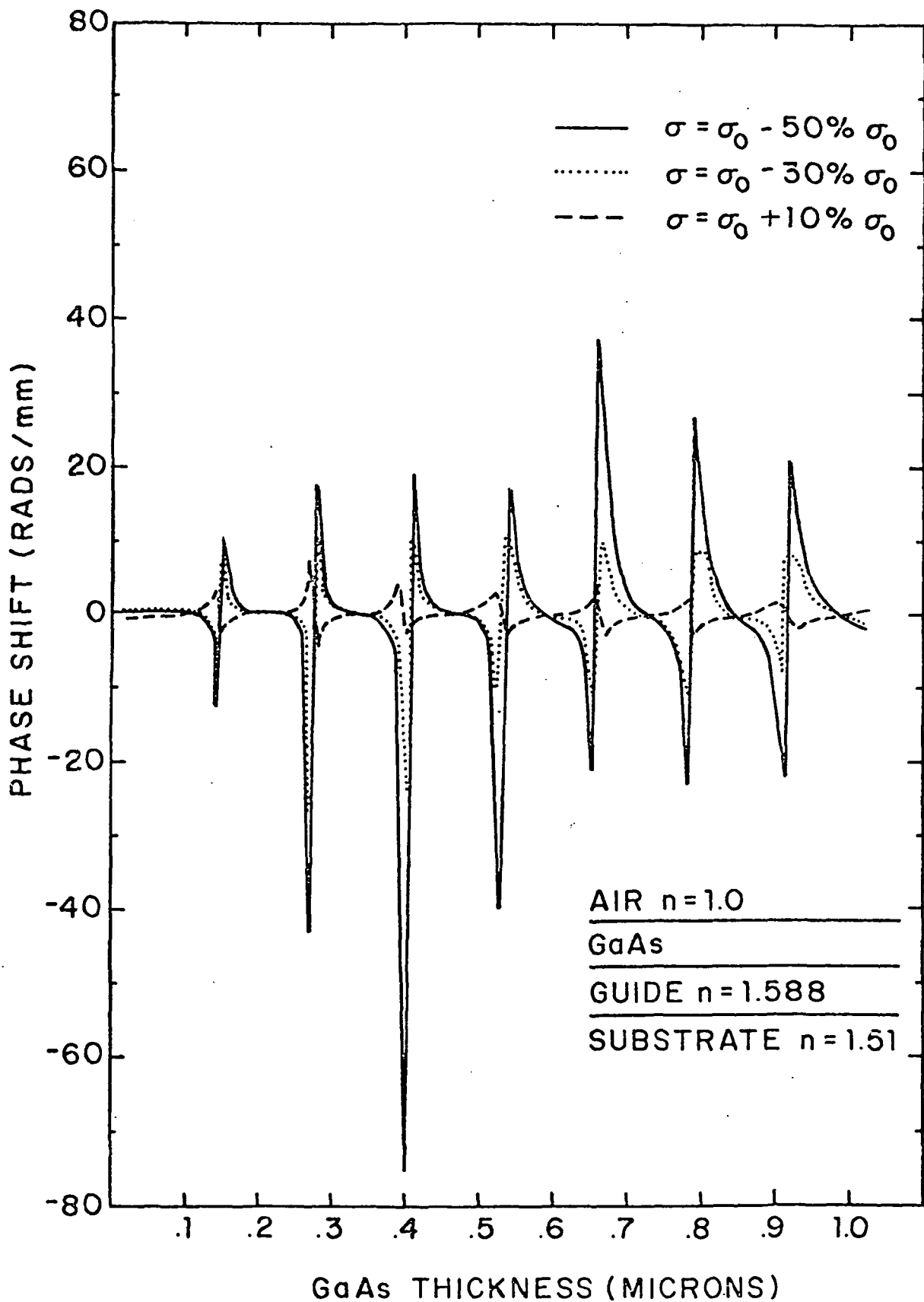
FIGURE #5.   CHANGE IN MODE INDEX WITH RELATIVE CHANGE IN
            CONDUCTIVITY (σ_0).
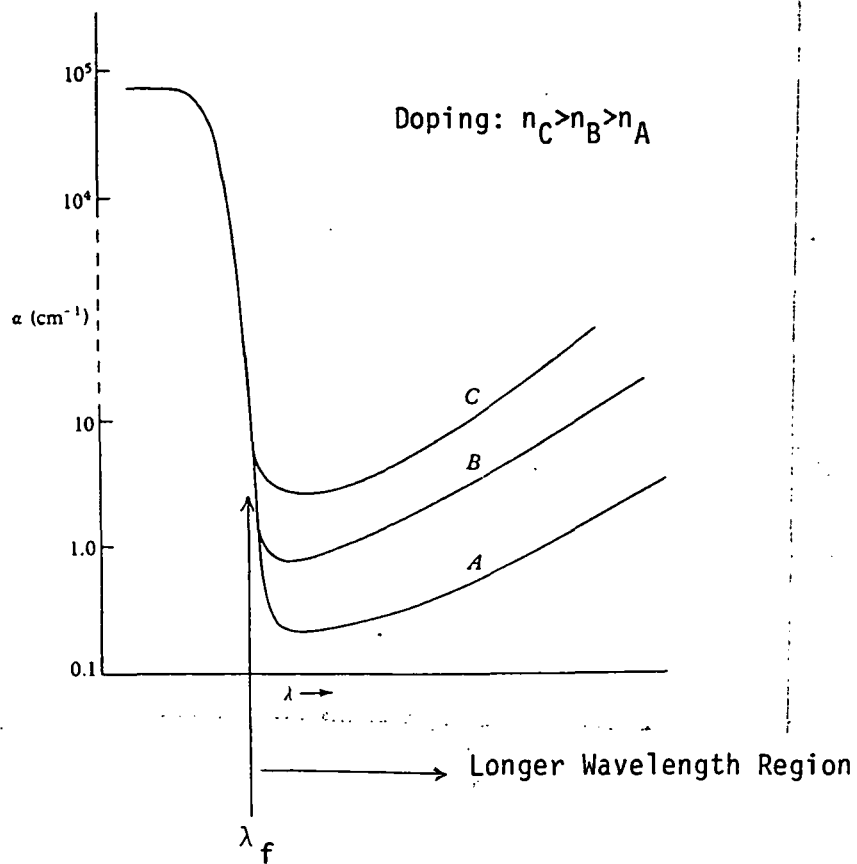
FIGURE #6. VARIATION OF ABSORPTION NEAR THE FUNDAMENTAL
ABSORPTION EDGE (λ_f).

Absorption: $A = e^{-\alpha x}$
Reflection: $R = 1 - A$

1.0 ⎯⎯⎯⎯⎯⎯⎯⎯⎯⎯⎯⎯⎯⎯

A

R

0 ⎯⎯⎯⎯⎯⎯⎯⎯⎯⎯⎯⎯⎯⎯⎯⎯⎯⎯⎯⎯⎯⎯⎯⎯⎯⎯⎯⎯⎯⎯⎯

Higher $\leftarrow \omega_p \rightarrow$ Lower $\omega = 2\pi c / \lambda$
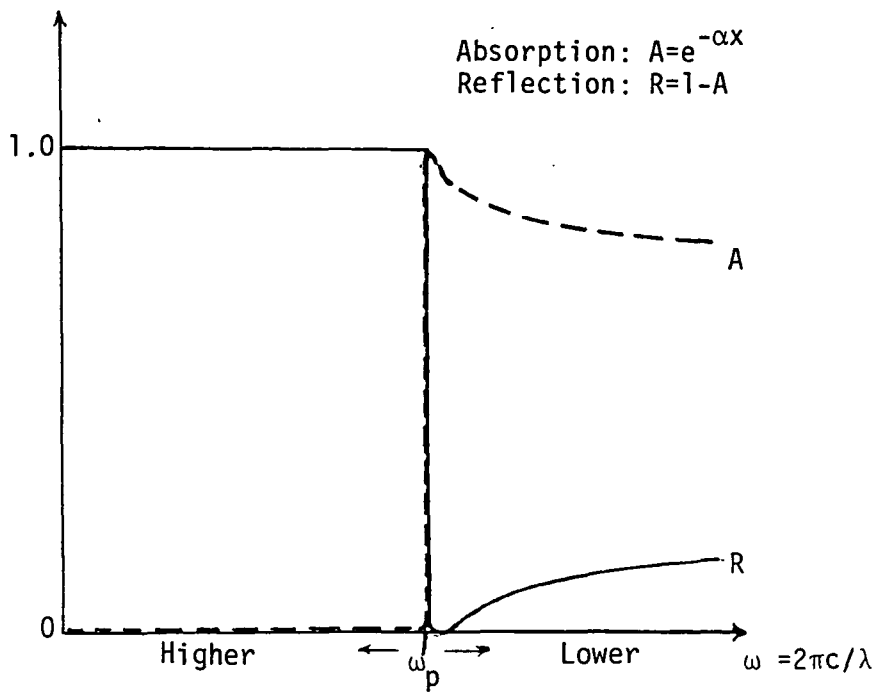
FIGURE #7. ABSORPTION AND REFLECTION NEAR THE PLASMA FREQUENCY (ω_p).

Laser In

Plasma Area

Input
mm wave

d

output
mm wave

d=plasma layer depth
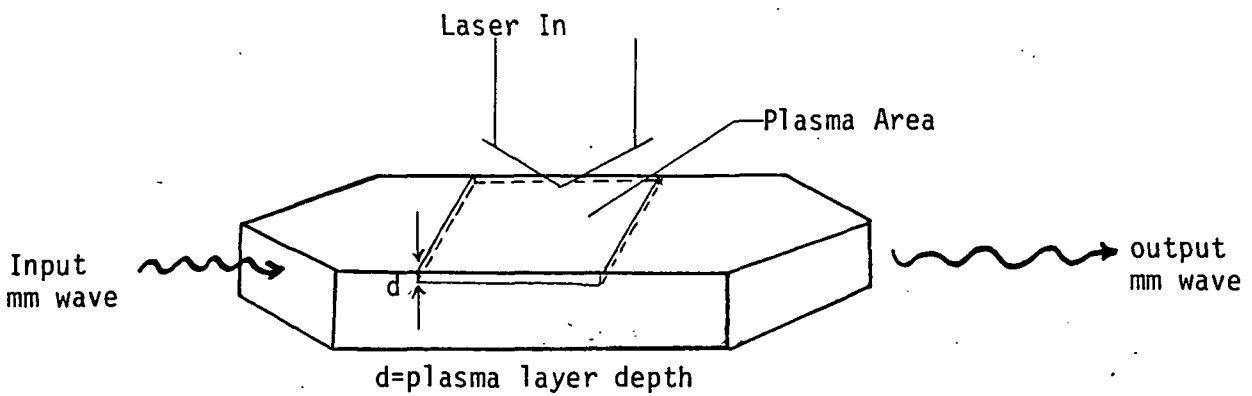
FIGURE #8. MILLIMETER WAVE MODULATOR.

42
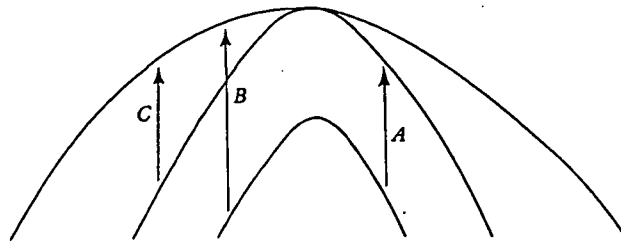
FIGURE #9. INTRA-BAND TRANSITIONS IN THE VALENCE BAND.

(a) Direct

$(E_g = E_c - E_v)$

(b) Indirect
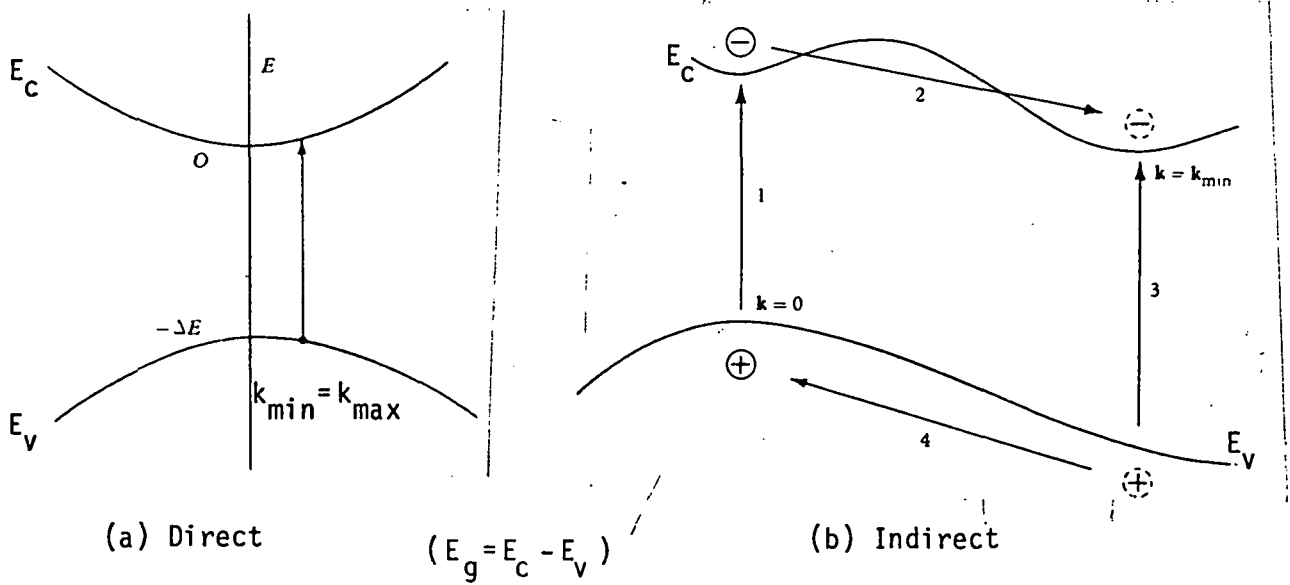
FIGURE #10. INTERBAND TRANSITIONS.

Sample No.	Doping (cm^{-3})
2.	1.3×10^{17}
3.	4.9×10^{17}
4.	1.09×10^{18}
5.	1.12×10^{18}
6.	5.40×10^{18}
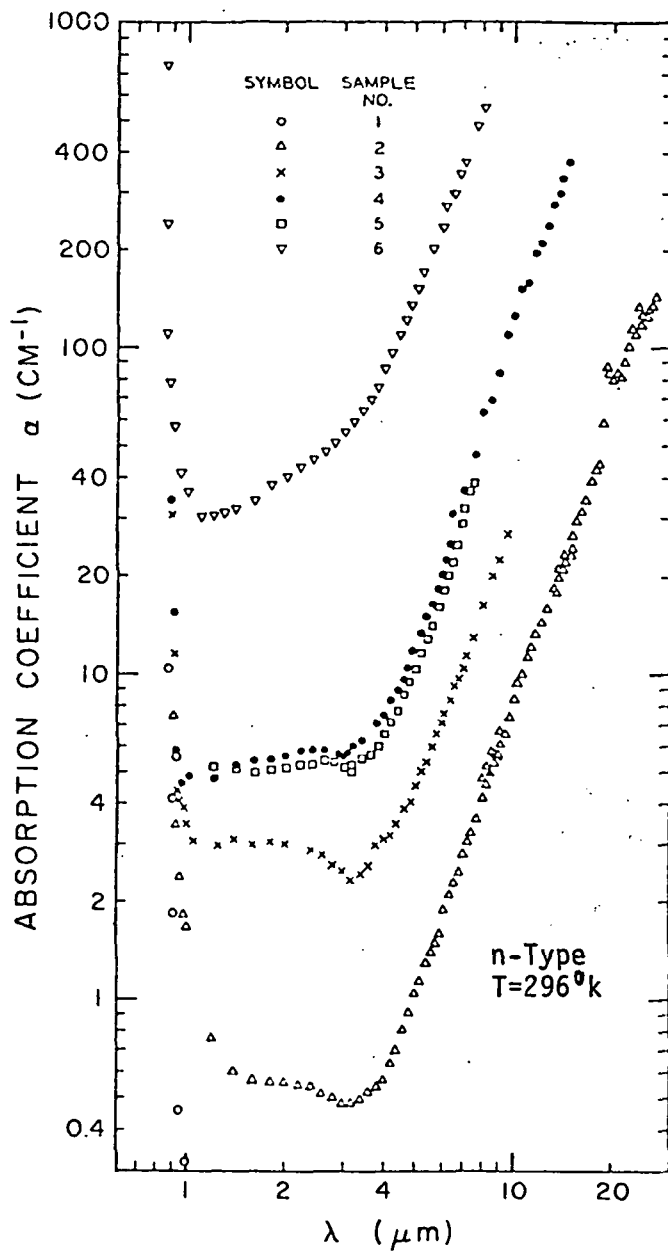
(a) Variations With Doping
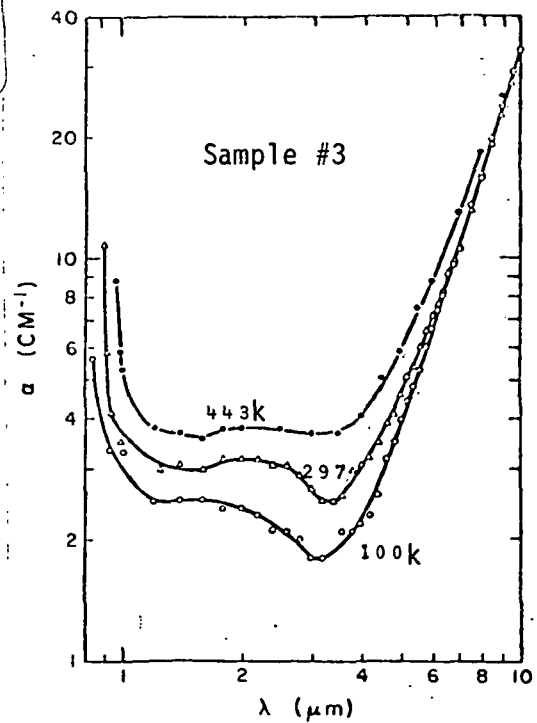
(b) Temperature Variations

FIGURE #11. ABSORPTION OF GaAs NEAR THE FUNDAMENTAL EDGE.
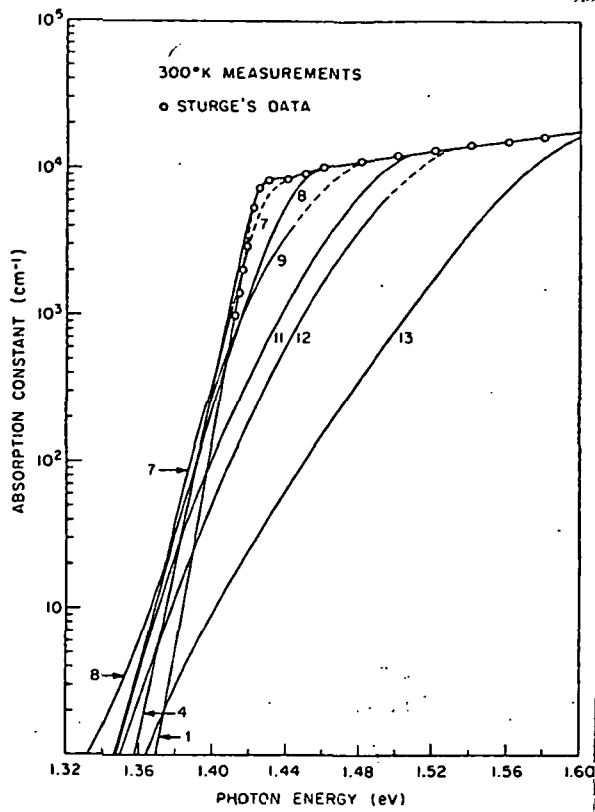
Crystal number	Crystal type	Carrier concentration (cm⁻³)	Mobility (cm²/V·sec)
1	HB[a]	2×10^{16}	3090
2	HB	5.6×10^{16}	2710
3	HB	1.1×10^{17}	3160
4	HB	2.2×10^{17}	3060
5	HB	5.3×10^{17}	3550
6	HB	6.5×10^{17}	2900
7	HB	7.2×10^{17}	2560
8	HB	1.2×10^{18}	2700
9	CZ[b]	1.62×10^{18}	2940
10	CZ	2.3×10^{18}	2662
11	CZ	3.15×10^{18}	2200
12	CZ	4.9×10^{18}	2360
13	CZ	6.5×10^{18}	1485

[a] HB Horizontal Bridgman.
[b] CZ Czochralski.

FIGURE #12. ABSORPTION OF N-TYPE GaAs NEAR THE FUNDAMENTAL EDGE.
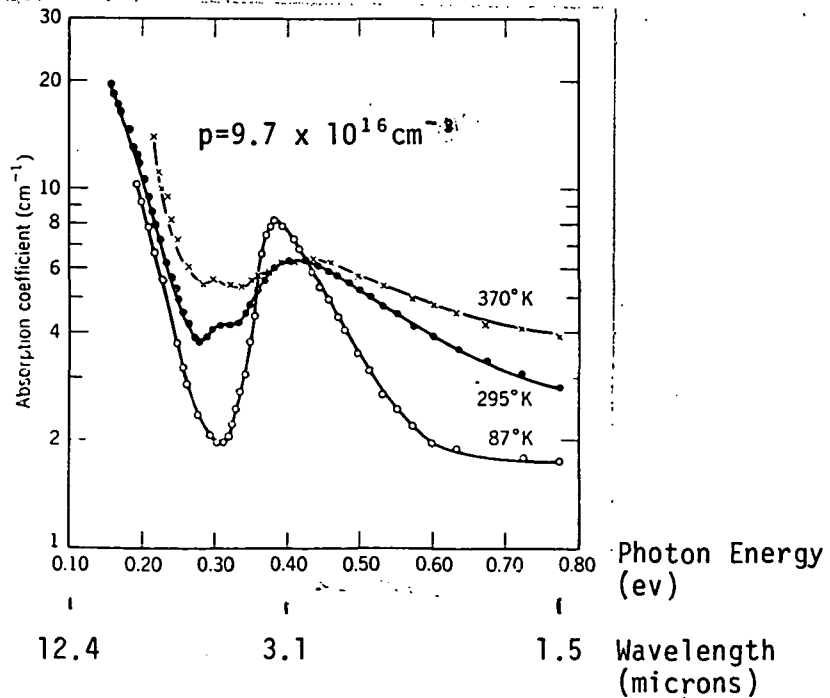
FIGURE #13. ABSORPTION OF P-TYPE GaAs IN THE INFRARED.

45
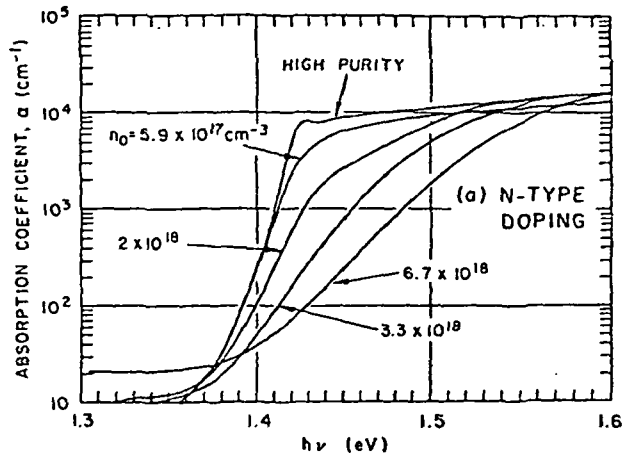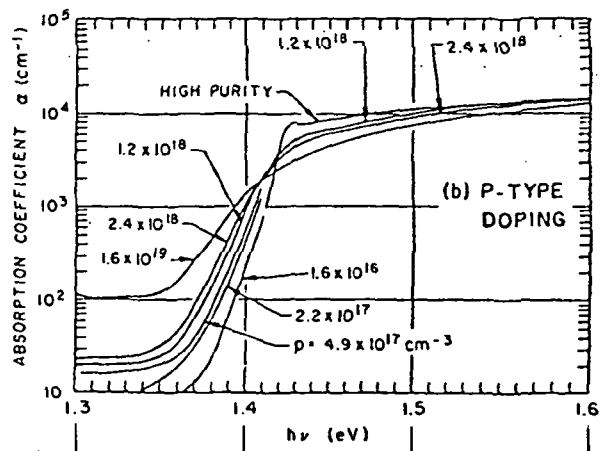
FIGURE #14. SHIFTS IN THE ABSORPTION EDGE WITH
VARIOUS DOPINGS.

46
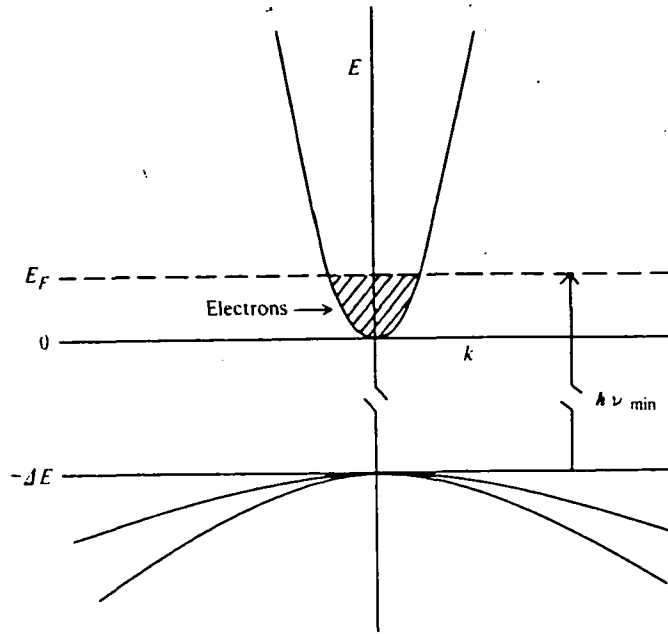
FIGURE #15. THE BURNSTIEN-MOSS EFFECT FOR HIGH
             DOPING.
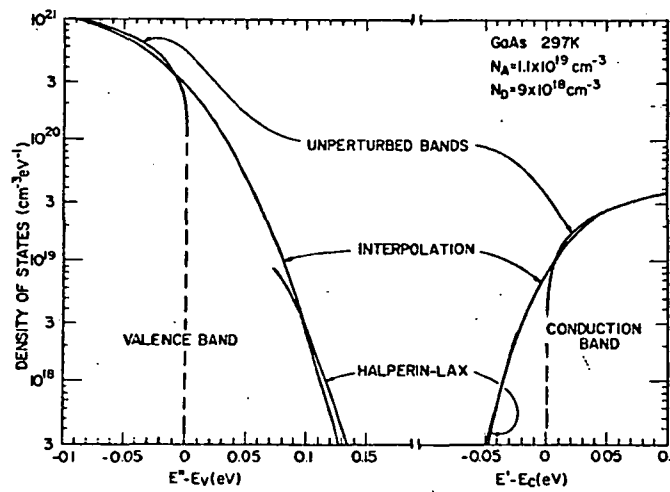
FIGURE #16. DENSITY OF STATES IN THE BAND TAILS.
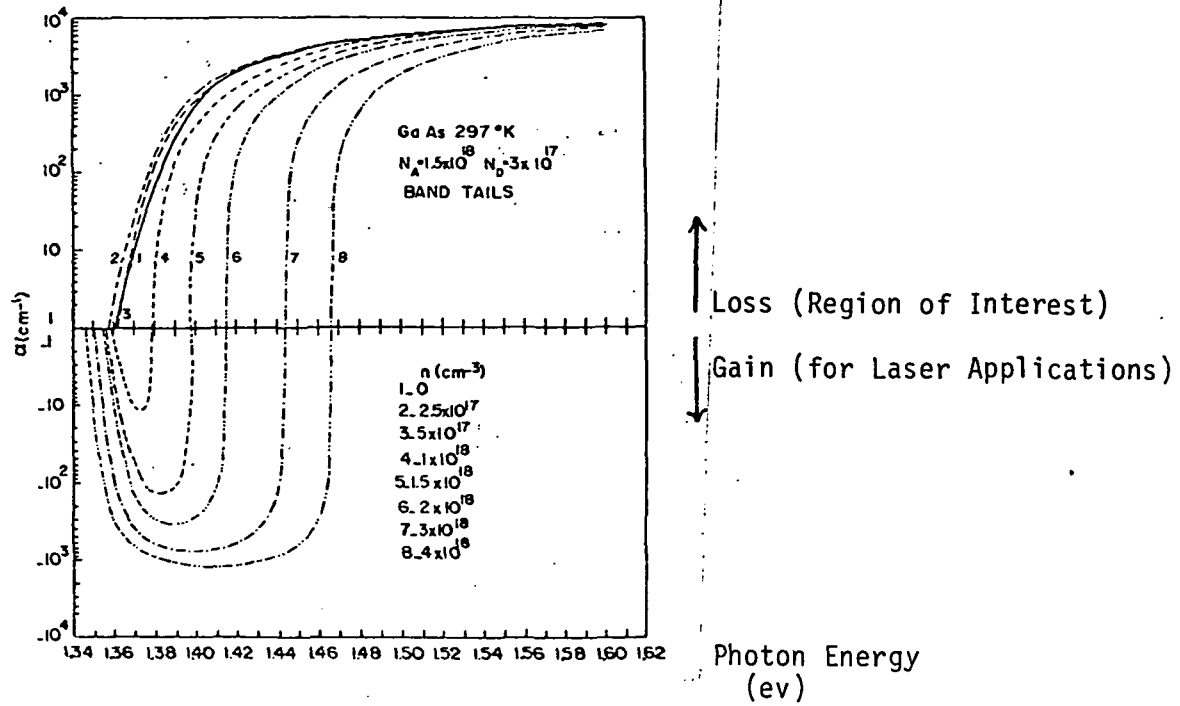
FIGURE #17. ABSORPTION COEFFICIENT VS. PHOTON ENERGY
FOR VARIOUS INJECTED CARRIER LEVELS.
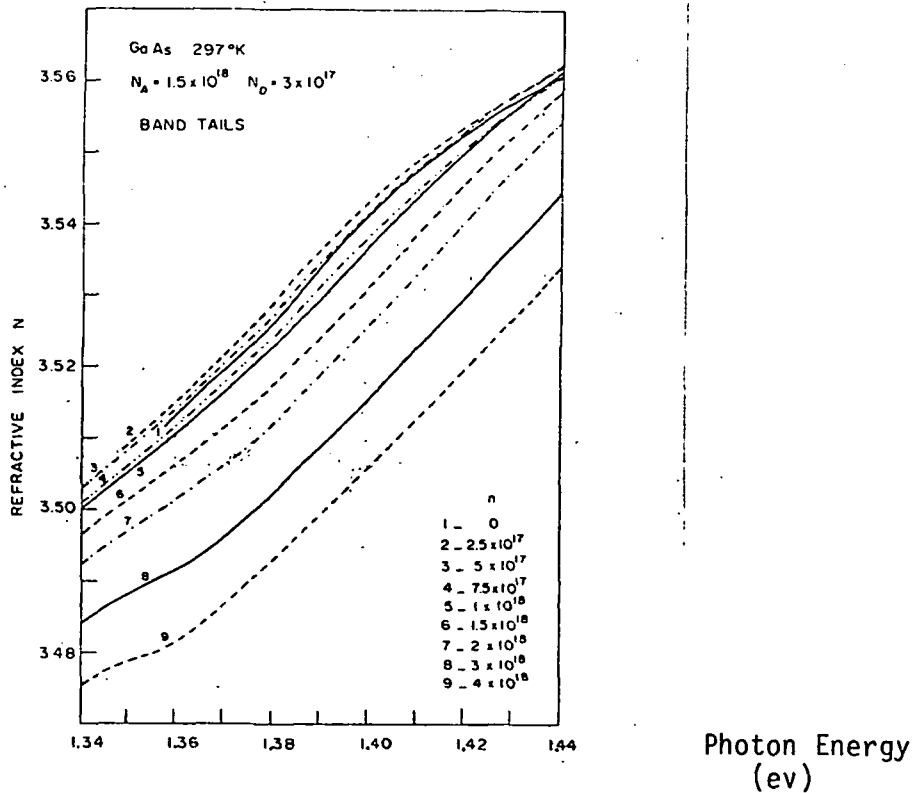
FIGURE #18. REFRACTIVE INDEX VARIATION FROM A
KRAMERS-KRONIG ANALYSIS OF THE DATA
FROM FIG. #17.
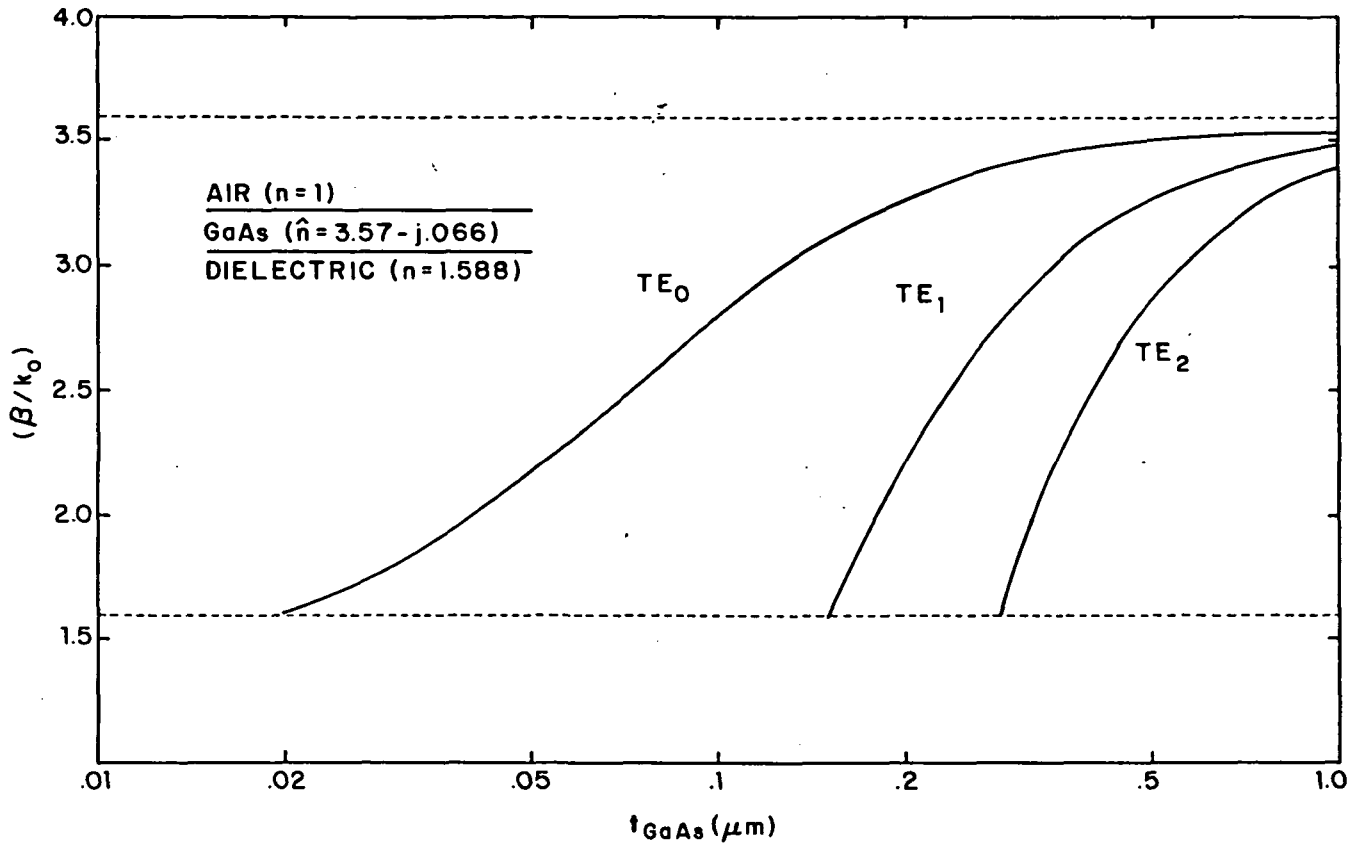
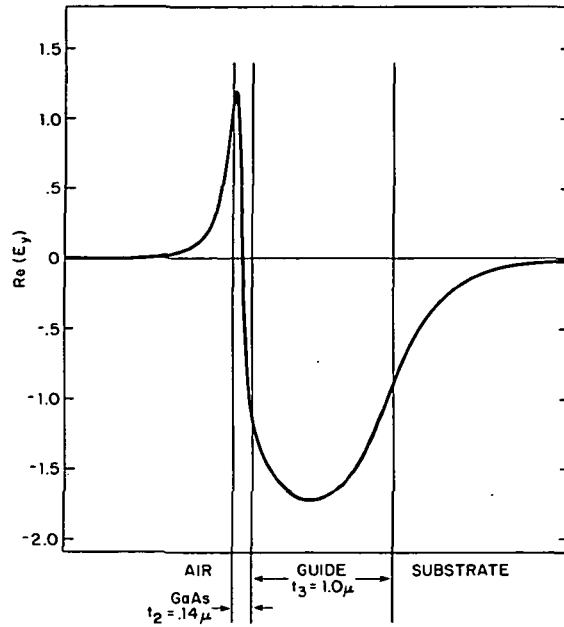FIGURE #19. MODE INDEX CHARACTERISTICS OF A 3-LAYER
GaAs WAVEGUIDE.

FIGURE #20. FIELD PROFILE FOR A GaAs THICKNESS OF
0.14 MICRONS (LOCAL MAXIMUM).
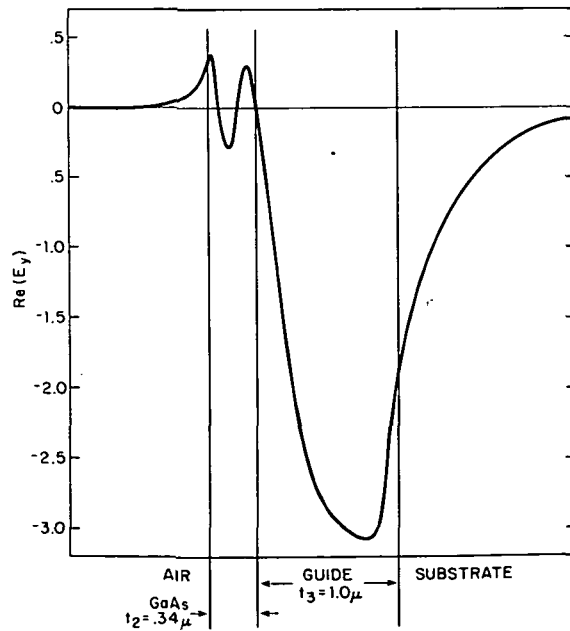
FIGURE #21. FIELD PROFILE FOR A GaAs THICKNESS OF
0.34 MICRONS (LOCAL MINIMUM).
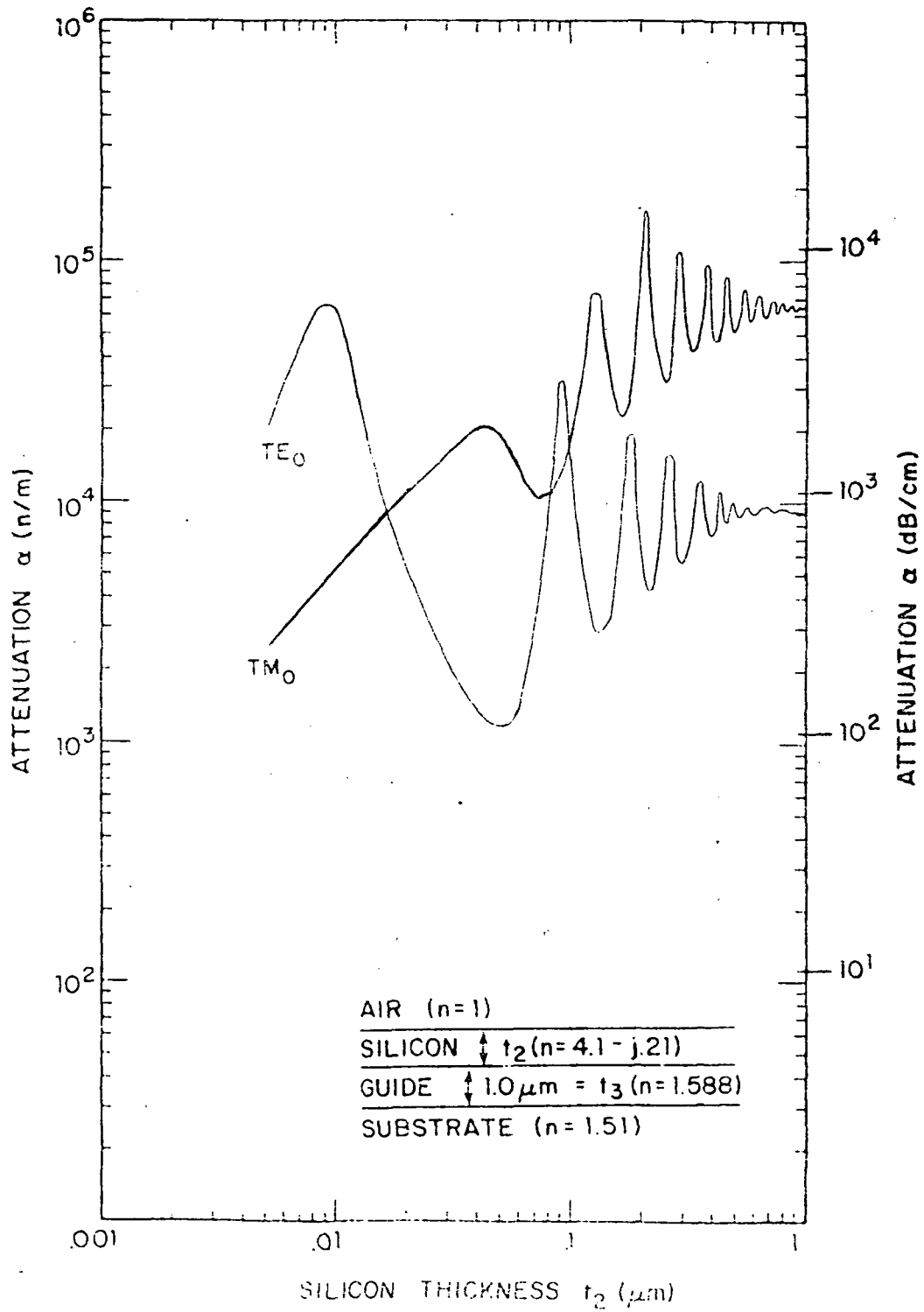
FIGURE #23. ATTENUATION CHARACTERISTICS OF A FOUR-
LAYER SILICON-CLAD WAVEGUIDE.
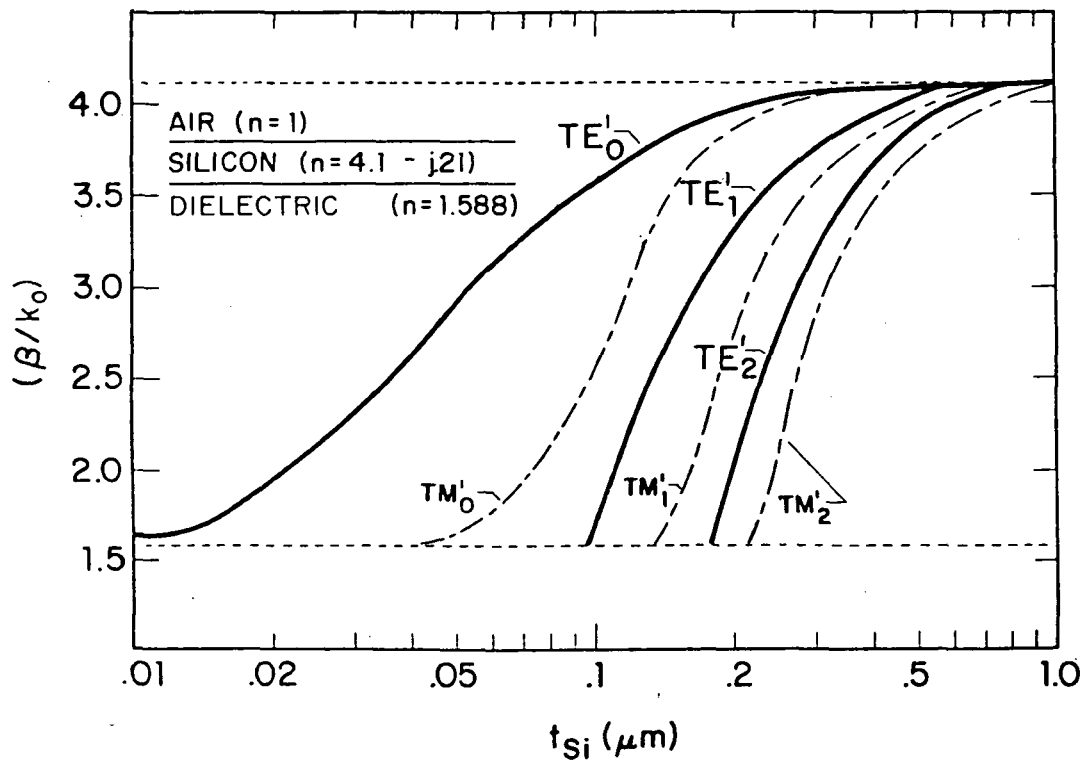
FIGURE #24. MODE INDICES OF A THREE-LAYER SILICON GUIDE.
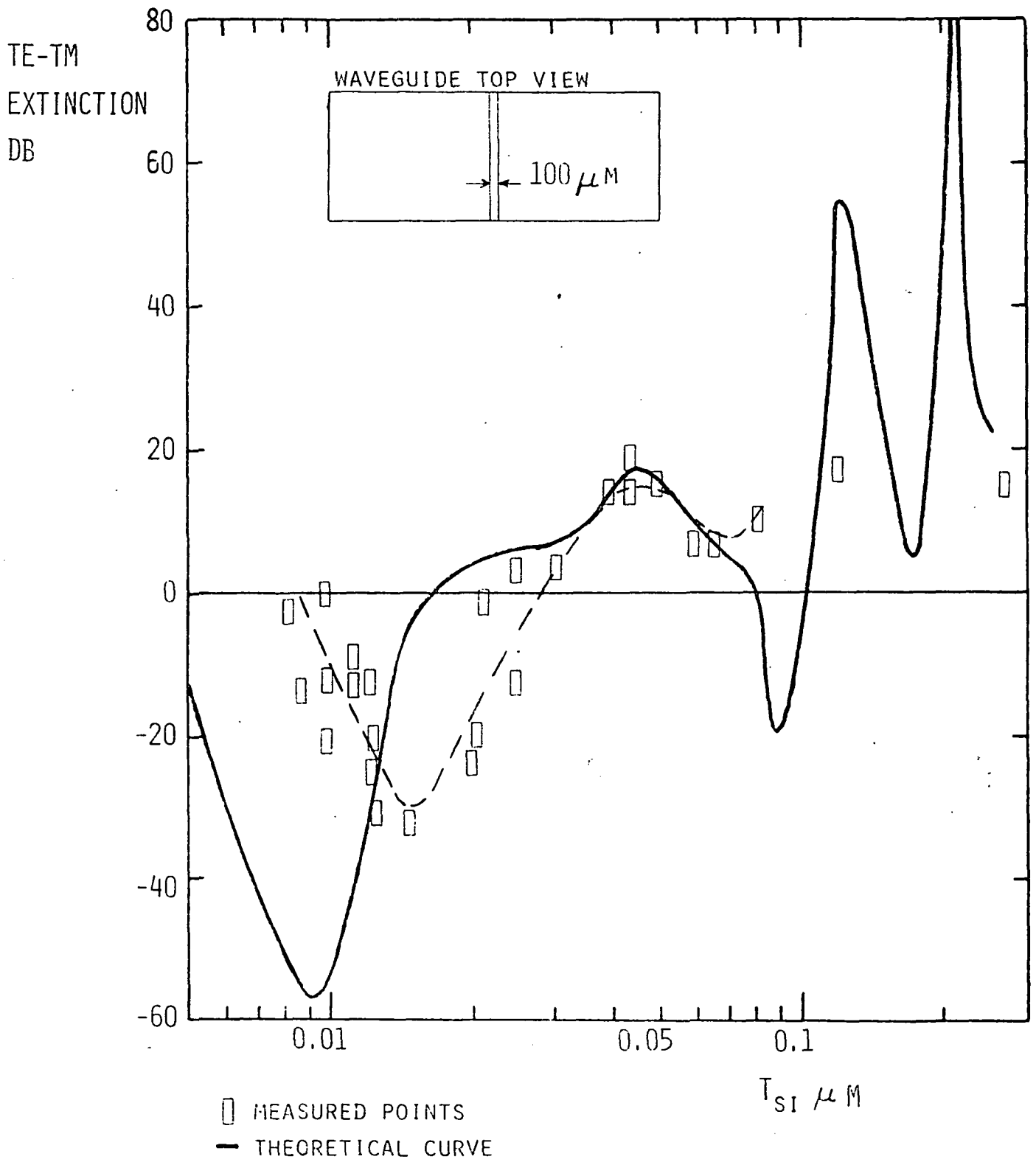
FIGURE #25. TE-TM MODE EXTINCTION FOR A 100 MICRON WIDTH OF
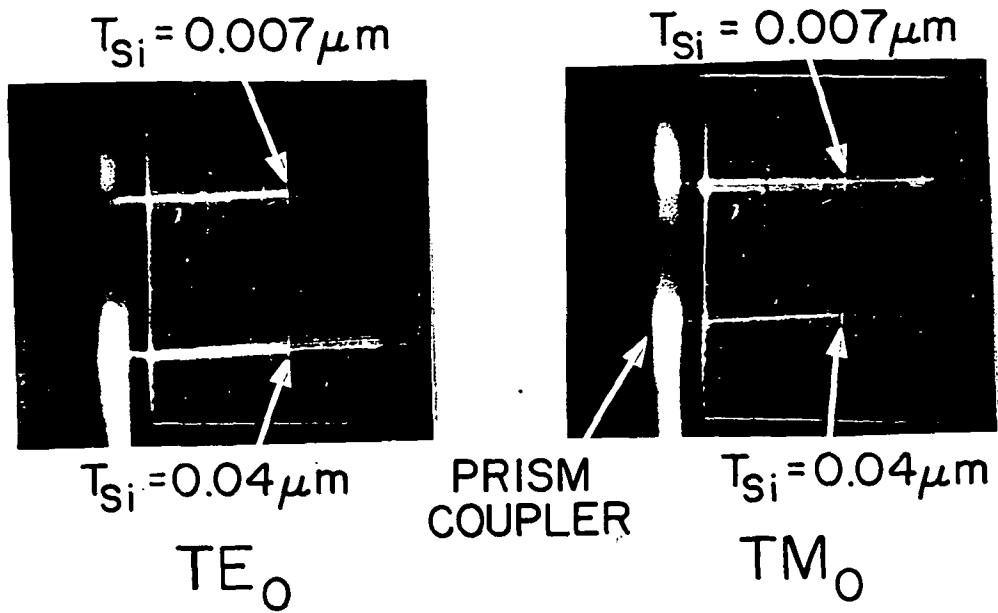SILICON CLADDING (SHOWN IN THE INSET) OF VARYING
THICKNESS.

$T_{Si} = 0.007 \mu m$

$T_{Si} = 0.007 \mu m$

$T_{Si} = 0.04 \mu m$

TE_O

PRISM
COUPLER

$T_{Si} = 0.04 \mu m$

TM_O

FIGURE #26. SCATTERED LIGHT VIEWS OF THE WAVEGUIDE FOR THE
TE AND TM MODES AT TWO SILICON THICKNESS VALUES.
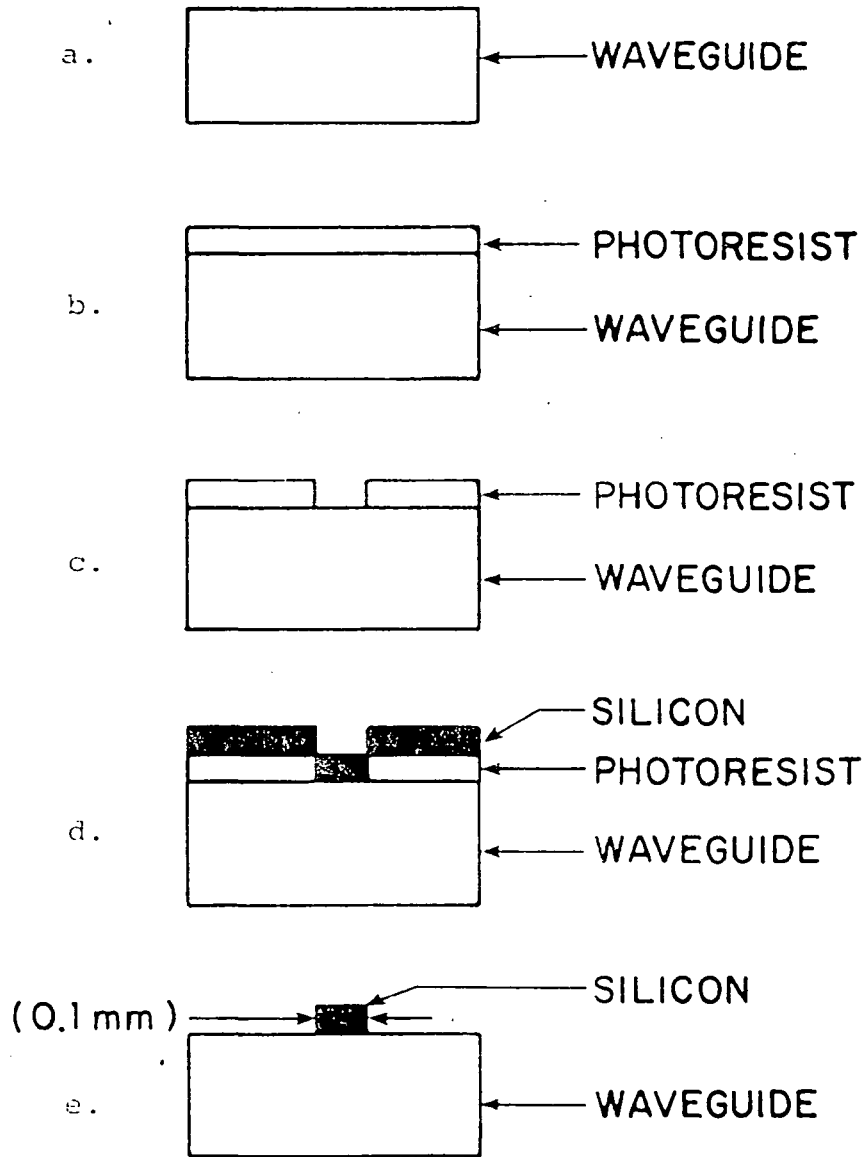
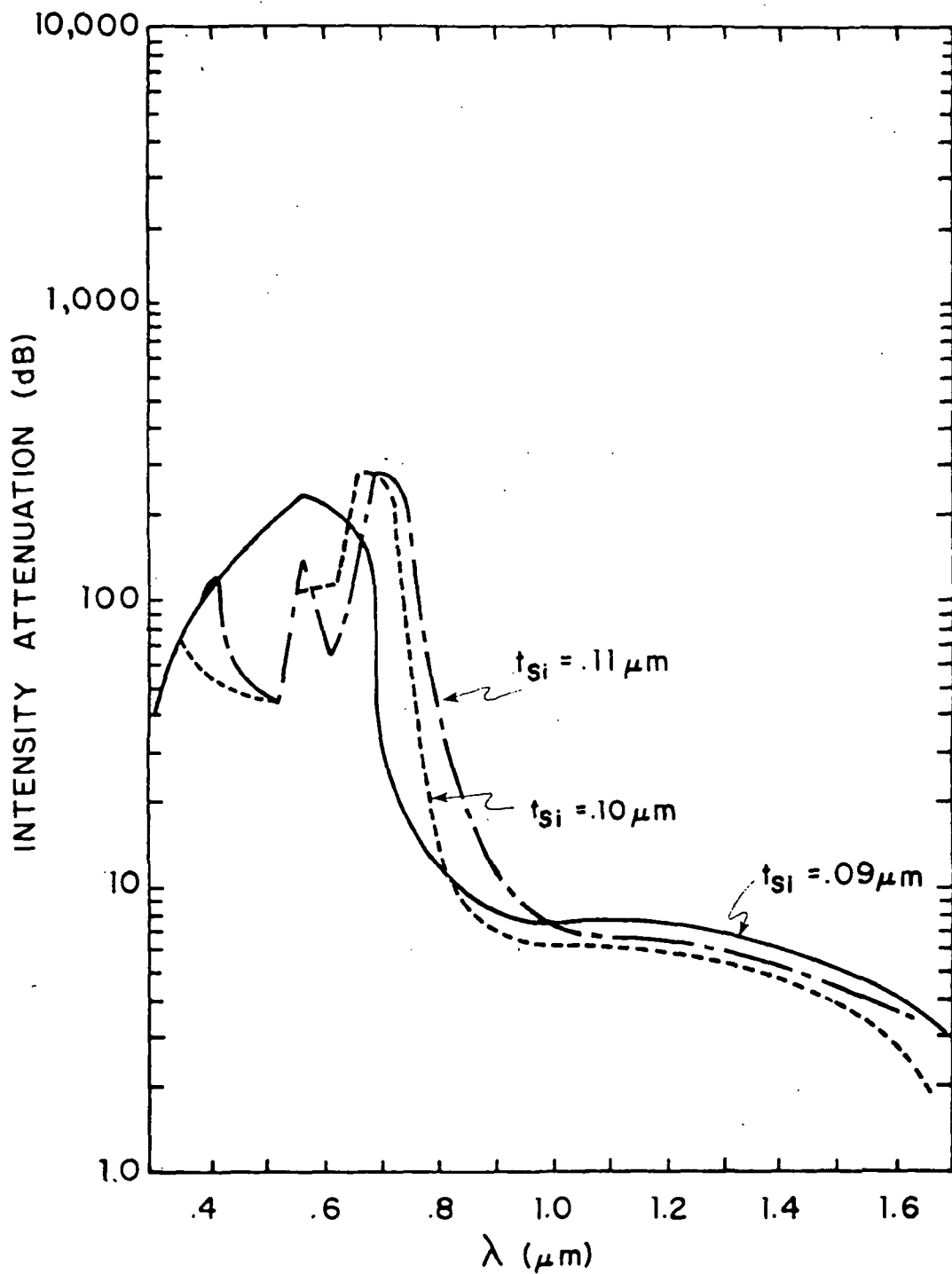FIGURE #27. PHOTOLITHOGRAPHIC PROCEDURE FOR GUIDE FABRICATION.

Figure 28.   Frequency response of silicon-clad
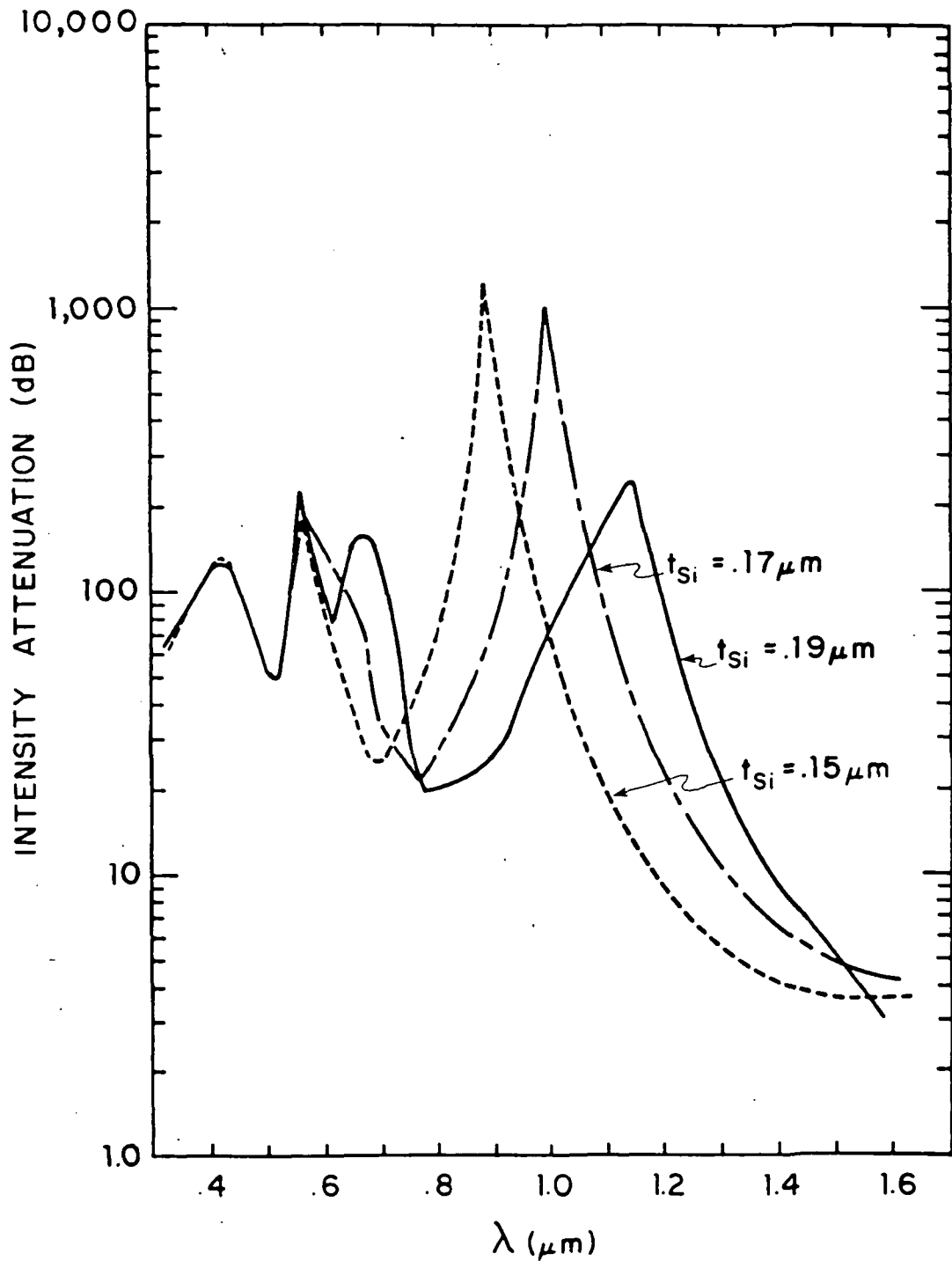   waveguide (t_{Si} = 0.09, 0.10, 0.11 µm)

Figure 29.   Frequency response of silicon-clad
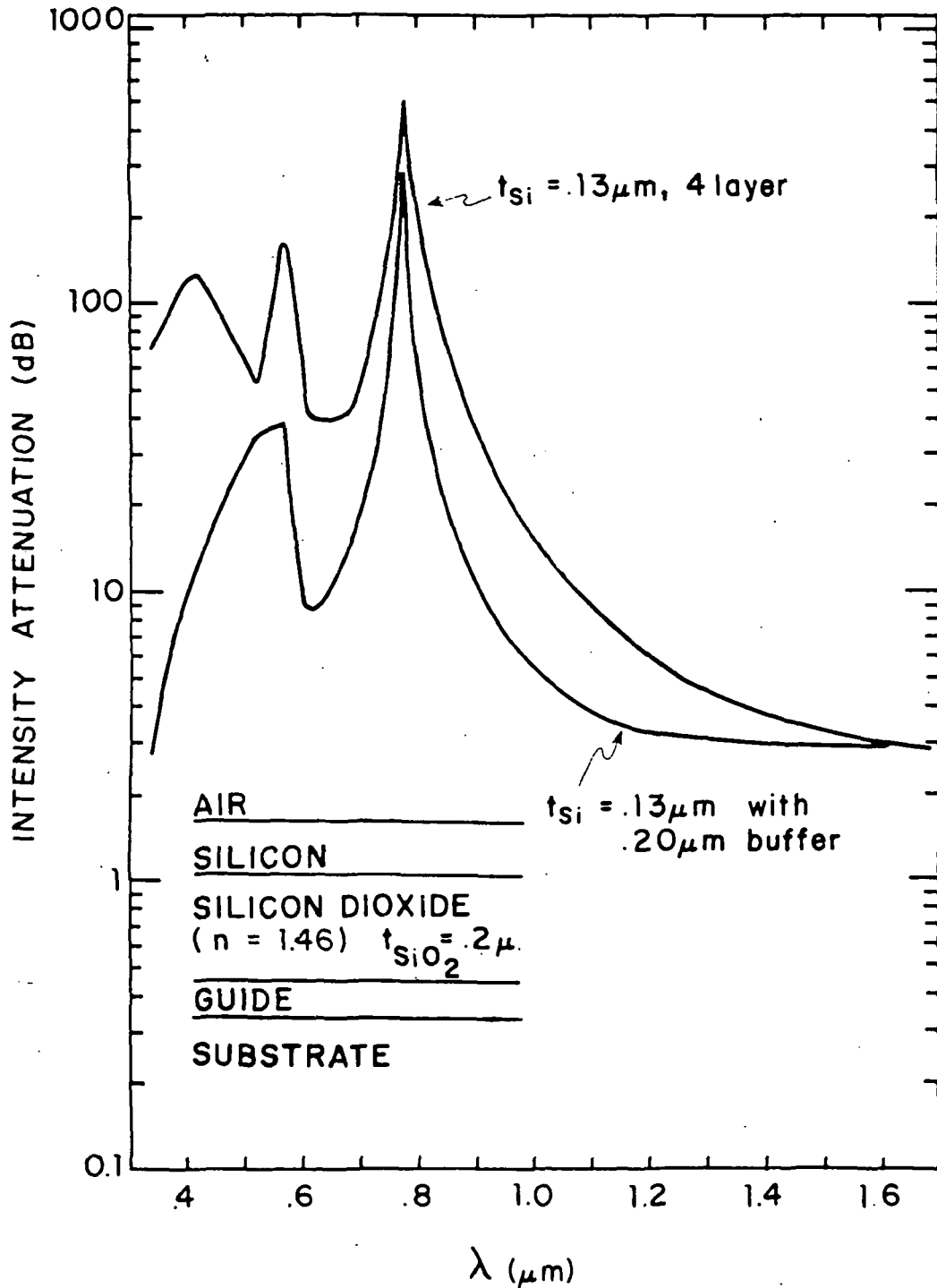   waveguide (t_{Si} = 0.15, 0.17, 0.19 µm)

Figure 30.   Reduction in attenuation of filter with
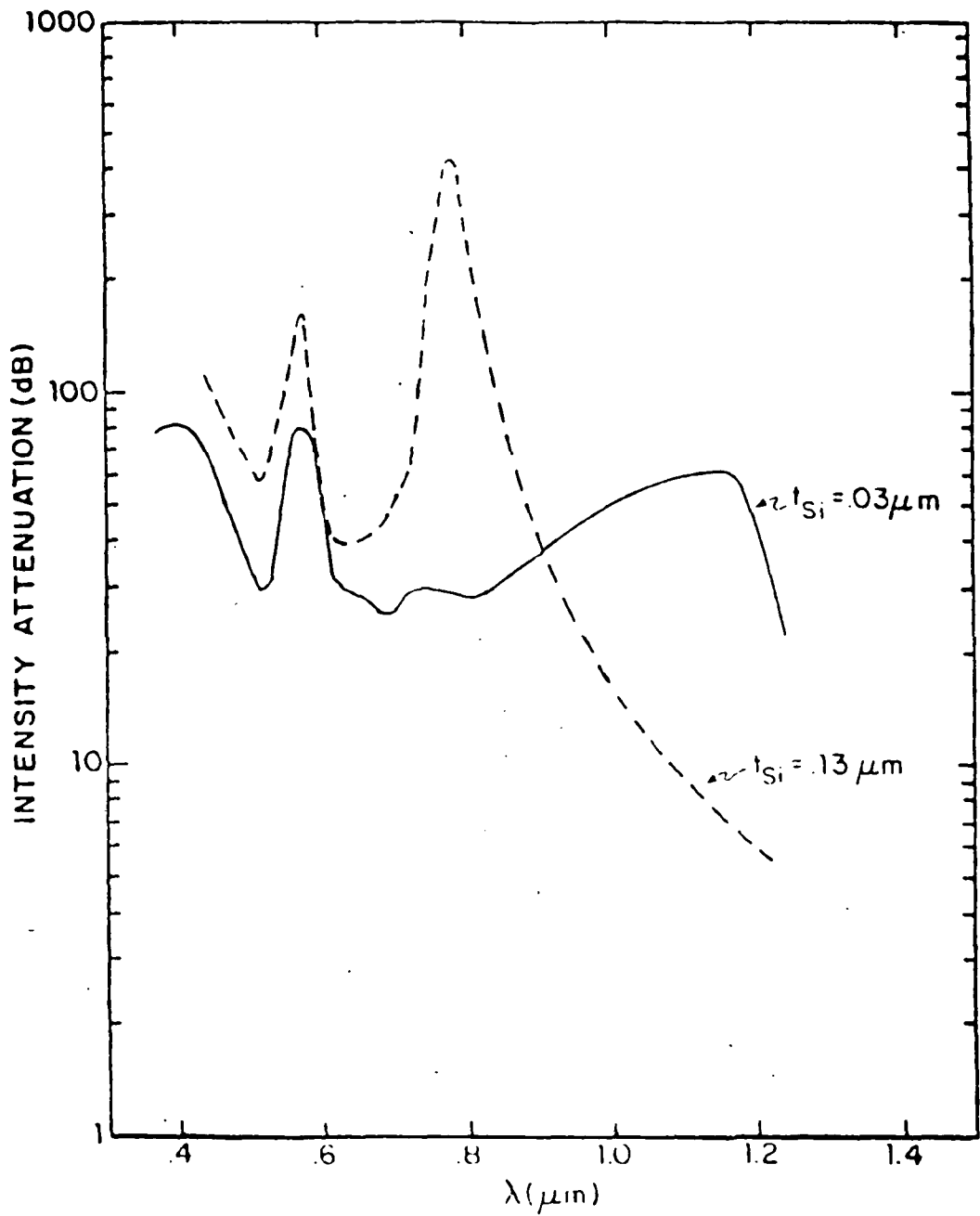 SiO_2 buffer layer (n = 1.46, t_{SiO_2} = 0.2 μm)

Figure 31.   Frequency response of silicon-clad
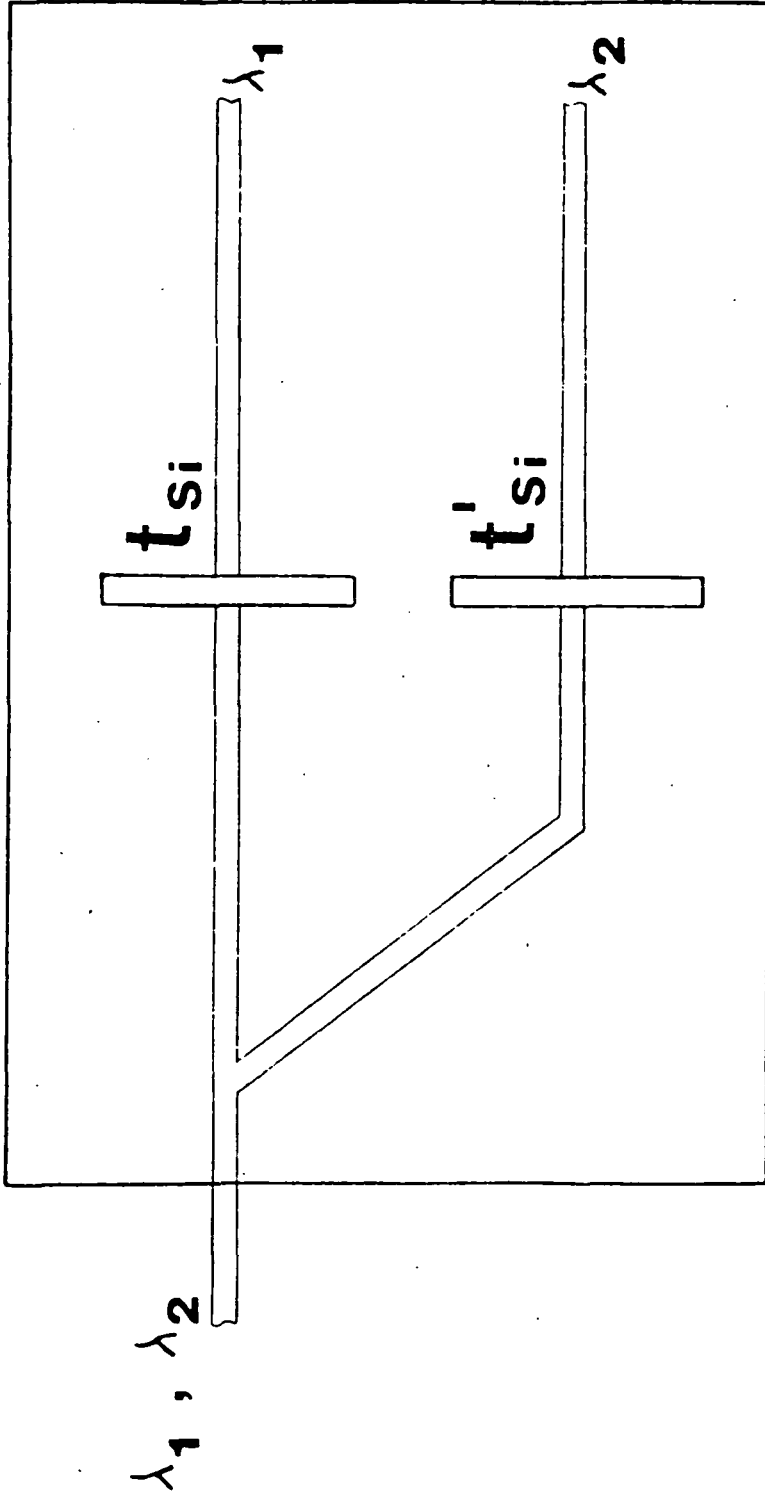   waveguide (t_{Si} = 0.03, 0.13 µm)

Figure 32.   Wavelength demultiplexer
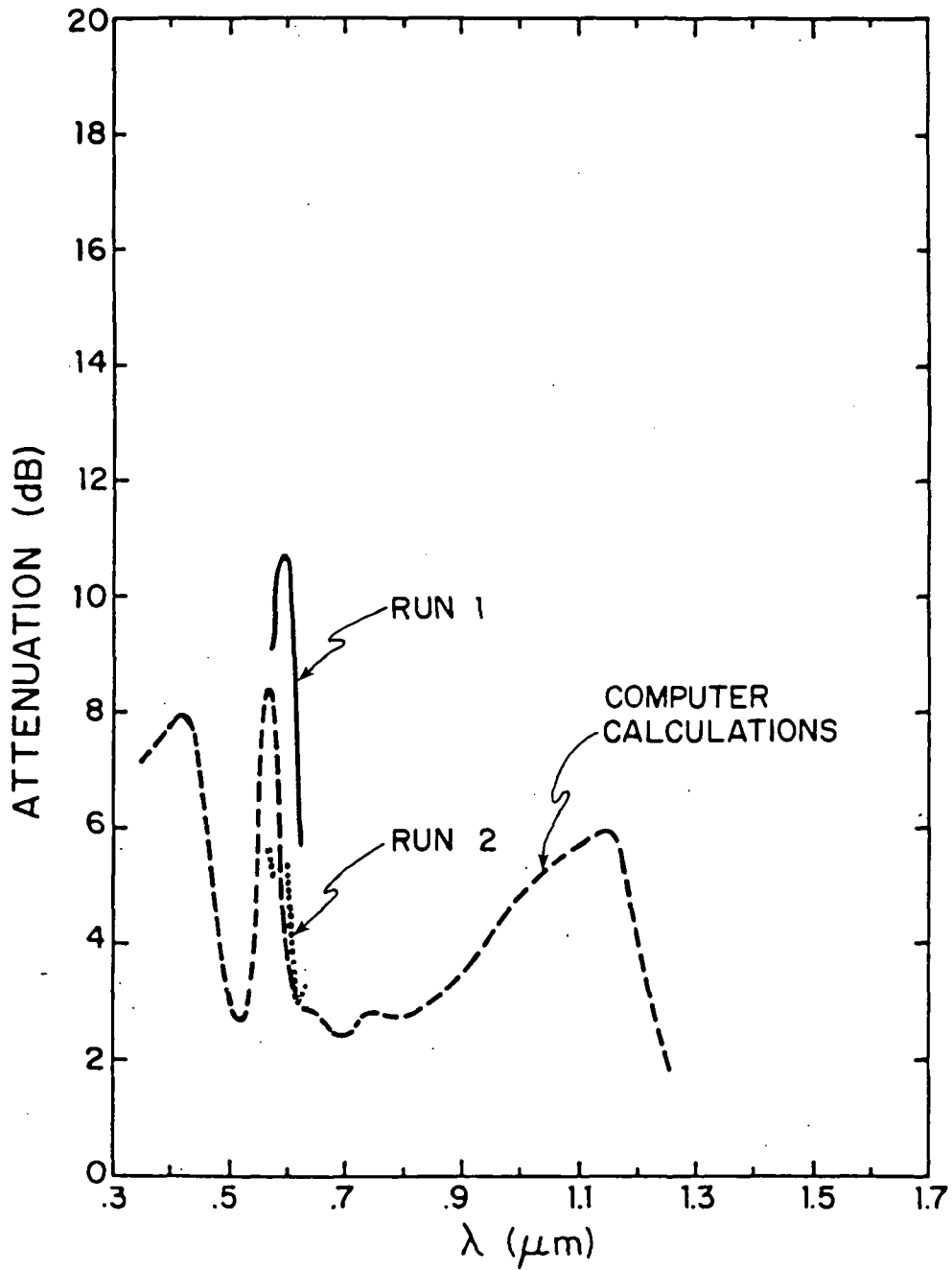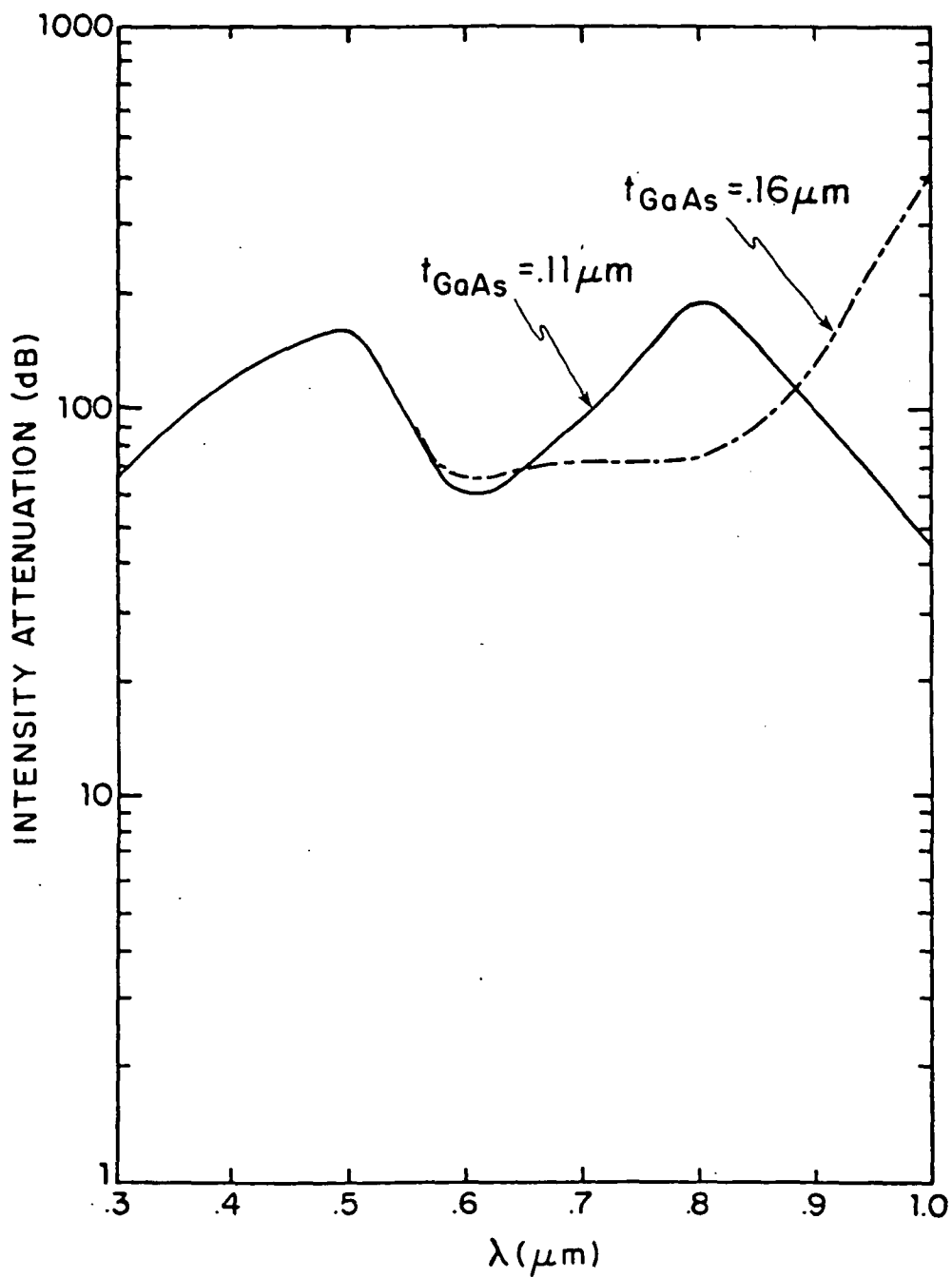
61

Figure 33. Filter response (t_{Si} = 0.03 μm)

Figure 34.   Frequency response of GaAs-clad
waveguide (t_{GaAs} = 0.11, 0.16 µm)
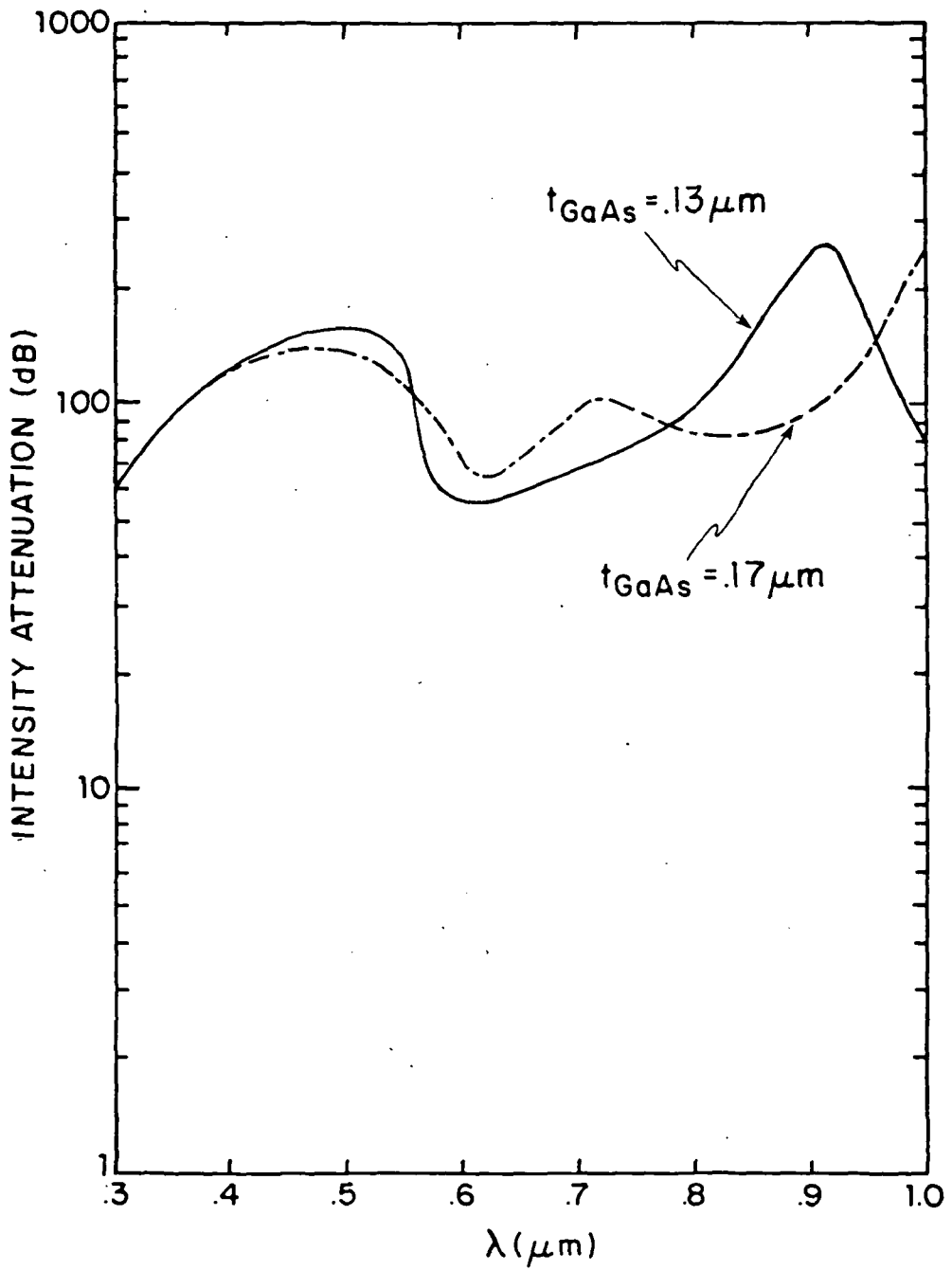
Figure 35.   Frequency response of GaAs-clad
waveguide (t_{GaAs} = 0.13, 0.17 µm)

Overlap Area Cross-Section

Overlap Area
100 Sqare
Microns

Au	5nm
Cr	2nm
Amorphous Si :H	100nm
Al	50nm
SiO₂	

Incident Light

Au/Cr

Al

V_bias

a-Si:H

Output

Ground Plane
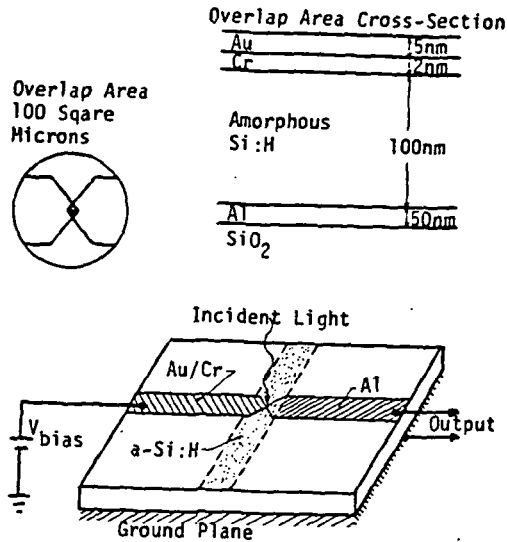
FIGURE #36. SCHEMATIC OF THE MICROSTRIPLINE THIN-FILM
PHOTODETECTOR.

Overlap Area Cross-Section

Overlap Area

Si

Al — Au/Cr

Al	5nm
Sputtered Silicon:H	T_3=10-200nm
Cr	2nm
Au	3nm
Dielectric Guide	1 micron
Glass Substrate	

Si

Al

Au/Cr

Output

V_b

Guided Light

Guide Layer

Substrate

Ground Plane

FIGURE #37. STRUCTURE OF THE THIN-FILM WAVEGUIDE PHOTODETECTOR.

FIGURE #38. ATTENUATION CHARACTERISTICS OF THE SEVEN-LAYER GUIDE.

FIGURE #39. MODE INDEX OF THE SIX-LAYER CLADDING.

FIGURE #40. TM FIELD PLOT FOR A SILICON THICKNESS OF
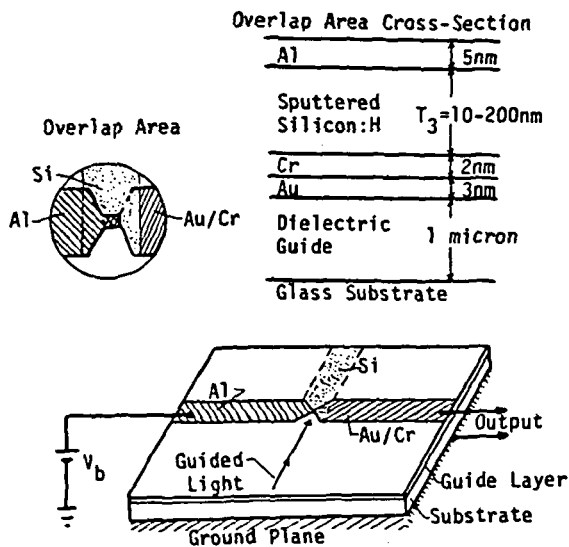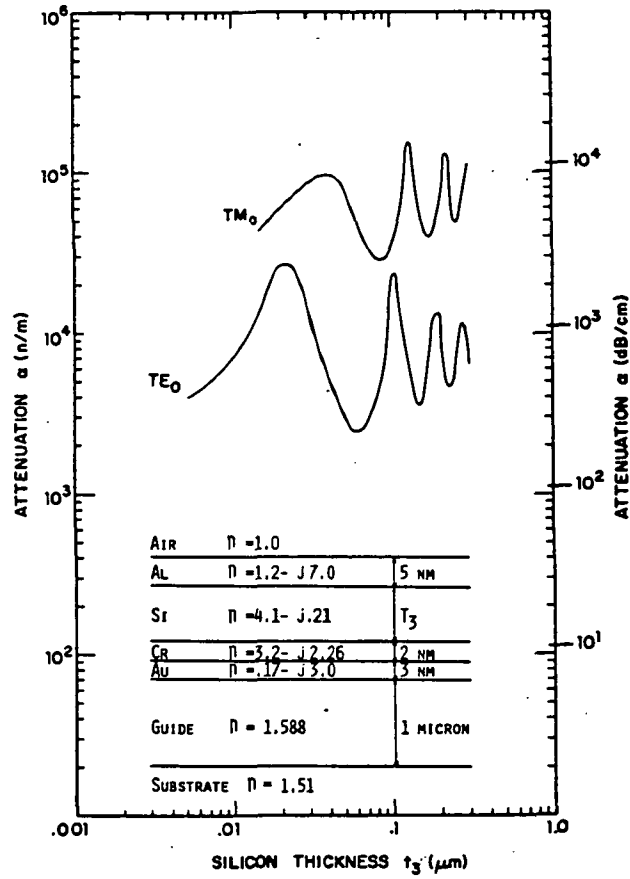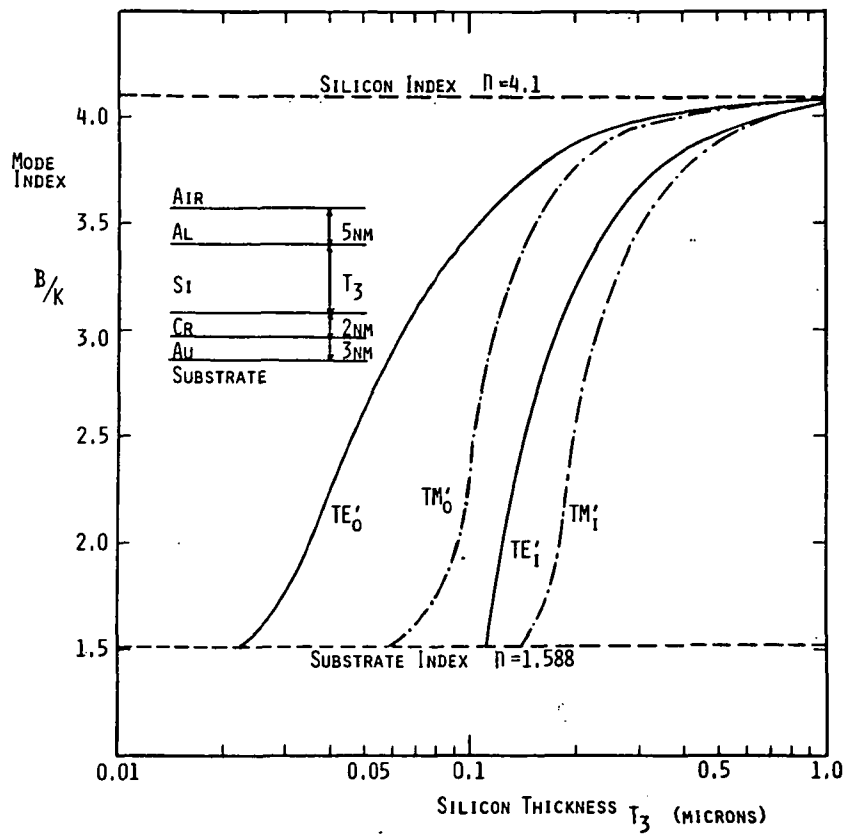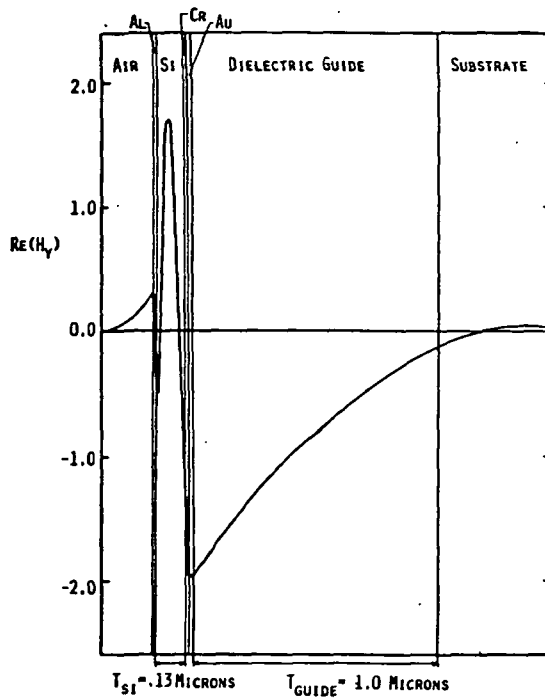0.13 MICRONS.

REFERENCES

1. D. L. Greenaway, G. Harbeke, Optical Properties and Band Structure of Semiconductors, Pergamon Press, (1968), pps. 4-12.

2. R. A. Smith, Semiconductors, 2nd Ed, Cambridge Press, (1978), Chapter 10 and pg. 462.

3. A. S. Jordon, "Determination of the Total Emittance of n-type GaAs with Application to Czochralski Growth", J. Appl. Phys. 51(4), (April 1980), pg. 2218.

4. G. H. B. Thompson, "A Theory for Filamentation in Semiconductor Lasers Including the Dependence of Dielectric Constant on Injected Carrier Density", Opto-electronics, 4 (1972), pps. 257-310.

5. G. M. McWright, T. E. Batchman, and R. F. Carson, "Gallium Arsenide Clad Waveguide Modulators", Proc. of the S.P.I.E., 409-25, (April 1983).

6. M. A. Omar, Elementry Solid State Physics, Addison-Wesley, (1975), p. 166.

7. C. H. Lee, et.al., "Optical Control of Millimeter-Wave Propagation in Dielectric Waveguides," IEEE J. of Quantum Electronics, QE-16-3, (March 1980), p. 277.

8. S. Sze, "Physics of Semiconductor Devices," 2nd ed., Wiley, (1981), p. 850.

9. W. C. Spitzer, J. M. Whelen, "Infrared Absorbtion and Electron Effective Mass in n-Type Gallium Arsenide", Phys, Rev., 114-1, (April 1, 1959), p. 59.

10. C. J. Hwang, "Optical Properties of n-Type GaAs. I. Determination of Hole Diffusion Length from Optical Absorption and Photoluminescence Measurements", J. Appl. Phys., 40-9, (August 1969), p. 3731.

11. J. S. Blakemore, "Semiconducting and Other Major Properties of Gallium Arsenide", J. Appl. Phys., 53-10. (October 1982), p. R123.

12. O. Madelung, Physics of III-V Compounds, Wiley, (1964), p. 68.

13. M. O. Sturge, "Optical Absorption of GaAs Between .6 and 2.75 eV", Phys. Rev., 127-3, (August 1962), p. 768.

14. H. C. Casey and F. Stern, "Concentration-Dependent Absorbtion and Spontaneous Emission of Heavily Doped GaAs", J. of Appl. Phys, 47-2, p. 631.

15. C. J. Hwang, "Properties of Spontaneous and Stimulated Emission in GaAs Junction Lasers I. Densities of States in the Active Region", Phys. Rev. B., vol. 2-10, (15 November 1970), p. 4117.

16. J. G. Mendoza-Alvarez, F. O. Nunes, and N. B. Patel, "Refraction Index Dependence on Free Carriers for GaAs", J. of Appl. Phys., 51-8, (August 1980), p. 4365.

17. T. E. Batchman, G. M. McWright, "Mode Coupling Between Dielectric and Semiconductor Planar Waveguides," I.E.E.E. J. of Quantum Electronics, QE-18-4, (April, 1982), p. 277.

18. W. Kern and R. C. Hiem, "Chemical Vapor Deposition of Silicate Glasses for Use with Silicon Devices," J. of Electrochemical Society, 117-4, (April, 1970), p. 568.

19. G. C. Marx, M. Gottlick, G. B. Barndt, "Integrated Optical Detector Array, Waveguide and Modulator Based on Silicon Technology," I.E.E.E. J. of Solid State Circuits, 5C-12-1 (February, 1977) p. 10.

20. R. F. Carson and T.E. Batchman, "Polarization Effects in Silicon-Clad Optical Waveguides," Applied Optics, Vol. 23, p. 2985 (1984).

21. Y. Yamamoto, T. Kamiya, and H. Yanai, "Characteristics of Optical Guided Modes in Multilayer Metal-Clad Planar Optical Guide with Low-Index Dielectric Buffer Layer," IEEE J. Quantum Electron. QE-11, 729 (1975).

22. F. K. Reinhart, J. C. Shelton, R. A. Logan, and B. W. Lee, "MOS Rib Waveguide Polarizers," Appl. Phys. Lett. 36, 237 (1980).

23. K. H. Rolke and W. Sohler, "Metal-Clad Waveguide as Cutoff Polarizer for Integrated Optics," IEEE J. Quantum Electron, QE-13, 141 (1977).

24. S. Uehara, T. Izawa, H. Nakagome, "Optical Waveguiding Polarizer," Appl. Opt. 13, 1753 (1974).

25. D. T. Pierce and W. E. Spicer, "Electronic Sturcture of Amorphous Si from Photoemission and Optical Studies," Phys. Rev. B-5, 3017 (1972).

26. G. L. Mitchell and W. D. Scott, "Calculation of Complex Propagating Modes in Arbitrary, Plane-Layered, Complex Dielectric Structures," NSF Report PB-277152 (National Technical Information Service, Springfield, VA, 1977).

27. K. Sasaki, Y. Kudo, H. Wantanabe, and O. Hamano, "Determining the Optical Constants of Vacuum Evaporated II-VI Compound Thin Films with Optical Waveguides," Appl. Opt. 20, 3715 (1981).

28. G. M. McWright, "Semiconductor-Clad Dielectric Optical Waveguides," Ph.D Dissertation, University of Virginia (August, 1983).

29. D. E. Gray, Ed. American Institute of Physics Handbook, 2nd ed., New York: McGraw-Hill, pp. 103-122, 1963.

30. J. Stuke and G. Zimmerer, "Optical properties of amorphous III-V compounds, Physica Status Solidi B, vol. 49, no. 2, pp. 513-523, February, 1972.

31. McWright, G. M., Carson, R. F., and Batchman, T. E., "Semi-conductor-Clad Optical Waveguides for Spectral Filtering in Integrated Optics," Paper THO4 Presented at the Conference on Lasers and Electro-Optics, May 19, 1983.

32. A. M. Johnson, A. M. Glass, D. H. Olsen, W. M. Simpson, and J. P. Harbison, "High Quantum Efficiency Amorphous Silicon Photodetectors With Picosecond Response Times," Applied Physics Letters, Vol. 44, p. 67 (1984).

APPENDIX A

MINIMIZING REFLECTIONS FROM THE GaAs CLADDING LAYER

In order to maximize the absorption of the normal-incidence signal beam, the reflection from the front surface of the GaAs (plane P_1 in Fig. A-1) must be minimized and the reflection from the rear surface (plane P_2) must be maximized.

For the analysis of this condition, we may treat the GaAs layer as lossless, in the 4 layer structure of Fig. A-1, and examine the reflection coefficients at each of the planes. The reflection coefficients at P_1 and P_2, respectively, are given by:

$$\Gamma_1 = \frac{n_{in1} - n_0}{n_{in1} + n_0} \qquad \Gamma_2 = \frac{n_{in2} - n_{GaAs}}{n_{in2} + n_{GaAs}} \qquad (A.1)$$

where n_0 is the intrinsic impedence: $n_0 = \sqrt{\mu_0/\epsilon_0}$ and $n_{GaAs} = \sqrt{\mu_{GaAs}/\epsilon_{GaAs}}$. Input impedence n_{in1} is given by:

$$n_{in1} = n_{GaAs} \frac{n_{in2} - jn_{GaAs} \tan(\frac{2\pi}{\lambda_{GaAs}} d)}{n_{GaAs} + jn_{GaAs} \tan(\frac{2\pi}{\lambda_{GaAs}})d} \qquad (A.2)$$

and n_{in2} is given similarly by the parameters of layers 3 and 4. We then solve for a free space wavelength that will minimize Γ_1 and maximize Γ_2 for the given GaAs layer thickness, d.

Layer #1
Air

Layer #2
GaAs

Layer #3
Guiding
Dielectric

Layer #4
Substrate

n_0

n_{GaAs}

n_3

n_4

$\leftarrow d \rightarrow$

Input
Light
Beam

Γ_1

Γ_2

n_{in_1}
Plane
P_1
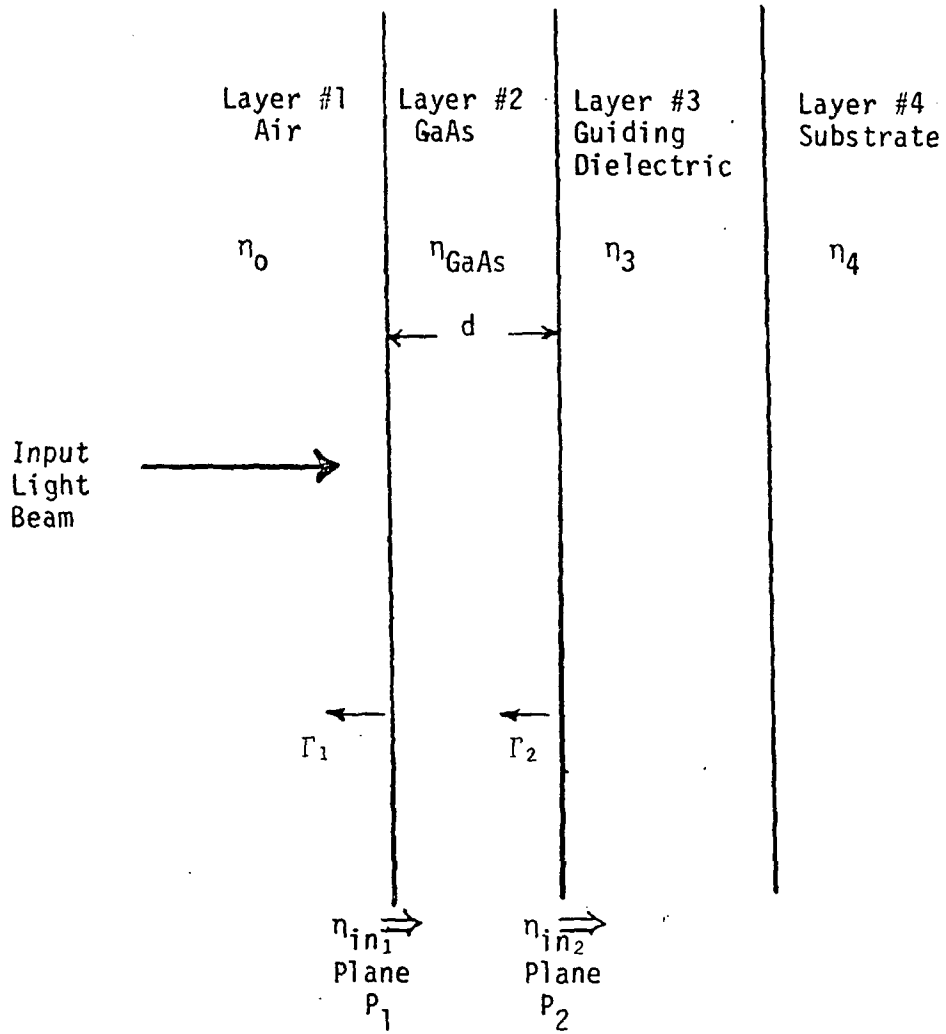
n_{in_2}
Plane
P_2

FIGURE A-1.   REFLECTIONS FROM THE FOUR LAYER STRUCTURE
(NORMAL INCIDENCE).

APPENDIX B

PUBLICATIONS

Polarization effects in silicon-clad optical waveguides

Richard F. Carson and Ted E. Batchman

By changing the thickness of a semiconductor cladding layer deposited on a planar dielectric waveguide, the TE or TM propagating modes may be selectively attenuated. This polarization effect is due to the periodic coupling between the lossless propagating modes of the dielectric slab waveguide and the lossy modes of the cladding layer. Experimental tests involving silicon claddings show high selectivity for either polarization.

Semiconductor-clad dielectric planar waveguides exhibit many interesting properties due to coupling between the lossless modes of the dielectric guiding layer and the lossy modes supported by the semiconductor cladding. Applications previously reported include studies of modulation by an external light source and spectral filtering using Ge, GaAs, and Si.[1-3] Here we report on the use of an easily deposited silicon cladding layer as a TE–TM polarizer at a free space wavelength of $\lambda_0 = 633$ nm.

Waveguide polarizers have been constructed by using selective attenuation in metal claddings,[4,5] cutoff effects in the waveguide due to cladding interaction,[6] or birefringent claddings such as calcite.[7] Unlike metal claddings on dielectric guides which mainly attenuate the TM mode,[4] a silicon cladding allows the selective attenuation of either the TE or TM polarization simply by choice of the thickness of the deposited cladding layer.

The planar waveguide structure analyzed is the four-layer cross section shown in the inset of Fig. 1. The air and the dielectric substrate layers are taken as semi-infinite, while the dielectric guiding layer is a constant (1-μm) thickness, and the silicon layer thickness t_2 is variable. The refractive indices used in the computer predictions are also shown in the inset, where the air and dielectric layers are considered to be lossless. The silicon layer, being absorptive at 633 nm, is characterized by a complex refractive index (for amorphous thin films)[8]:

$$\eta = 4.1 - j0.21 \qquad (1)$$

or a relative permittivity of

$$\epsilon_r = \epsilon' - j\epsilon'' = 16.76 - j1.75, \qquad (2)$$

where the imaginary portion gives a measure of the absorption of light in the material. For a plane wave traveling in the +z direction of propagation in a waveguide, the attenuation and phase characteristics for the electric and magnetic fields are then given by

$$\bar{E} = \bar{E} \exp(-j\beta z) \exp(\alpha z),$$

$$\bar{H} = \bar{H} \exp(-j\beta z) \exp(\alpha z), \qquad (3)$$

where α is the attenuation constant and β is the propagation or phase constant.

A computer program was used to solve the Maxwell equations and associated boundary conditions for the four-layer structure discussed.[9] The resulting effective mode index,

$$\beta/k = (\lambda_0 \beta)/2\pi, \qquad (4)$$

and the attenuation constant α of the entire guided-wave structure were generated at various thickness values of the silicon cladding layer for both the TM_0 and TE_0 modes. As illustrated in Fig. 1 and discussed in previous references for the TE_0 case, the attenuation constant for the four-layer guide exhibits a damped oscillatory behavior as the silicon layer thickness is increased from 0.005 to 1.0 μm.[3] These oscillations are due to coupling between the zero-order mode propagating in the dielectric waveguide and the various orders of the modes which are supported by the silicon layer. As the silicon thickness is increased, each successive maximum on the attenuation curve represents a point where the silicon layer is supporting a successively higher-order mode.

To study the modes of the silicon layer itself, the TE_0' and TM_0' mode indices are generated for an equivalent three-layer air–silicon–dielectric guide, where the dielectric substrate now has the $\eta = 1.588$ index value of the dielectric guide in the four-layer structure. The

74

Fig. 1. Attenuation characteristics of a four-layer silicon-clad waveguide.

Figure 1 labels:

AIR (n=1)

SILICON t_2(n= 4.1 - j.21)

GUIDE 1.0μm = t_3 (n= 1.588)

SUBSTRATE (n= 1.51)

Fig. 2. Mode indices of a three-layer silicon guide.

Fig. 3. TE-TM mode extinction for a 100-μm width of silicon cladding (shown in the inset) of varying thickness.

results, shown in Fig. 2, indicate that a given mode in the silicon can only exist at thickness values which allow the mode index to be >1.588 for that mode. When the silicon is too thin, the mode index falls below 1.588 for a given mode, which is then said to be in cutoff. When the mode index is just above 1.588, the mode still propagates, but it is matched with the substrate, and there is a large exchange of energy across the silicon-dielectric boundary. In the four-layer guide, these match points correspond to large amounts of energy being coupled from the dielectric guide into the absorptive silicon. Thus, as shown by comparing the mode index curve of Fig. 2 with the attenuation curve of Fig. 1, the attenuation maxima for the four-layer guide correspond to the cutoff thickness values for the three-layer air–silicon–dielectric case. Similar behavior has been seen by Sasaki et al.[10] in II–VI compounds for the TE_0 case.

Of special interest here is the fact that, for the TM′ case, the three-layer silicon waveguide is below the cutoff thickness and hence does not support any modes below 0.04 μm. It follows that the attenuation of the TM_0 mode in the four-layer guide of Fig. 1 drops steadily as the silicon thickness is decreased below the value due to the fact that very little energy couples into the lossy silicon. The TE_0' mode is supported down to
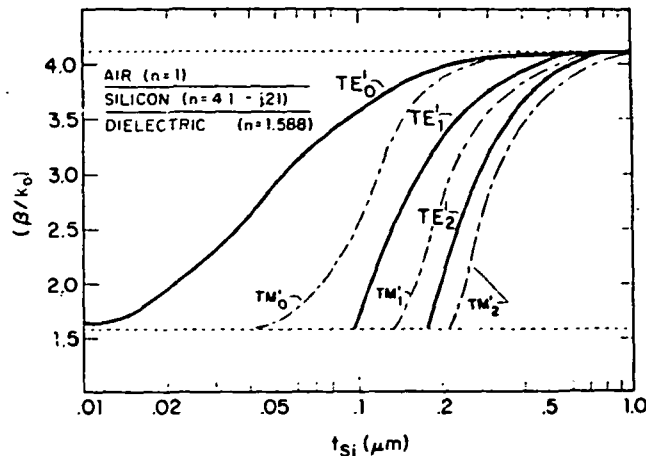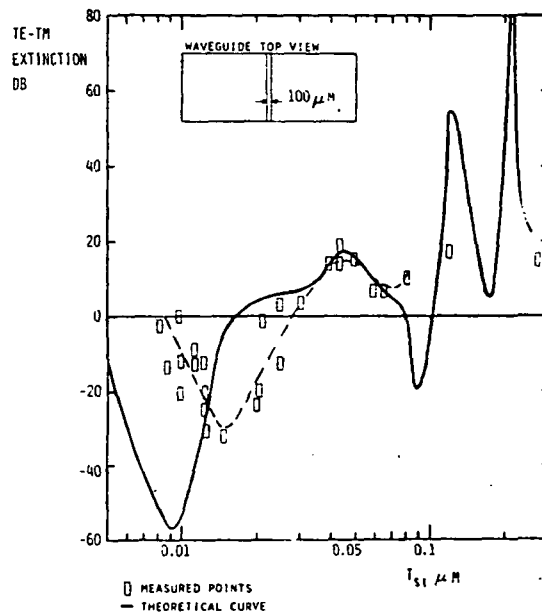
a cutoff thickness of 0.008 μm as indicated by Fig. 2. Thus the TE_0 mode of the four-layer guide has an attenuation peak in Fig. 1 at a silicon thickness of 0.008 μm. These characteristics create regions of cladding thickness where the TE_0 or TM_0 modes may be selectively absorbed into the silicon and thus are attenuated in the guide.

This extinction ratio between the TM_0 and TE_0 modes is plotted in Fig. 3, where the theoretical intensity relation between the two modes is plotted by the solid line using data from Fig. 1. The extinction is defined as

$$\text{TE-TM extinction (dB)} = 10 \log(I_{TE}/I_{TM}), \qquad (5)$$

and the ratio of output intensities is

$$\frac{I_{TE}}{I_{TM}} = \exp[-(\alpha_{TE} - \alpha_{TM})z], \qquad (6)$$
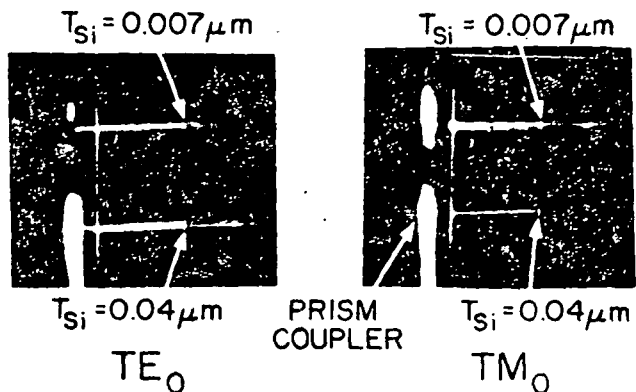
75

$T_{Si} = 0.007 \mu m$ $\qquad$ $T_{Si} = 0.007 \mu m$

$T_{Si} = 0.04 \mu m$ $\qquad$ PRISM COUPLER $\qquad$ $T_{Si} = 0.04 \mu m$

TE$_0$ $\qquad\qquad\qquad$ TM$_0$

Fig. 4. Scattered light views of the waveguide for the TE$_0$ and TM$_0$ modes at two silicon thickness values.

We have shown here that silicon claddings on dielectric planar waveguides offer a simple method for selectively polarizing guided light. Because the attenuation mechanism is absorptive, semiconductor claddings might be used in p-n and Schottky barrier junction structures as polarization-sensitive photodetectors. Such possibilities are currently being investigated.

where z is the 100-μm width of silicon shown on the top view of the waveguide in the inset. The rectangles along the dotted curve show actual experimental measurements taken by measuring the prism-coupled input and output of waveguides with a 100-μm wide strip of sputtered amorphous silicon cladding having the thickness values shown. The predictions and results indicate that high extinctions can be obtained for either mode simply by changing the thickness of the silicon cladding layer.

The suppression in the negative peak of the experimental data is due to the large amount of scattered and stray light in the measurement system, which caused the noise level to be at about -40 dB. The slight shift in the negative peak may be due to the fact that the experimental waveguides are ion-exchange graded-index guides rather than the slab guides analyzed by the computer program. The refractive index of the sputtered silicon may also be different from that used in the computer predictions due to varying sputtering conditions.

Views of the scattered light in the guide are shown for both polarizations in Fig. 4. For the TE$_0$ mode, the beam passing under the 0.04-μm thick (100-μm wide) silicon strip is much less attenuated than the beam which encounters the 0.007-μm thick silicon. When the polarization is changed to the TM$_0$ mode the 0.04-μm thick silicon layer attentuates the beam much more than the 0.007-μm thick layer.

References

1. G. M. McWright, T. E. Batchman, and R. F. Carson, "Gallium Arsenide Clad Optical Waveguide Modulators," Proc. Soc. Photo-Opt. Instrum. Eng. 408, 149 (1983).
2. G. M. McWright, R. F. Carson, T. E. Batchman, in Technical Digest, Conference on Lasers and Electrooptics (Optical Society of America, Washington, D.C., 1983), paper THO4.
3. G. M. McWright, T. E. Batchman, and M. S. Stanziano, "Measurement and Analysis of Periodic Coupling in Silicon-Clad Planar Waveguides," IEEE J. Quantum Electron. QE-18, (1982).
4. Y. Yamamoto, T. Kamiya, and H. Yanai, "Characteristics of Optical Guided Modes in Multilayer Metal-Clad Planar Optical Guide with Low-Index Dielectric Buffer Layer," IEEE J. Quantum Electron. QE-11, 729 (1975).
5. F. K. Reinhart, J. C. Shelton, R. A. Logan, and B. W. Lee, "MOS Rib Waveguide Polarizers," Appl. Phys. Lett. 36, 237 (1980).
6. K. H. Rolke and W. Sohler, "Metal-Clad Waveguide as Cutoff Polarizer for Integrated Optics," IEEE J. Quantum Electron. QE-13, 141 (1977).
7. S. Uehara, T. Izawa, H. Nakagome, "Optical Waveguiding Polarizer," Appl. Opt. 13, 1753 (1974).
8. D. T. Pierce and W. E. Spicer, "Electronic Structure of Amorphous Si from Photoemission and Optical Studies," Phys. Rev. B 5, 3017 (1972).
9. G. L. Mitchell and W. D. Scott, "Calculation of Complex Propagating Modes in Arbitrary, Plane-Layered, Complex Dielectric Structures," NSF Report PB-277152 (National Technical Information Service, Springfield, Va., 1977).
10. K. Sasaki, Y. Kudo, H. Wantanabe, and O. Hamano, "Determining the Optical Constants of Vacuum Evaporated II–VI Compound Thin Films with Optical Waveguides," Appl. Opt. 20, 3715 (1981).

76

Measurement and Analysis of Periodic Coupling in Silicon-Clad Planar Waveguides

GLEN M. MC WRIGHT, STUDENT MEMBER, IEEE, T. E. BATCHMAN, MEMBER, IEEE, AND
M. S. STANZIANO, STUDENT MEMBER, IEEE

Abstract—Computer modeling studies indicate that planar dielectric waveguides clad with silicon exhibit a damped periodic oscillation in their attenuation and phase characteristics. The effect is due to a periodic coupling between the lossy, guided modes in the silicon film and the TE_0 mode of the dielectric waveguide. Experimental confirmation of the periodic coupling for a wavelength of 632.8 nm is presented. Propagation characteristics for a wavelength of 1150 nm were investigated for application in integrated optical modulators. Frequency filtering properties of silicon-clad waveguides are also examined and it is shown that the silicon thickness controls the filter response curve.

I. INTRODUCTION

METAL-clad optical waveguides have been studied extensively and have found considerable application in electrooptic and magnetooptic modulators [1]-[5]. Semiconductor-clad or positive permittivity metal-clad waveguides are characterized by high attenuations which have severely limited their application, although they may be useful as cutoff polarizers or attenuators [6], and more recently, for optical control of millimeter wave propagation [7], [8]. We discuss further applications for these semiconductor-clad waveguides [9] and report, in this paper, the experimental confirmation of the predicted characteristics. Frequency filtering is also suggested as an application for these clad guides in the optical propagation region based on predictions presented here.

The permittivity of a semiconductor is given by

$$\epsilon_R = \epsilon' - j\epsilon'' = \epsilon' - \frac{j\sigma}{\omega\epsilon_o} \qquad (1)$$

where σ is the conductivity of the material at frequency ω. This can also be expressed in terms of the refractive index of the semiconductor as

$$\hat{n} = \epsilon^{1/2} = n - jk \qquad (2)$$

where n and k are the real and imaginary parts of the refractive index, respectively. Values for the thin amorphous semiconductor films of interest are highly dependent on the preparation technique used [10].

Lee et al. [7] have shown that both the real and imaginary portions of the permittivity vary with incident light; however, the variation in the real part is small compared to the imaginary portion. It is assumed, then, that if light is incident on the semiconductor film, electron-hole pairs are created and only the conductivity varies according to

$$\sigma = \sigma_o e \Delta n(\mu_e + \mu_h)$$

where μ_e and μ_h are the electron and hole mobilities, respectively, and Δn is the number of generated electron-hole pairs. The imaginary portion of the permittivity is thus changed proportional to the number of generated pairs.

As previously reported [9], planar waveguide structures utilizing this externally induced conductivity change have been analyzed and it was shown that the attenuation and mode index of the propagating mode are significantly altered by conductivity changes in the semiconductor cladding. An amplitude modulator and phase modulator were proposed using these results. Furthermore, it was noted that the planar waveguide structures exhibit a periodic coupling between modes in the dielectric waveguide and semiconductor cladding. The experimental confirmation of the periodic coupling from the waveguide modes to the semiconductor cladding is discussed in Section II for propagation at 632.8 nm. Section III examines the waveguide characteristics at a wavelength below the bandgap of the silicon cladding (1150 nm). Based on the previous analysis of the characteristics of the guide at 632.8 nm and the results of Section III, it was observed that the silicon film could be used as a frequency filter. The frequency characteristics are investigated in detail in Section IV and these results suggest the use of such clad waveguides as coarse frequency filters.

II. THEORY AND EXPERIMENTAL VERIFICATION

Computer modeling studies of four-layer, silicon-clad, planar optical waveguides indicate that the attenuation behaves as a damped sinusoid with increasing semiconductor thickness [9]. Experimental confirmation of this predicted effect is presented after a brief review of previous predictions.

The four-layer planar waveguide structure under consideration is shown in Fig. 1 where the guided light is propagating in the z direction in the dielectric (N_3), and it is assumed there is no variation in the y direction. All materials are lossless except for the silicon (N_2). The dispersion relations for this structure are well known and two methods of solution
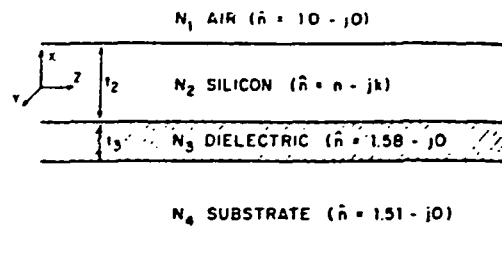

Fig. 1. Four-layer planar waveguide structure.

for the complex mode propagation constant $(\alpha + j\beta)$ have been described previously [11], [12].

The waveguide consists of a semi-infinite glass substrate, dielectric core of thickness 1 μm, a silicon cladding varying from 0.01 to 10 μm in thickness, and a semi-infinite layer of air. A free-space wavelength of 632.8 nm was assumed and a material parameters shown in Fig. 1 are for this wavelength. It should be noted that permittivity values for thin amorphous semiconductor films depend on the method of deposition and any impurities deliberately or accidentally added to the semiconductor [13], [14]. Thus, values assumed in these calculations may vary from those of the experimental films since no attempts were made to measure the permittivity of the experimental films at optical frequencies.

Silicon was investigated as a semiconductor cladding and the attenuation curve of Fig. 2 was generated by varying the cladding thickness from 0.01 to 10 μm. All other parameters were held constant in the calculations and results were confirmed using the two computer solution techniques [11], [12]. It was initially expected that decreasing the lossy cladding thickness to 0.01 μm would reduce the attenuation to zero in a well-behaved manner; however, the results were not as expected below a silicon thickness of 1.0 μm.

Experimental confirmation of the oscillatory behavior of the attenuation versus silicon thickness curve was subsequently attempted. Low-loss, single-mode optical waveguides were diffused into soda-lime glass from a sodium nitrate/silver nitrate melt using an ion-exchange fabrication technique [15]-[18]. Uniform silicon films 1 mm wide and extending across the waveguide were deposited using a radio-frequency sputtering system [19]-[21]. For each run, the system was prepumped to a base pressure less than 5×10^{-6} torr and all sputtering was performed in an argon atmosphere at a pressure of 10^{-2} torr. A number of uniform silicon films with thicknesses in the range of 0.02-0.4 μm were fabricated. High predicted attenuations in the silicon-clad guide along with severe experimental inaccuracies in either the fluid coupler or the sliding-prism attenuation measurement technique [3] has made quantitative confirmation difficult. Thus, a photographic technique was employed for confirmation of the behavior shown in Fig. 2.

As Fig. 3 indicates, qualitative confirmation of the damped oscillatory behavior of the attenuation versus silicon thickness curve has been successful. A 5 mW He-Ne (632.8 nm) laser was coupled into the silicon-clad guide using a prism coupler. Fig. 3 is a top view of the coupler and silicon-clad planar waveguide with propagation from left to right. In each of the three photographs, the coupling into the waveguide was
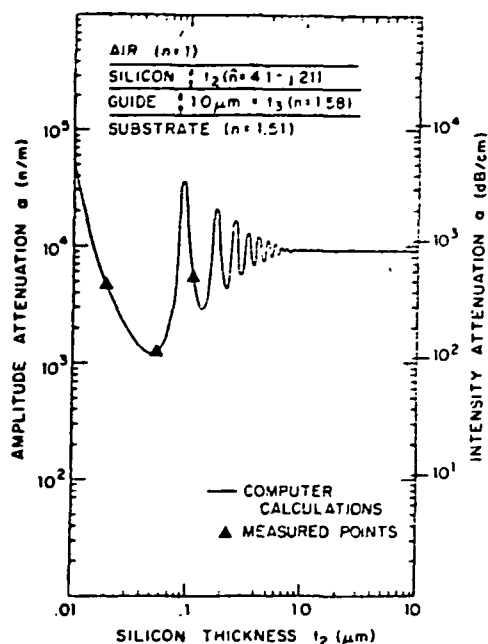
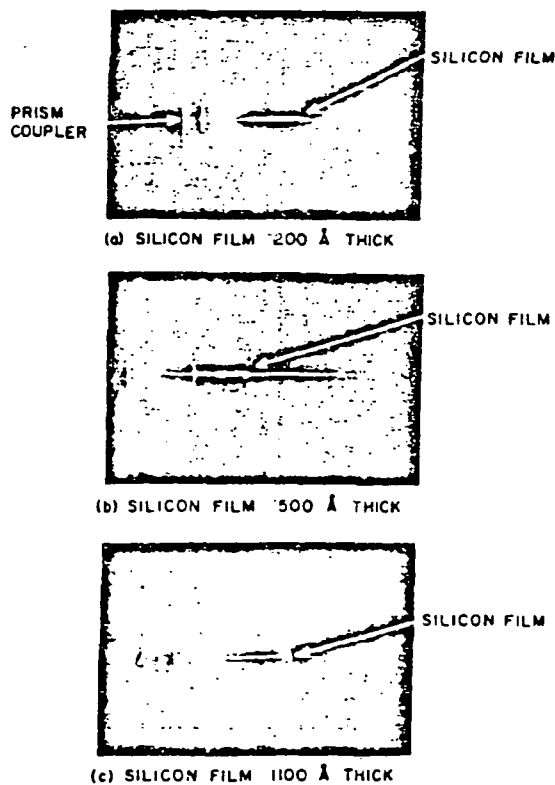Fig. 2. Attenuation characteristics of silicon-clad waveguide (TE$_0$ mode, wavelength = 632.8 nm).

(a) SILICON FILM 200 Å THICK

(b) SILICON FILM 500 Å THICK

(c) SILICON FILM 1100 Å THICK

Fig. 3. Experimental measurements of waveguide attenuation.

maximized. All photographic exposures are 5 s, f2, ASA 400 film. Uninterrupted propagation occurs until the beam encounters the 1 mm wide silicon film at which point it may suffer a large attenuation. Slight differences in the beam intensity to the left of the silicon film are due to differences in coupling efficiency and scattering in the individual waveguides. For a silicon film 200 Å thick [Fig. 3(a)], the beam is clearly attenuated as computer calculations predict. For a film 500 Å thick (a predicted minimum on the attenuation thickness curve of Fig. 2) nearly uninterrupted propagation occurs

[Fig. 3(b)], and for a film 1100 Å thick (a predicted region of high attenuation), the beam is again attenuated [Fig. 3(c)]. The three points labeled "measured" in Fig. 2 correspond to the film thicknesses at which the photographic exposures were taken and are not quantitative amplitude measurements. The principal conclusion which can be drawn from the data is that there is at least one minimum in attenuation which occurs in the thickness range 200-1100 Å. The existence of this local minimum between 200 and 1100 Å was similarly verified with a different set of silicon-clad waveguides. It should be noted that accurate thickness measurements are difficult for silicon films less than 200 Å and that the values for the refractive indexes used in the computer calculations may differ from those of the actual silicon-clad waveguides. Furthermore, predicted high attenuations for subsequent peaks and valleys of the attenuation versus silicon thickness curve make confirmation of the oscillatory behavior for thicker silicon films extremely difficult (i.e., the attenuation for subsequent peaks is greater than 1000 dB/cm). Additional measurements will be required to confirm the absolute attenuation levels observed.

III. CALCULATIONS AND ANALYSIS AT 1150 nm

It has been predicted that the attenuation and mode index of the four-layer silicon-clad guide are significantly altered by conductivity changes in the silicon, and amplitude and phase modulators have been proposed using these results [9]. Calculations were presented for a wavelength of 632.8 nm, and modulation would be accomplished as a result of a change in the semiconductor conductivity via an incident light beam with photon energy above the bandgap of the silicon. It is evident, however, that the 632.8 nm guided wave will inadvertently excite the silicon cladding since it is above the bandgap. To circumvent this problem the wavelength was changed to 1150 nm and the amplitude and phase characteristics of the guide were analyzed. This wavelength is such that the absorption coefficient of amorphous silicon is minimal [22], [27] and appreciable excitation of the silicon cladding due to the 1150 nm guided wave is unlikely. Direct optical modulation, however, would still be realized by altering the conductivity of the silicon with a light beam with photon energy above the bandgap of silicon (in the visible region). Computer predictions of the propagation characteristics of the four-layer silicon-clad planar waveguide at 1150 nm are presented in this section.

The attenuation and phase constant curves of Figs. 4 and 5 were generated by varying the silicon cladding thickness from 0.01 to 1.0 μm (the phase constant β has been normalized by $k_o = 2\pi/\lambda_o$ so that all curves show the mode index). Material parameters shown in Figs. 4 and 5 are for a 1150 nm wavelength. The curves are again similar to exponentially damped sinusoids with extreme values of the mode index (β/k_o) corresponding to the median values (maximum slope) in the attenuation (α) curves. Extreme values of the α curve correspond to median values in the β/k_o curves and the oscillations in both curves approach a median value at 10 μm. Similar behavior was observed for a wavelength of 632.8 nm and results were described as a periodic coupling be-
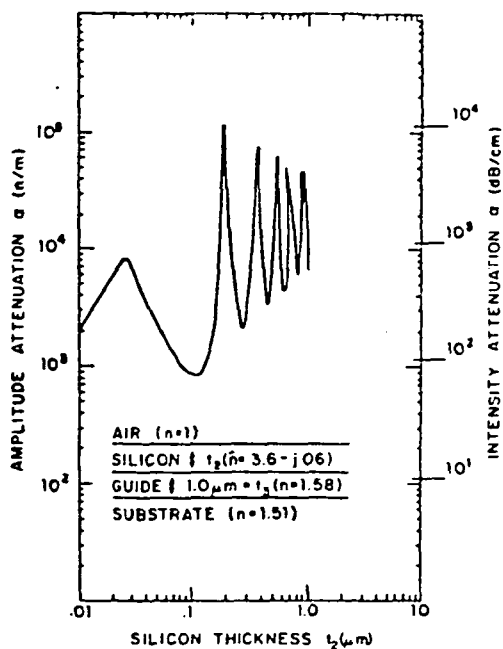
Fig. 4. Attenuation characteristics of silicon-clad waveguide (TE_0 mode, wavelength = 1150 nm).

Fig. 5. Mode index characteristics of silicon-clad waveguide (TE_0 mode, wavelength = 1150 nm).

Fig. 6. Mode index characteristics of silicon waveguide (wavelength = 1150 nm).
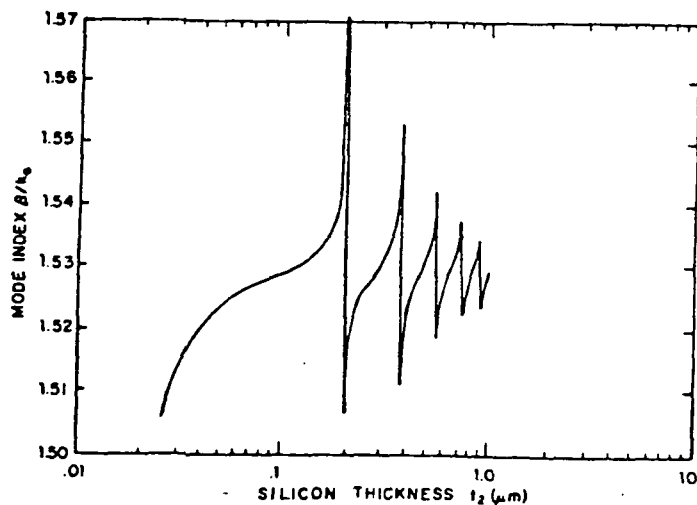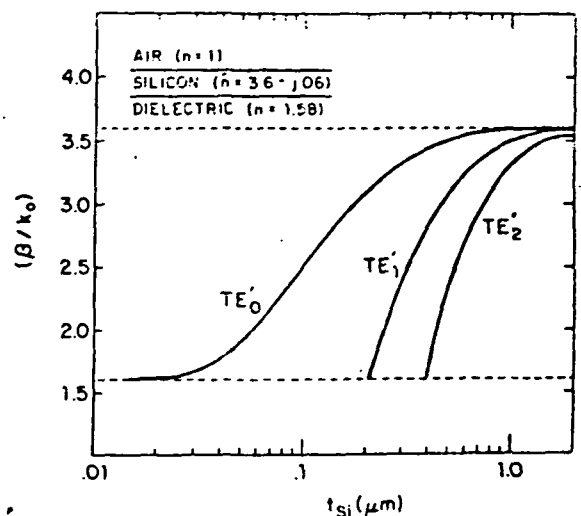

Fig. 7. Attenuation characteristics of silicon waveguide (wavelength = 1150 nm).

tween the guided mode (TE_0) in the dielectric and the lossy TE' modes[1] of the semiconductor guide [9]. Figs. 4 and 5 show that such coupling still occurs and the amplitude of the oscillations has increased.

This coupling (or lack thereof) has a profound effect on the attenuation and phase characteristics of the original four-layer waveguide. Therefore, a partial structure consisting of a silicon guiding region surrounded by semi-infinite layers of air and dielectric was analyzed.

The mode index and attenuation constants for the first few low order TE' modes in the silicon waveguide are shown in Figs. 6 and 7. All modes (except, perhaps the lowest order TE'_0 mode) are very lossy and the attenuation increases for the higher order modes. In Figs. 5 and 6, note that a phase

match condition occurs between the TE_0 mode in the waveguide and the TE'_1 mode in the partial structure (air–silicon–dielectric) at $t_{Si} = 0.2$ μm. This phase match is present at each of the successively higher order TE' mode cutoff thicknesses and corresponds to the respective attenuation peaks in Fig. 4 for the total structure. The sharp nulls in the attenuation curve, indicating very low coupling efficiency, occur at thicknesses midway between the cutoff value of two adjacent lossy TE' modes. Note, however, that the first peak on the four-layer attenuation curve (Fig. 4) is considerably lower than the subsequent peaks. This behavior is unlike that of the attenuation curve presented at 632.8 nm (Fig. 2). Observe that the TE'_0 mode of the three-layer guide (Fig. 7) is reasonably low-loss, and that, although nearly complete transfer of energy between the guide and the silicon occurs for $t_{Si} = 0.25$ μm, coupling is into a low-loss mode. For the subsequent peaks on the attenuation curve (Fig. 4), coupling is into high-loss modes of the partial structure and the attenuation of the four-layer guide is thus greater. For large silicon thickness, however, the four-layer attenuation curve (Fig. 4) exponen-

[1] TE'_i denotes guided modes in the semiconductor and TE_i denotes guided modes in the dielectric.

tially approaches that of the three-layer structures previously analyzed [23], where the semiconductor layer is considered semi-infinite. Similarly, the abrupt transitions on the mode index curve of the complete structure (Fig. 5) occur when the phase match condition is satisfied and the guided waves couple into successively higher order modes of the partial structure. These results are similar to the power transfer calculations for linearly tapered directional couplers [24]–[26]. Finally, note that the period and amplitude of the attenuation characteristics of the silicon-clad guide are a function of the material permittivities for a given wavelength as Fig. 2 (λ = 632.8 nm) and Fig. 4 (λ = 1150 nm) indicate.

Calculations presented in this section demonstrate that the attenuation and mode index of the four-layer silicon clad planar dielectric waveguide behave as exponentially damped sinusoids for a wavelength of 1150 nm. The effect may be explained as a coupling between the basic TE_0 mode of the dielectric waveguide and the high loss TE' modes of the semiconductor guide. The oscillatory behavior of the attenuation and mode index curves, a necessary prerequisite for the direct modulation of the guided beam, is still apparent and detailed calculations of a direct optical modulation scheme at 632.8 nm are presented elsewhere [9]. These calculations at 1150 nm demonstrate that the required modulation technique is still feasible without inadvertent excitation of the silicon cladding by the guided light wave.

IV. Selective Frequency Filtering

The attenuation characteristics of silicon-clad waveguides are a function of the material permittivities for a particular wavelength as Fig. 2 (λ_o = 632.8 nm) and Fig. 4 (λ_o = 1150 nm) indicate. Based on the observed change in period and amplitude of the attenuation curve oscillations as the material parameters vary with wavelength, it is evident that selective frequency filtering can be realized with a silicon-clad waveguide. In particular, for a given silicon-cladding thickness, the attenuation will vary drastically as the material permittivities vary with wavelength, and through optimization of the semiconductor cladding thickness, a particular frequency filtering response may be obtained with the clad guide. For example, note that a silicon thickness t_{Si} = 0.10 μm lies in a range of high attenuation ($\alpha > 10^4$ n/m) on Fig. 2 (λ = 632.8 nm), while it is in a region of low attenuation ($\alpha < 10^3$ n/m) on Fig. 4 (λ = 1150 nm). It is this effect which will be used for frequency filtering. The permittivities of all four materials (air, silicon, guide, substrate) in the planar waveguide structure of interest vary with wavelength; however amorphous silicon is particularly sensitive to frequency variations as Table I indicates [27]. The predicted frequency filtering effect is due almost solely to a change in silicon permittivity. It should be again noted that the permittivity of amorphous silicon is highly dependent upon the method of preparation.

Attenuation versus silicon thickness curves similar to those of Figs. 2 and 4 were generated as the wavelength was allowed to change from 0.35 to 1.55 μm and the permittivities of the four layers consequently varied [10], [27]. All attenuation curves retained their characteristic oscillations; however, the amplitude and period of the oscillations were significantly

TABLE I
AMORPHOUS SILICON PARAMETERS AS A FUNCTION OF WAVELENGTH

Wavelength (microns)	Refractive Index n	Refractive Index k	Relative Permittivity ε'_R	Relative Permittivity ε''_R
0.35	3.63	2.860	5.0	20.80
0.42	4.53	1.479	18.4	13.40
0.47	4.43	0.900	19.4	8.00
0.52	4.21	0.540	17.3	5.60
0.62	4.11	0.384	16.8	3.20
0.55	4.04	0.289	16.3	2.35
0.69	3.97	0.188	15.8	1.50
0.72	3.88	0.155	15.0	1.20
0.80	3.67	0.068	13.5	0.50
1.00	3.65	0.062	12.3	0.45
1.15	3.59	0.055	12.9	0.40
1.24	3.55	0.039	12.6	0.28
1.55	3.52	0.028	12.4	0.20

altered. Similarly, the mode index versus silicon thickness curves retained their characteristic oscillatory behavior although the frequency and amplitude of the oscillations changed.

Figs. 8–10 were obtained by assuming a given silicon thickness in the four-layer planar structure and allowing the wavelength to vary (and consequently, the material permittivities). The resulting attenuation (dB) for a 1 mm wide silicon bar is plotted vertically in Figs. 8–10.

A high-pass frequency filter is realized in Fig. 8. Insertion loss is less than 7 dB for a wavelength greater than 1.0 μm for the three silicon thicknesses considered (t_{Si} = 0.09, 0.10, 0.11 μm), and the extinction for wavelengths less than 0.7 μm is more than 50 dB. The particular filter characteristics in the wavelength region of 0.7–1.0 μm may be adjusted by changing the thickness of the silicon cladding.

Filters with passband wavelengths of 0.7–0.9 μm are shown in Fig. 9. Note that the exact location of the passband may be varied for the three silicon thicknesses of interest (t_{Si} = 0.15, 0.17, 0.19 μm) and that high attenuation (>100 dB) occurs immediately outside of this passband region. Insertion loss, however, is approximately 20 dB.

Even relatively short sections of silicon-clad waveguides are lossy, and for a practical device the insertion loss must be reduced significantly. Thin dielectric buffer layers have been used to lower the attenuation losses of metal-clad dielectric waveguides [28]. These layers are placed between the dielectric core and the metal and act as buffers to remove a large portion of the field from the metal cladding. The effect of a silicon dioxide (SiO_2) buffer layer on the filter response curve was investigated. The results are shown in Fig. 10. A silicon thickness t_{Si} = 0.13 μm was assumed and the attenuation versus wavelength was calculated for a four-layer structure. Note that an insertion loss of approximately 40 dB is apparent in the passband region of 632.8 nm, although rapid extinction is evident (>400 dB) immediately outside of the passband region. A silicon dioxide buffer layer (t_{Si} = 0.2 μm) of refractive index n = 1.46 was then added, and the filter response curve for the five-layer structure was calculated. Insertion loss is now less than 9 dB at a wavelength of 632.8 nm while rapid extinction (>200 dB) is still evident immediately outside of this passband. Further reduction of the passband attenuation may result from optimization of the buffer layer and silicon thicknesses. Although no attempt has been made to optimize the filter characteristics, Figs. 8 and 9 indicate the low fre-
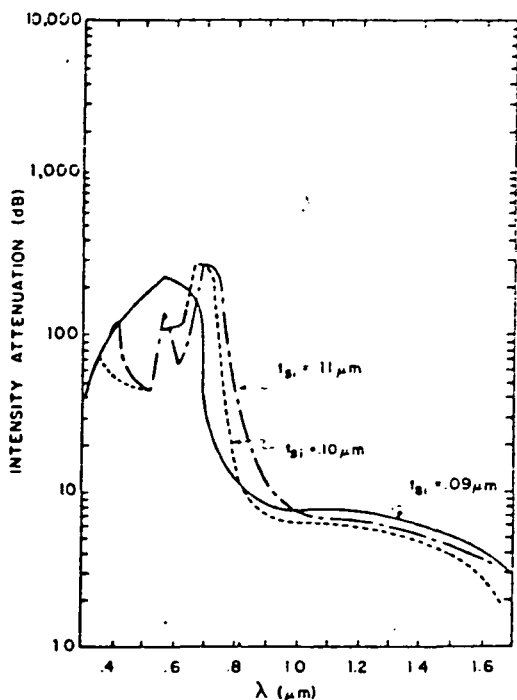
Fig. 8. Frequency response of silicon-clad waveguide (t_{Si} = 0.09, 0.10, 0.11 μm).

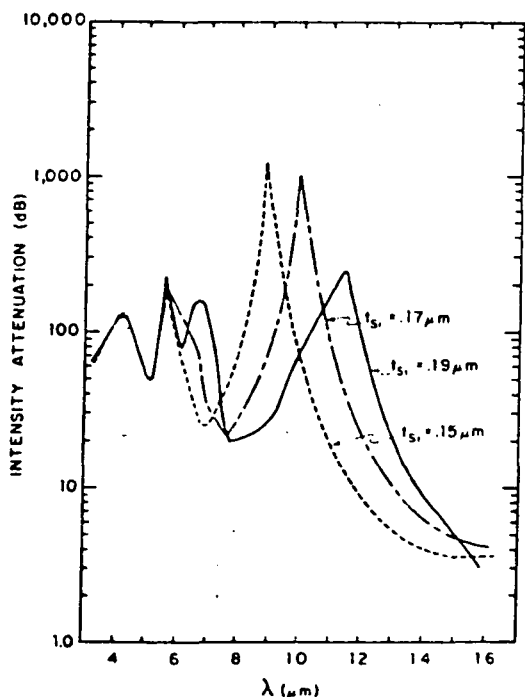Fig. 10. Reduction in attenuation of filter with SiO_2 buffer laye (n = 1.46, t_{SiO_2} = 0.2 μm).

Fig. 9. Frequency response of silicon-clad waveguide (t_{Si} = 0.15, 0.17, 0.19 μm).

quency cutoff and the attenuation peaks may be adjusted by proper choice of cladding thickness.

V. CONCLUSIONS

It has been shown that planar dielectric waveguides clad with silicon exhibit a damped periodic oscillation in their attenuation and phase characteristics. The effect is due to a periodic coupling between the lossy guided modes in the silicon film and the TE_0 mode of the dielectric waveguide. Experimental confirmation of this periodic coupling for a
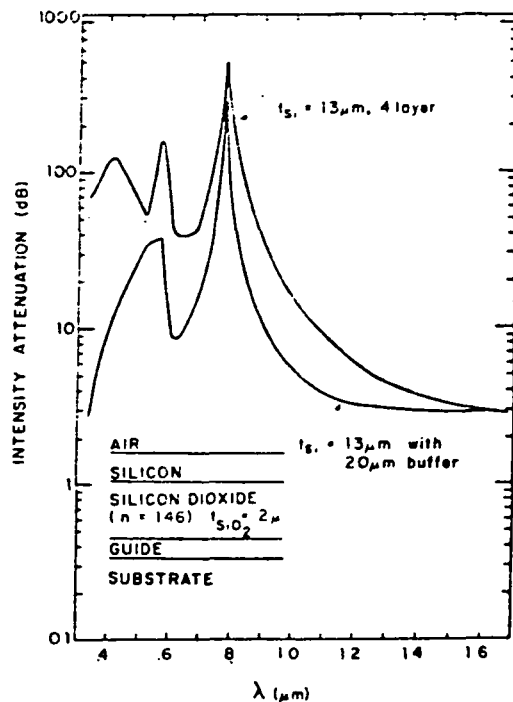
wavelength of 632.8 nm has been achieved. Calculations for wavelength of 1150 nm indicate that the attenuation and mode index still retain their oscillatory behavior. Thus, direct optical modulation scheme through excitation of th silicon cladding is still applicable without inadvertent excita tion of the cladding by the guided wave. The silicon-cla guide may also be used as a frequency filter, and the charac teristics may be adjusted through optimization of the silico thickness and through control of a buffer layer. Practica devices are currently being constructed to confirm their pre dicted characteristics.

REFERENCES

[1] J. N. Polky and G. L. Mitchell, "Metal-clad planar dielectri waveguide for integrated optics," *J. Opt. Soc. Amer.*, vol. 64, pr 274-279, Mar. 1974.

[2] S. C. Rashleigh, "Four-layer metal-clad thin film optical wave guides," *Opt. & Quantum Electron.*, vol. 8; pp. 49-60, Jan. 1976

[3] I. P. Kaminow, W. L. Mammel, and H. P. Weber, "Metal-cla optical waveguides: Analytical and experimental study," *Appl Opt.*, vol. 13, pp. 396-405, Feb. 1974.

[4] T. Takano and J. Hamasaki, "Propagating modes of a metal-cla dielectric-slab waveguide for integrated optics," *IEEE J. Quan tum Electron.*, part II, vol. QE-8, pp. 206-212, Feb. 1972.

[5] E. M. Garmire and H. Stoll, "Propagation losses in metal-film substrate optical waveguides," *IEEE J. Quantum Electron.*, vo. QE-8, pp. 763-766, Oct. 1972.

[6] T. E. Batchman and J. R. Peeler, "Gallium arsenide clad optica waveguides," *IEEE J. Quantum Electron.*, vol. QE-14, pp. 327 329, May 1978.

[7] C. H. Lee, P. S. Mak, and A. P. DeFonzo, "Optical control o millimeter wave propagation in dielectric waveguides," *IEEE J Quantum Electron.*, vol. QE-16, pp. 277-288, Mar. 1980.

[8] C. H. Lee and V. K. Mathur, "Picosecond photoconductivity an its application," *IEEE J. Quantum Electron.*, vol. QE-17, pp 2098-2112, Nov. 1981.

[9] T. E. Batchman and G. M. McWright, "Mode coupling betwee dielectric and semiconductor planar waveguides," *IEEE J. Quan tum Electron.*, vol. QE-18, pp. 782-788, Apr. 1982.

[10] D. E. Gray, Ed., *American Institute of Physics Handbook*, 2n ed. New York: McGraw-Hill, 1963, ch. 6, pp. 103-122.

[1] T. E., Batchman and S. C. Rashleigh, "Mode-selective properties of a metal-clad dielectric-slab waveguide for integrated optics," *IEEE J. Quantum Electron.*, vol. QE-8, pp. 848-850, Nov. 1972.

[2] R. B. Smith and G. L. Mitchell, "Calculation of complex propagating modes in arbitrary plan-layered complex dielectric structures," E. E. Tech. Rep. 206, University of Washington. National Science Foundation Grant Eng 76-09937, Dec. 1977.

[3] D. E. Carson, "Photo voltaics V: Amorphous silicon cells," *IEEE Spectrum*, pp. 39-41, Feb. 1980.

[4] D. E. Ackley and J. Tauc, "Silicon films as selective absorbers for solar energy conversion," *Appl. Opt.*, vol. 16, no. 11, pp. 2806-2809, Nov. 1977.

[5] G. Stewart, C. A. Miller, P.J.R. Laybourn, C.D.W. Wilkinson, and R. M. DeLaRue, "Planar optical waveguides formed by silver-ion migration in glass," *IEEE J. Quantum Electron.*, vol. QE-13, pp. 192-200, Apr. 1977.

[6] G. Stewart and P.J.R. Laybourn, "Fabrication of ion-exchanged optical waveguides from dilute silver nitrate melts," *IEEE J. Quantum Electron.*, vol. QE-14, pp. 930-934, Dec. 1978.

[7] T. G. Giallorenzi, E. J. West, R. Kirk, R. Ginther, and R. A. Andrews, "Optical waveguides formed by thermal migration of ions in glass," *Appl. Opt.*, vol. 12, no. 6, pp. 1240-1245, June 1973.

[8] A. Gedeon, "Formation and characteristics of graded-index optical waveguides buried in glass," *Appl. Phys.*, vol. 6, pp. 223-228, Mar. 1975.

[9] R. C. Ross and R. Messier, "Microstructure and properties of rf-sputtered amorphous hydrogenated films," *J. Appl. Phys.*, vol. 52, pp. 5329-5339, Aug. 1981.

[10] W. T. Pawlewicz, "Influence of deposition conditions on sputter-deposited amorphous silicon," *J. Appl. Phys.*, vol. 49, no. 11, pp. 5595-5600, Nov. 1978.

[11] J. C. Bruyere, A. Deneuville, A. Mini, J. Foutenilie, and R. Danielou. "Influence of hydrogen on optical properties of a-Si:H," *J. Appl. Phys.*, vol. 51, no. 4, pp. 2199-2205, Apr. 1980.

[12] M. H. Brodsky, Ed., "Amorphous semiconductors," *Topics in Appl. Physics*, vol. 36. New York: Spring-Verlag, 1979, pp. 1-7.

[13] T. E. Batchman and K. A. McMillan, "Measurement on positive-permittivity metal-clad waveguides," *IEEE J. Quantum Electron.*, vol. QE-13, pp. 187-192, Apr. 1977.

[24] A. L. Jones, "Coupling of optical fibers and scattering in fibers," *J. Opt. Soc. Amer.*, vol. 55, pp. 261-271, Mar. 1965.

[25] T. K. Lim, B. K. Garside, and J. P. Marton, "An analysis of optical waveguide tapers," *Appl. Phys.*, vol. 18, pp. 53-62, Jan. 1979.

[26] R. B. Smith, "Analytic solutions for linearly tapered directional couplers," *J. Opt. Soc. Amer.*, vol. 66, pp. 882-892, Sept. 1976.

[27] D. T. Pierce and W. E. Spicer, "Electronic structure of amorphous Si from photoemission and optical studies," *Phys. Rev. B*, vol. 5, pp. 3017-3029, Apr. 15, 1972.

[28] Y. Yamamoto, T. Kamiya and H. Yanai, "Characteristics of optical guided modes in multi-layer metal-clad planar optical guide with low-index dielectric buffer layer," *IEEE J. Quantum Electron.*, vol. QE-11, pp. 729-736, Sept. 1975.

Glen M. McWright (S'81), for a photograph and biography, see p. 788 of the April 1982 issue of this JOURNAL.

T. E. Batchman (S'61-M'66), for a photograph and biography, see p. 788 of the April 1982 issue of this JOURNAL.

M. S. Stanziano (S'79) was born in Washington, DC, on March 28, 1957. He received the B.S. degree in electrical engineering from the University of Virginia, Charlottesville, in 1980.

During the summer he has been employed with the Hazeltine Corporation, Electro-Acoustics Systems Laboratory, and with the Submarine Signal Division, Raytheon Company. He is currently completing studies towards the M.E. degree at the University of Virginia.

83

DISTRIBUTION LIST

Copy No.

1 - 3   National Aeronautics and Space Administration
         Langley Research Center
         Hampton, Virginia 23665

         Attention: IRD

4 - 5   NASA Scientific & Technical Information Facility
         P.O. Box 8757
         Baltimore/Washington International Airport
         Maryland 21240

  6   Gilbert Hay

7 - 11   T. E. Batchman

 12   E. H. Pancake
         Science/Technology Information Center
         Clark Hall

 13   SEAS Publications Files

JO#5793:wn

UNIVERSITY OF VIRGINIA

School of Engineering and Applied Science

The University of Virginia's School of Engineering and Applied Science has an undergraduate enrollment of approximately 1,400 students with a graduate enrollment of approximately 600. There are 125 faculty members, a majority of whom conduct research in addition to teaching.

Research is an integral part of the educational program and interests parallel academic specialties. These range from the classical engineering departments of Chemical, Civil, Electrical, and Mechanical and Aerospace to departments of Biomedical Engineering, Engineering Science and Systems, Materials Science, Nuclear Engineering and Engineering Physics, and Applied Mathematics and Computer Science. In addition to these departments, there are interdepartmental groups in the areas of Automatic Controls and Applied Mechanics. All departments offer the doctorate; the Biomedical and Materials Science Departments grant only graduate degrees.

The School of Engineering and Applied Science is an integral part of the University (approximately 1,530 full-time faculty with a total enrollment of about 16,000 full-time students), which also has professional schools of Architecture, Law, Medicine, Commerce, Business Administration, and Education. In addition, the College of Arts and Sciences houses departments of Mathematics, Physics, Chemistry and others relevant to the engineering research program. This University community provides opportunities for interdisciplinary work in pursuit of the basic goals of education, research, and public service.